ESPOO 2004 VTT PUBLICATIONS 552

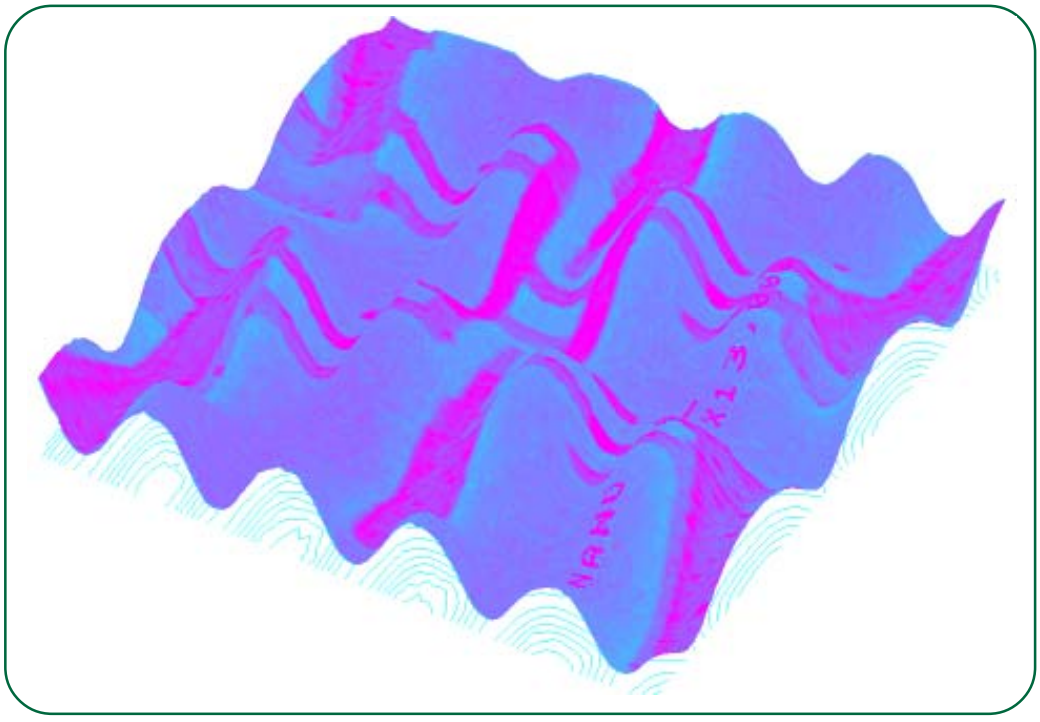

Antti O. Niskanen

Control of Quantum Evolution and Josephson Junction Circuits

VTT PUBLICATIONS 552

Control of Quantum Evolution and Josephson Junction Circuits

Antti O. Niskanen

VTT Information Technology

Dissertation for the degree of Doctor of Science in Technology to be presented with due permission of the Department of Engineering Physics and Mathematics for public examination and debate in Auditorium F1 at Helsinki University of Technology (Espoo, Finland) on the 26th of November, 2004, at 12 noon.

ISBN 951–38–6420–0 (soft back ed.)
ISSN 1235–0621 (soft back ed.)

ISBN 951–38–6421–9 (URL: http://www.vtt.fi/inf/pdf/)
ISSN 1455–0849 (URL: http://www.vtt.fi/inf/pdf/)

JULKAISIJA – UTGIVARE – PUBLISHER

VTT, Vuorimiehentie 5, PL 2000, 02044 VTT
puh. vaihde (09) 4561, faksi (09) 456 4374

VTT, Bergsmansvägen 5, PB 2000, 02044 VTT
tel. växel (09) 4561, fax (09) 456 4374

VTT Technical Research Centre of Finland, Vuorimiehentie 5, P.O.Box 2000, FIN–02044 VTT, Finland
phone internat. + 358 9 4561, fax + 358 9 456 4374

VTT Tietotekniikka, Tietotie 3, PL 1207, 02044 VTT
puh. vaihde (09) 4561, faksi (09) 456 7012

VTT Informationsteknik, Datavägen 3, PB 1207, 02044 VTT
tel. växel (09) 4561, fax (09) 456 7012

VTT Information Technology, Tietotie 3, P.O.Box 1207, FIN–02044 VTT, Finland
phone internat. + 358 9 4561, fax + 358 9 456 7012

Technical editing Leena Ukskoski

Otamedia Oy, Espoo 2004

Niskanen, Antti O. Control of Quantum Evolution and Josephson Junction Circuits. Espoo 2004. VTT Publications 552. 46 p. + app. 61 p.

Keywords quantum systems, quantum mechanics, quantum computing, quantum algorithms, Cooper pair pumping

Abstract

Ever since Peter Shor's ground-breaking discovery in 1994 of an algorithm capable of factoring large integers on a quantum-mechanical computer exponentially faster than using any known classical method, research on quantum computing has boomed. Quantum information – a unique mixture of computer science, physics and mathematics – has developed into a new branch of information theory. On the experimental side, physicists from many different disciplines including atomic, solid-state and low-temperature physics, as well as optics, are striving today towards a practical quantum computer. All the candidate quantum bit (qubit) technologies have one thing in common: They rely on the controlled time-evolution of a closed quantum system, a seemingly paradoxical task.

In this Thesis the temporal control of quantum systems is studied. The topics included can be divided into two according to the type of temporal evolution; geometrical or dynamical. Geometrical realization-independent methods for quantum computing are studied first. Then the study is extended into dynamical quantum computing and the so-called Josephson charge-qubit register is considered as a test bench. Finally, a spin-off application of the geometrical evolution of a Josephson junction system is studied, i.e. Cooper pair pumping. A novel Cooper pair pump, the Cooper pair "sluice", is introduced.

The work on quantum computing reported in this Thesis is theoretical while the Cooper pair "sluice" is studied both theoretically and experimentally. Numerical simulations, both sequential and parallel, are used extensively throughout the Thesis. The experiments were carried out under cryogenic mK conditions and the sample fabrication was done using e-beam nanolithography.

Because the execution time of a quantum algorithm is always limited by the inevitable process of decoherence, it is important to utilize any measure available for accelerating quantum computations. It is found that practical quantum algorithms could greatly benefit from classical computer-aided optimization. Moreover, it is found that even a modest demonstrator of a full quantum algorithm using Josephson charge qubits is just barely realizable within present-day coherence times. However, the experimental part of this Thesis shows clear evidence of the functioning of the "sluice". While the worldwide effort of improving the coherence properties of qubits is underway, the "sluice" could well find practical use, e.g., in metrology in the foreseeable future.

Preface

The incentive for this work was obtained when I attended prof. Mikio Nakahara's course *Quantum Computing* in 2001 at Helsinki University of Technology (HUT) while he was in Finland as a visiting professor from Kinki University, Osaka. Later, in 2002, I had the privilege of writing my Master's Thesis under prof. Nakahara's guidance at the Materials Physics Laboratory of HUT. The Master's Thesis titled *Holonomic Quantum Computing*, lead to the first two papers of this Thesis. The next three papers of the work were on a slightly different subject, but still, they were a natural continuation of my Master's Thesis. I am grateful to prof. Nakahara for his guidance. I also wish to thank my Finnish co-authors at the Materials Physics Laboratory, namely prof. Martti Salomaa and M.Sc. Juha Vartiainen, for fruitful collaboration. In particular, I am indebted to prof. Salomaa for making my work on quantum computing possible. Enlightening discussions with M.Sc. Teemu Ojanen and M.Sc. Mikko Möttönen in the "Theory Room" are gratefully acknowledged.

Since the beginning of the year 2003 I have worked in the Quantronics group lead by Dr. Panu Helistö at Microsensing of VTT Information Technology. Almost from the beginning of 2003 I have also had the opportunity to broaden my perspective on physics by working partially in acad. prof. Jukka Pekola's group in the Low Temperature Laboratory at HUT. This arrangement has proven more than great. I am extremely grateful to acad. prof. Pekola for his dedicated guidance. I would also like to thank my group members at VTT and in particular prof. Heikki Seppä for guidance and stimulating discussions. In addition, I would like to thank M.Sc. Jani Kivioja for the long but fun days that we have spent next to the cryostat. I am also grateful to those who I have not explicitly mentioned but who have been helpful along the way.

I wish to thank the Research Foundation of Helsinki University of Technology for funding my Master's Thesis work. I would also like to thank the Academy of Finland for funding during my time in the Materials Physics Laboratory through the Graduate School in Technical Physics. Since 2003, my research has been funded by VTT internal funding and the Academy of Finland for which I am grateful. I would also like to acknowledge the European Science Foundation PiShift program, the EU-IST-FET SQUBIT, and the Magnus Ehrnrooth Foundation for travel support. The excellent computing resources of CSC Finland are gratefully acknowledged.

I would also like to thank my parents Juha and Merja for support and everything else during my 26+ years. Thanks go also to my brother Ville and sister Johanna. Finally, the greatest of thanks go to my wife Katriina and our little wonder girl Alina.

List of Publications

This Thesis is a review of the author's work on the control of the temporal evolution of quantum systems in general and of Josephson junction systems in particular. It consists of an overview and the following publications:

I. A. O. Niskanen, M. Nakahara, and M. M. Salomaa, *Realization of arbitrary gates in holonomic quantum computation*, Physical Review A **67**, 012319 (2003).

II. A. O. Niskanen, M. Nakahara, and M. M. Salomaa, *Optimal holonomic quantum gates*, Quantum Information and Computation **2**, 560–577 (2002).

III. A. O. Niskanen, J. J. Vartiainen, and M. M. Salomaa, *Optimal multiqubit operations for Josephson charge qubits*, Physical Review Letters **90**, 197901 (2003).

IV. J. J. Vartiainen, A. O. Niskanen, M. Nakahara, and M. M. Salomaa, *Acceleration of quantum algorithms using three-qubit gates*, International Journal of Quantum Information **2**, 1–10 (2004).

V. J. J. Vartiainen, A. O. Niskanen, M. Nakahara, and M. M. Salomaa, *Implementing Shor's algorithm on Josephson charge qubits*, Physical Review A **70**, 012319 (2004).

VI. A. O. Niskanen, J. P. Pekola, and H. Seppä, *Fast and accurate single-island charge pump: Implementation of a Cooper pair pump*, Physical Review Letters **91**, 177003 (2003).

VII. A. O. Niskanen, J. M. Kivioja, H. Seppä, and J. P. Pekola, *Evidence of Cooper pair pumping with combined flux and voltage control*, submitted, 4 pages (2004); cond-mat/0410758.

Throughout the overview the above articles are referred to by their Roman numerals.

Author's Contribution

The research reported in this Thesis has been carried out in the Materials Physics Laboratory at Helsinki University of Technology in 2002 (Publications I–III) and in 2003–2004 (Publications VI and VII) jointly at Microsensing of VTT Information Technology and the Low Temperature Laboratory at Helsinki University of Technology. During 2003–2004 the author has also continued, out of academic interest, part-time the research initiated at the Materials Physics Laboratory in 2002 (Publications IV and V).

The author has had a central role in all aspects of the work reported in this Thesis. The author has written the manuscripts for Publications I–III, VI and VII and actively participated in writing Publications IV and V. The computer programs used in Publications I, II and VI were developed by the author. The author was a co-developer of the parallel programs and methods used in Publications III–V, which are based on the author's original sequential algorithms used in Publications I and II. Publication VI, the theory of the Cooper pair "sluice", is based on the author's original idea. Publication VII is a report of the experimental verification of this idea. The author fabricated the samples used in the experiment, actively participated in the low-temperature measurements and analyzed the data of Publication VII.

In addition, the author has presented the results of the work at major international conferences including the Erato Workshop on Quantum Information Science (EQIS) in Tokyo (Japan) 2002, the 6^{th} European Conference on Applied Superconductivity (EUCAS) in Sorrento (Italy) 2003 and the 39^{th} Rencontres de Moriond on Quantum Information and Decoherence in Nanosystems in La Thuile (Italy) 2004. Some results of the Thesis were also presented in the Applied Superconductivity Conference (ASC) in Jacksonville (Florida, USA) 2004.

Contents

1 Introduction

The temporal control of pure quantum systems has two competing requirements. On one hand, it is desired that the system under scrutiny is well isolated from its environment such that the dynamics may be assumed to be unitary. On the other hand, however, any temporal control implies a time dependence in the Hamiltonian which can only be an effective approximation and a result of an interaction with the environment such that the system cannot stay pure indefinitely. Despite this, ever since the emergence of Shor's algorithm [1] for factoring large composite integers on a quantum computer [2–5] the control of the temporal evolution of quantum systems has been a topic of intensive investigations in physics. The "killer application" of Shor's algorithm would be the breaking of the RSA cryptosystem. This could have a remarkable societal impact, and not necessarily a negative one. To complement the possible emergence of a quantum computer, quantum cryptography [6] is quite advanced already today. Nevertheless, in order to perform calculations on a quantum computer, the quantum programmer needs to have full control over the time-evolution of the system. Moreover, the system needs to stay pure in the quantum-mechanical sense. It is possible to have quantum control that does not maintain the purity, and the difference between the control of an impure state and that of a pure state should be distinguished. Roughly speaking, in the control of pure states not only the probabilities of different states but also the quantum-mechanical phases are of interest. This Thesis discusses the control of pure or almost pure quantum systems.

Quantum control has been studied in the past particularly in the context of nuclear magnetic resonance (NMR) [7] and, e.g., within molecular dynamics [8]. Quite complicated quantum-computing experiments have also been carried out in NMR with the most spectacular achievement of a seven-qubit algorithm for factoring the number fifteen [9]. The topic of controlling the macroscopic quantum state of a system such as the nanoelectronic superconducting Cooper pair box [10] is less thoroughly explored. Nevertheless, many steps have been taken in recent years towards an experimental realization of a Josephson junction based quantum computer. In the experiments by Nakamura et al. [11–13], the coherent oscillations of a Cooper pair box were first observed. The coherent operation of a coupled Cooper pair box system has also been demonstrated [14, 15]. The dual realization, i.e. the superconducting qubit taking advantage of the flux degree of freedom [16, 17] has been experimentally verified as well [18, 19]. The macroscopic coherent behavior of a current-biased large Josephson junction, or the phase qubit, was recently realized [20, 21] with as high as μs coherence times reported in Ref. [20]. Coherence times on the same order were measured in the so-called quantronium circuit [22] in Saclay. A generalization of the current-biased Josephson junction, the current-biased SQUID, has also been demonstrated to exhibit coherent behavior [23]. Exotic scenarios, such as the tetrahedral qubit [24], have been suggested as well. For a review of various superconducting qubits up to year 2001 see in particular Ref. [25].

The control of adiabatic Cooper pair pumps (CPPs) [26–28] is an instance of the geometrical control of a superconducting system similar to superconducting qubits. While in

superconducting qubits the control is typically achieved via ordinary dynamical temporal evolution, the CPPs are controlled adiabatically and cyclically such that no transitions between states occur. In quantum computing unitary transformations are pursued while in Cooper pair pumping the time-integral of the current is of interest. It is however possible, at least in principle, to achieve also general unitary transformations via adiabatic evolutions as holonomies. This branch of quantum information is called holonomic quantum computing (HQC) [29]. This Thesis contains examples of both adiabatic and dynamical quantum computing as well as Cooper pair pumping.

The Overview is organized as follows. Section 2 briefly discusses the unitary evolution of quantum systems in general and the concept of geometrical evolution in particular. Section 3 discusses the optimization of quantum algorithms developed in detail in Publications I–V. Finding unitary operations within a realization-independent model of holonomic quantum computing (Publications I and II) is studied first. Then the construction of dynamical quantum gates (Publications III–V) for a model identical to a Cooper pair box array is explored. The highlight of the Section is a theoretical study of carrying out the simplest nontrivial application of Shor's factorization algorithm on Josephson charge qubits. The topic of Section 4 is the adiabatic Cooper pair pump and especially the so-called Cooper pair "sluice" of Publications VI and VII. This topic is an illustration of the multitude of present-day applications achievable with almost identical techniques and structures as those intended to be used in quantum computing. As explained below this device aimed at a metrological application has many common features with superconducting qubits and it is further closely related to the concept of Berry's phase. Cooper pair pumping has been studied extensively in the past but has never proven even nearly as accurate as, e.g., single-electron pumping [30]. The sluice is hoped to bridge this gap. Finally, Section 5 is dedicated to a discussion of the results in this Thesis.

2 Controlled Evolution of Quantum Systems

The topics discussed in this Thesis rely on the cyclic control of quantum systems achieved via manipulating their Hamiltonians in time. That is, in all the applications considered the parameters of a Hamiltonian go around loops in the parameter space in order to achieve some desired effect. These controlled cyclic temporal evolutions may roughly be divided into two main categories: Evolution may be either dynamical or geometrical in nature. Geometrical evolution may arise if the time dependence is slow enough compared to the relevant energy level separations, i.e., all the controllable parameters of the Hamiltonian are tuned adiabatically. As the term geometrical implies, only the geometry of the loop matters and not the speed at which it is traversed. Geometrical, or adiabatic, evolutions may further be divided into Abelian and non-Abelian ones. Abelian evolutions are commuting, i.e. the order in which the loops are arranged does not matter, while non-Abelian evolutions do not commute. Abelian evolutions give rise to Berry's phase [31] while non-Abelian evolutions may not be characterized by a simple phase but rather unitary matrices are needed as pointed out by Wilczek and Zee [32]. They are called holonomies.

Decoherence mechanisms and open quantum systems (see, e.g., Ref. [33, 34]) are not considered in detail in this Thesis. Many studies on the decoherence mechanisms in superconducting circuits exist in the literature, see e.g. Refs. [25, 35–39] and references therein. In Subsection 2.1 below we give a brief introduction to the concepts of quantum mechanics that are important for the present work including general dynamical evolution. We then proceed to discuss geometrical evolution in Subsection 2.2. For a critical discussion of the fundamentals of quantum mechanics, see e.g. Ref. [40]. Publications I, II, VI and VII are related to adiabatic evolution while Publications III–V discuss dynamical evolutions.

2.1 Quantum mechanics and dynamical temporal evolution

The state of a pure quantum system is described by a state vector $|\psi\rangle$ in a complete inner-product space called the Hilbert space. A physical state vector $|\psi\rangle$ can always be normalized to unity $\langle\psi|\psi\rangle = 1$. It may occur, however, that the state is not pure but rather mixed in which case the system is described with a state operator, or a density matrix (operator) ρ with $\mathrm{Tr}\,\rho = 1$. The system is pure if and only if $\mathrm{Tr}\,\rho^2 = 1$ in which case one may use the state vector to describe the system. Given a state vector, the corresponding density operator may be formed via $\rho = |\psi\rangle\langle\psi|$. The state vector and the state operator are not themselves directly observable quantities in quantum mechanics. Namely, every observable has an associated self-adjoint operator $\mathcal{O} = \mathcal{O}^\dagger$. In the spirit of the statistical interpretation of quantum mechanics, the expectation value for the k^{th} moment of an observable is given by either $\langle\mathcal{O}^k\rangle = \mathrm{Tr}\,\left(\rho\mathcal{O}^k\right)$ or alternatively by $\langle\mathcal{O}^k\rangle = \langle\psi|\mathcal{O}^k|\psi\rangle$ in the special case of a pure system. The measurement of the observable always yields an eigenvalue of the operator $\mathcal{O}$. Even if the state $|\psi\rangle$ is not an eigenstate of $\mathcal{O}$, then owing to the self-adjointness of $\mathcal{O}$ we may utilize the complete

eigenbasis to expand the state. That is, we may write

$$|\psi\rangle = \sum_{\alpha} c_\alpha |\psi_\alpha\rangle, \tag{1}$$

where $\mathcal{O}|\psi_\alpha\rangle = \omega_\alpha|\psi_\alpha\rangle$, $\sum_\alpha |c_\alpha|^2 = 1$, $\langle\psi_\beta|\psi_\alpha\rangle = \delta_{\alpha\beta}$ and $\omega_\alpha \in \mathbb{R}$. An ideal projective measurement will result in ω_α with the probability $|c_\alpha|^2$. Immediately following the measurement, the system will reside in the state $|\psi_\alpha\rangle$.

For every quantum system, there exists a Hamiltonian operator $\mathcal{H}$ which describes the energy of the system. This dictates the exact form of the temporal evolution. Namely, the dynamics of an isolated quantum system is governed by the Schrödinger equation

$$i\hbar\frac{d}{dt}|\psi(t)\rangle = \mathcal{H}|\psi(t)\rangle. \tag{2}$$

The corresponding equation for the density operator is

$$i\hbar\dot{\rho}(t) = [\mathcal{H}, \rho]. \tag{3}$$

For a time-independent Hamiltonian Eq. (2) may be simply solved using operator exponentiation, i.e. $|\psi(t_1)\rangle = \exp(-i\mathcal{H}(t_1 - t_0)/\hbar)|\psi(t_0)\rangle$. If the Hamiltonian has a general time dependence $\mathcal{H} \equiv \mathcal{H}_{\mathbf{q}(t)}$ the situation is considerably more complicated since the Hamiltonian may have a non-vanishing commutator with itself at different instants of time. In this work the Hamiltonian is taken to depend on a set of tunable parameters. These parameters are described by a vector-valued function of time $\mathbf{q}(t)$. This vector naturally contains all the parameters that we have control over. We can, even then, still formally solve for the time evolution using the time-ordering operator $\mathcal{T}$, which results in

$$|\psi(t_1)\rangle = \mathcal{T}\exp\left(-i\int_{t_0}^{t_1}\mathcal{H}_{\mathbf{q}(t)}dt/\hbar\right)|\psi(t_0)\rangle. \tag{4}$$

In spite of the integral, the above expression does not involve integration in the ordinary sense but it is rather a product integral. The effect of $\mathcal{T}$ is to arrange a sequence of operators, each of which is associated with an instant in time, such that the operators associated with earlier times are always to the right from those associated with later instants. Regardless of the exact details, however, the dynamics of an isolated quantum system is always unitary. We may write $|\psi(t_1)\rangle = U(t_1, t_0)|\psi(t_0)\rangle$ where in the general case the unitary operator $U(t_1, t_0)$ is given by

$$U(t_1, t_0) = \mathcal{T}\exp\left(-i\int_{t_0}^{t_1}\mathcal{H}_{\mathbf{q}(t)}dt/\hbar\right). \tag{5}$$

Due to unitarity, the quantum-temporal evolution of a closed system is always reversible: $U(t_1, t_0)^{-1} = U(t_1, t_0)^\dagger$. The norm is also preserved, i.e.

$$\langle\psi(t_1)|\psi(t_1)\rangle = \langle\psi(t_0)|U(t_1, t_0)^\dagger U(t_1, t_0)|\psi(t_0)\rangle = \langle\psi(t_0)|\psi(t_0)\rangle = 1, \tag{6}$$

which is consistent with the probability interpretation of quantum mechanics. The unitary temporal evolution of a mixed state may be expressed also very concisely as $\rho(t_1) = U(t_1, t_0)\rho(t_0)U(t_1, t_0)^\dagger$.

Equation (5) is quite general and comprises all forms of unitary evolution, i.e. both adiabatic and non-adiabatic behaviors. It serves as the natural starting point for numerical calculations. Depending on the application, one either aims at realizing a certain unitary evolution (quantum computing) or a certain consequence of evolutions (e.g., quantum pumping). The unitarity of the temporal evolution only breaks down when the system in consideration is no longer isolated. The quantum measurement mentioned briefly above is clearly non-unitary and, as a matter of fact, it is just through interactions that the actual measurements take place. This brings us to the problem of combining quantum systems. Two quantum systems with separate Hilbert spaces may be combined by considering their tensor product. That is, for any $|\psi_1\rangle$ (ρ_1) and $|\psi_2\rangle$ (ρ_2) the combined state is $|\psi_1\rangle \otimes |\psi_2\rangle$ ($\rho_1 \otimes \rho_2$). In the case of finite-dimensional spaces the tensor product is just the Kronecker product for matrices. The total Hamiltonian is, on the other hand $\mathcal{H}_{\text{tot}} = \mathcal{H}_1 \otimes I + I \otimes \mathcal{H}_2$. However, it may be that the two systems are non-isolated such that the total Hamiltonian may not be written as a sum of two terms each of which acts non-trivially only on the subspace of one of the systems but rather $\mathcal{H}_{\text{tot}} = \mathcal{H}_1 \otimes I + I \otimes \mathcal{H}_2 + \mathcal{H}_{\text{int}}$. It may also be the case that two initially separate pure systems cannot be described by $|\psi_1\rangle \otimes |\psi_2\rangle$. Then the total system is called entangled. To obtain the state operator for a certain subsystem of a possibly entangled total system one simply traces over the degrees of freedom of the uninteresting part of the Hilbert space. That is, if we have two systems 1 and 2, then $\rho_1 = \text{Tr}_2\rho$ is the state operator of subsystem 1. This partial trace combined with unitary global evolution may result in non-unitary temporal evolution.

2.2 Geometrical temporal evolution

In the special case when the temporal evolution of a quantum system may be considered to be adiabatic, Eq. (5) may be further refined. Adiabaticity in quantum mechanics means that if the quantum system in question, described by some Hamiltonian $\mathcal{H}_{\mathbf{q}(t)}$, is initially in the k^{th} eigenstate of energy, then we may also assume that it stays in the corresponding k^{th} eigenstate. This is the case when the dynamics is slow compared to the energy-level separations. Clearly no level crossings can be allowed such that the ordering of the states is possible and the separations remain nonzero. In this Thesis we consider only adiabatic systems in the ground state. Thus, for our purposes, the adiabaticity criterion means that all the related frequencies are much lower than the resonant frequency between the ground state and the first exited state. This resonant frequency may of course also depend on time, and thus the condition must hold at all times.

This basic assumption has quite nontrivial consequences [31,32,41]. For our purposes it is sufficient to concentrate on what happens to the ground state. Let us assume that the ground state has g degenerate eigenstates denoted by $|0\alpha;\mathbf{q}\rangle$ ($\alpha = 1, ..., g$) and that no level crossings occur at least between the ground state and the higher excited states. The eigenvalue of the ground state is $\varepsilon_{\mathbf{q}}$, such that

$$\mathcal{H}_{\mathbf{q}}|0\alpha;\mathbf{q}\rangle = \varepsilon_{\mathbf{q}}|0\alpha;\mathbf{q}\rangle \tag{7}$$

and

$$\langle 0\alpha;\mathbf{q}|0\beta;\mathbf{q}\rangle = \delta_{\alpha\beta}. \tag{8}$$

Moreover, the eigenvectors of the ground-state subspace are also orthogonal to the higher excited states. Let us assume that the state of the system is initially any one of orthonormal ground states $|\alpha;\mathbf{q}(t_0)\rangle$ and that the system evolves adiabatically over time $t \in [t_0, t_1]$ and also that the parameters go around a loop such that $\mathbf{q}(t_0) = \mathbf{q}(t_1)$. Then we may write the state of the system $|\psi_\alpha(t)\rangle$ at time t as

$$|\psi_\alpha(t)\rangle = \sum_{\theta=1}^{g} U_{\theta\alpha}(t,t_0)|0\theta;\mathbf{q}(t)\rangle \tag{9}$$

with some complex coefficients $U_{\beta\alpha}(t,t_0)$ that must satisfy $U_{\beta\alpha}(t_0,t_0) = \delta_{\beta\alpha}$. Plugging this into the Schrödinger equation, multiplying from the left by $\langle 0\beta;\mathbf{q}(t)|$ and using the orthonormality of the states yields

$$\frac{dU_{\beta\alpha}(t,t_0)}{dt} = -\sum_{\theta=1}^{g}\langle 0\beta;\mathbf{q}(t)|\frac{d}{dt}|0\theta;\mathbf{q}(t)\rangle U_{\theta\alpha}(t,t_0) - i\varepsilon_{\mathbf{q}(t)}U_{\beta\alpha}(t,t_0)/\hbar. \tag{10}$$

This has the solution

$$U(t,t_0) = e^{-i\int_{t_0}^{t}\varepsilon_{\mathbf{q}(\tau)}d\tau/\hbar}\mathcal{T}\exp\left(-\int_{t_0}^{t}\mathbf{A}(\tau)d\tau\right), \tag{11}$$

where $\mathbf{A}(t)$ is a matrix whose entries $\mathbf{A}_{\beta\alpha}(t)$ are given by

$$\mathbf{A}_{\beta\alpha}(t) = \langle 0\beta;\mathbf{q}(t)|\frac{d}{dt}|0\alpha;\mathbf{q}(t)\rangle. \tag{12}$$

Neglecting the dynamical phase $\theta_{\text{dyn}} = -\int_{t_0}^{t}\varepsilon_{\mathbf{q}(\tau)}d\tau/\hbar$ for now and introducing the connection matrices $\mathcal{A}_i$ whose elements are

$$\mathcal{A}_{i;\beta\alpha} = \langle 0\beta;\mathbf{q}|\frac{\partial}{\partial\mathbf{q}_i}|0\alpha;\mathbf{q}\rangle \tag{13}$$

allows us to rewrite Eq. (11) at the instant $t = t_1$ as

$$U(t_1,t_0) \equiv U_\gamma = \mathcal{P}\exp\left(-\oint_\gamma \mathcal{A}_i d\mathbf{q}^i\right), \tag{14}$$

where γ is the loop around which we traverse. The quantity $\mathcal{A}_i d\mathbf{q}^i$ is sometimes called the Wilczek-Zee connection one-form. Einstein's summation convention over all the components of the control parameter vector, i.e. the index i, is assumed. The path-ordering operator $\mathcal{P}$ is used above. Its operation is similar to that of $\mathcal{T}$.

Now if instead of the state $|\alpha;\mathbf{q}(t_0)\rangle$ we were initially to start from an arbitrary superposition $\sum_{\alpha=1}^{g} c_\alpha|\alpha;\mathbf{q}(t_0)\rangle$ then at time t_1 the state of the system would be

$$|\psi(t_1)\rangle = \sum_{\alpha=1}^{g} c_\alpha|\psi_\alpha(t_1)\rangle \tag{15}$$

or

$$|\psi(t_1)\rangle = \sum_{\alpha,\beta=1}^{g} U_{\beta\alpha}(t_1,t_0)c_\alpha|\beta;\mathbf{q}(t_1)\rangle = \sum_{\alpha,\beta=1}^{g}(U_\gamma)_{\beta\alpha}c_\alpha|\beta;\mathbf{q}_0\rangle. \tag{16}$$

We see form this that U_γ is indeed the unitary matrix that describes how the quantum state evolves during each loop based at $\mathbf{q}(t_0)=\mathbf{q}_0$. This is called a non-Abelian holonomy [32,41] in the degenerate case (Publications I and II) and Berry's phase [31] (Publications VI and VII) in the nondegenerate case, i.e. $U_\gamma = e^{i\theta_{\text{Berry}}}$ if $g=1$. In the nondegenerate case we may denote the ground state simply as $|0;\mathbf{q}\rangle$ and since the path ordering is then meaningless, Berry's phase is simply

$$\theta_{\text{Berry}} = i\oint_\gamma \langle 0;\mathbf{q}|\frac{\partial}{\partial\mathbf{q}_i}|0;\mathbf{q}\rangle d\mathbf{q}^i = i\oint_\gamma \langle 0;\mathbf{q}(t)|\nabla_{\mathbf{q}}|0;\mathbf{q}(t)\rangle\cdot d\mathbf{q}. \tag{17}$$

Thus, the cyclic quantum evolution of the ground state in the adiabatic limit has two contributions; the more-or-less trivial dynamical factor $e^{-i\int_{t_0}^{t_1}\varepsilon_{\mathbf{q}(t)}dt/\hbar}$ that can be neglected in e.g. quantum computing applications and the geometrical contribution U_γ. To obtain some desired holonomic evolution one needs to describe a loop γ in the parameter space spanned by all the controllable parameters. Whereas in general the speed at which a loop is traversed plays a role, in the adiabatic evolution only the geometry of the path (not its parameterization) matters. It may appear at first sight that for a nondegenerate system in its ground state, Berry's phase would be meaningless since it only describes a global phase. This is not the case as will be seen in Section 4 where we discuss Cooper pair pumps. For universal quantum computation based solely on ground-state adiabatic control, however, a degenerate system is required.

3 Optimization of Quantum Algorithms

Quantum computing is potentially a very spectacular application of the temporal control of quantum systems. Basically any collection of two-state (or more) quantum systems that can be controlled, and moreover, the couplings of which we have control over, or can take into account somehow, is a potential quantum computer. Provided that the quantum system is sufficiently well isolated from its environment, we may assume the dynamics to be unitary as in the previous Section. However, the parameters of the Hamiltonian need to be tunable and thus the isolation must not be perfect. In this Section we shall first introduce the concept of quantum computing. Many excellent overviews of this subject may be found in the literature, see e.g. Refs. [2–5]. It will turn out that a quantum algorithm is nothing but a unitary operator. It is programmed by finding a proper control pulse $\mathbf{q}(t)$ and executed by applying the pulse on the quantum system. In Subsection 3.2 we consider a realization–independent approach for finding physical implementations of holonomic quantum computations. Subsection 3.3 describes a similar approach for finding optimized logical dynamical quantum gates on Josephson charge qubits. All the methods presented rely on intensive numerical optimization. The key point of this Section is that instead of using sequences of elementary operations, we pursue a method of finding direct implementations of single and multiple qubit operations in a single pulse sequence. We demonstrate that it is in practice much more advantageous to implement a quantum algorithm via first finding, using ordinary computers, a direct implementation for as large a multiqubit operation as possible and then implementing this optimized operation on a quantum computer rather than using some limited set of elementary operations.

3.1 Quantum computing

Quantum computers can solve certain problems that are classically considered to require exponential resources (time and space) in polynomial time and space. The idea of quantum computing is to take advantage of the global properties of a very high-dimensional multi-partite Hilbert space. A quantum computer is a quantum system typically consisting of multiple two-state subsystems called quantum bits, or qubits. A prototype for a qubit is the spin degree of freedom of a spin-1/2 particle. Information is encoded in the states of the qubits such that one state of the qubit corresponds to the "0" of a classical digital bit while the other corresponds to "1". Let us denote the basis states of the collection of N qubits by $|0_j\rangle$ and $|1_j\rangle$ with $j \in \{1, \ldots, N\}$. One often uses the vector notation

$$|0_j\rangle = \begin{pmatrix} 1 \\ 0 \end{pmatrix} \quad \text{and} \quad |1_j\rangle = \begin{pmatrix} 0 \\ 1 \end{pmatrix} \tag{18}$$

for these states. If the states of the individual qubits are $|\psi_j\rangle$ with $\psi_j = 0, 1$ then the state of the composite system may be expressed using the tensor product as

$$|\Psi\rangle = \bigotimes_{j=1}^{N} |\psi_i\rangle = |\psi_N\rangle \otimes \ldots \otimes |\psi_1\rangle = |\psi_N \ldots \psi_1\rangle \,, \tag{19}$$

where the last form is an often used abbreviation. In the absence of superpositions the quantum information contained in this quantum register is interpreted just like the information in a classical bit register; the data is just a binary number. The strength of a quantum computer, however, emerges from the fact that the quantum register may evolve into a superposition of all the possible 2^N states. That is, if $|\Psi_\alpha\rangle$ is some N-qubit state corresponding to a binary number, then the state of the quantum computer can be

$$|\Psi\rangle = \sum_{\alpha=1}^{2^N} c_\alpha |\Psi_\alpha\rangle \,, \tag{20}$$

with $\langle\Psi|\Psi\rangle = 1$. The prototype of an entangled superposition is the so-called Bell state for two qubits

$$|\Psi\rangle = \frac{1}{\sqrt{2}} \left(|0\rangle \otimes |0\rangle + |1\rangle \otimes |1\rangle \right). \tag{21}$$

The interpretation of the data contained in this register is entirely non-classical; with probability one half the bits are either both zeros or ones. Moreover, the measurement of one of the qubits immediately tells us the result that the measurement of the second qubit would give. This has some very counterintuitive implications and the interpretation of this kind of state even confused Einstein [42]. Entangled states, such as the Bell state above, can be used for so-called (deterministic) quantum teleportation that has been recently realized using ion traps [43, 44].

The quantum algorithm is nothing but a 2^N-dimensional unitary operator of Eq. (5) which dictates the temporal evolution of the quantum register, i.e.

$$|\Psi(t_1)\rangle = U(t_1, t_0)|\Psi(t_0)\rangle. \tag{22}$$

The evolution of the quantum computer is governed by the Hamiltonian $\mathcal{H}_{\mathbf{q}(t)}$ whose time-dependence the experimenter must have control over. The control is mediated by the parameters $\mathbf{q}(t)$ and different formal expressions for the algorithm U can be derived as discussed in the previous Section. Clearly the number of degrees of freedom for the algorithm is immense; it takes $2^{2N} - 1$ real numbers to describe the most general kind of an algorithm while for applications $N \gg 100$. Luckily, practical algorithms exist too. Typically, we would desire the operator U to perform, for instance, the quantum part of Shor's algorithm [1] or the Grover search [45] both of which can be carried out by applying a polynomial number of so-called elementary operations [46]. Shor's algorithm can factor large integers in polynomial time, which is otherwise believed to be exponentially hard, while Grover's search can be used to carry out a database search of an unsorted database in time proportional to the square root of the entries in it. The best known decompositions of arbitrary multiqubit gates have been reported in Refs. [47, 48] but, nevertheless, the number of required gates scales exponentially with the number of qubits.

The unique property of quantum mechanics that makes quantum computing attractive is that unitary operator "processes" all orthogonal basis states independently. In other words, the quantum algorithm may process 2^N different inputs at once if the register is initialized for instance in an equal superposition. This is sometimes called quantum

parallelism. The task carried out e.g. in Shor's algorithm is the evaluation of a certain modular function, see e.g. Refs. [1, 2] or Paper V. With $N \sim 10^3$ the number of states is already immense and beyond the capacity of all classical computers. However, after the unitary temporal evolution one has to measure the state of the system. Each qubit is found in either the state $|0\rangle$ or $|1\rangle$. If the state of the register prior to measurement is $|\Psi\rangle$, then the probability of obtaining the result $|\tilde{\Psi}\rangle = \bigotimes_{j=1}^{N} |\tilde{\psi}_j\rangle$ ($\tilde{\psi}_j = 0$ or $\tilde{\psi}_j = 1$) is given by

$$P(\Psi) = \langle\Psi|\tilde{\Psi}\rangle\langle\tilde{\Psi}|\Psi\rangle = |\langle\Psi|\tilde{\Psi}\rangle|^2. \tag{23}$$

This is the tricky part. No matter how many orthogonal basis states have non-vanishing amplitudes in the superposition, upon measurement only one of them survives. Moreover, the result is stochastic. The quantum measurement makes it impossible to obtain more than one output. The trick that can be used then is to further process the information in the quantum register before measurement and to look for "global" properties in it. In Shor's algorithm one is interested in the period of the modular function and luckily the quantum equivalent of the fast Fourier transform may be carried out efficiently. This causes the quantum register to form strong interference patterns and upon measurement it is possible, stochastically, to deduce the period. Thus the true strength of quantum computing is only unleashed in a certain class of applications in which some well-defined global property is known.

We list the requirements for practical quantum computing following DiVincenzo [49]. One needs to have:

- a scalable physical system with well characterized qubits
- the ability to initialize the state of the qubits to a simple fiducial state
- long relevant decoherence times, much longer than the gate operation time
- a universal set of quantum gates
- a qubit-specific measurement capability.

All of these points are necessary and it seems that all the existing suggestions for physical realizations of quantum computing possess strengths in some of these areas but not in each one of them. In this work we are primarily interested in how to carry out the unitary transformations, i.e. the quantum gates.

As mentioned above, typically the unitary operator U is decomposed into a sequence of so-called elementary gates [46] that act non-trivially only on one or two qubits. These are analogous with the basic logical operations of an ordinary computer. The physical implementation for these is often found by hand and the Hamiltonian is sometimes even considered piecewise constant in time. This leads to abrupt switchings in the parameter sequences which are hard if not impossible to implement. Finite rise and fall times of real pulses lead to errors [50]. Furthermore, in general only a limited number of logically different gates are assumed to be available. Thus the logical gate sequences may get prohibitively long. In the next two subsections methods for finding arbitrary single and

multiple qubit gates avoiding abrupt switchings are considered. The motivation for this is that the more complicated gates we may perform in a single step, the more of the valuable execution time we save. This is extremely important due to the presence of decoherence which inevitably limits the total execution time of the algorithm. In Subsection 3.2, methods for finding the adiabatic loop γ in the control-parameter space for any one-qubit and two-qubit operation for a certain toy model is presented, while in Subsection 3.3 control sequences realizing up to three-qubit operations for Josephson charge qubits are found. The developments presented here have recently obtained experimental verification when Nakahara et al. demonstrated [51] the acceleration of the two-qubit Grover search at best by four times by first optimizing the algorithm and then by carrying it out experimentally in an NMR setup.

3.2 Adiabatic non-Abelian quantum gates

Holonomic quantum computing (HQC) [29, 52–55] is a subfield of quantum information processing in which the quantum register is assumed to be fully degenerate and the quantum control is implemented using Eq. (14). The reason for studying holonomic quantum computing is that it is hoped to be robust against decoherence due to the degeneracy of the spectrum. A clear benefit is also the fact that the exact timing of the pulses is not crucial since the evolution is purely geometrical as long as the adiabaticity is maintained. Additional features include the absence of unwanted phases on idle qubits that inevitably accumulate in any scenario in which the logical states are energetically different.

Thus in HQC each unitary gate is associated with a loop in the parameter space, and a sequence of loops forms the full quantum algorithm. Holonomic or adiabatic non-Abelian gates in a three-state model are studied in papers I and II. The results obtained are quite general and are not limited to any particular physical system. For various suggestions for the realization of non-Abelian holonomies with Josephson junction structures, see Refs. [56–58]. Also optical [59] and semiconductor [60] HQC has been suggested. Berry's Abelian geometrical phase has been envisaged to be used for universal quantum computation in superconducting systems by Falci et al. [61], but there the system under study is not in the ground state such that differences in Berry phases are of interest and, furthermore, sudden changes in the parameters are also used. In HQC purely ground state systems and strictly adiabatic control is used.

The problem considered is the following: Given a unitary quantum gate $\hat{U}$, what is the parameter loop γ that produces $\hat{U}$ through Eq. (14), i.e. under which conditions $U_\gamma = \mathcal{P}\exp\left(-\oint_\gamma \mathcal{A}_i d\mathbf{q}^i\right)$ equals $\hat{U}$? It is straightforward to solve the direct problem but the solution of the inverse problem turns out to involve heavy computations. However, this is clearly the relevant question from the point of view of holonomic quantum computing since γ is just the experimental control sequence. A possible way of finding a path γ that realizes $\hat{U}$ is to use numerical optimization. Namely, let us define

$$f(\gamma) = \|\hat{U} - U_\gamma\|, \tag{24}$$

where $\|\cdot\|$ is some specified norm. In this Thesis we use the Frobenius norm $\|\cdot\|_F$ defined as $\|\mathbf{A}\|_F = \sqrt{\mathrm{Tr}\,(A^\dagger A)}$. Then finding the minimum of $f(\gamma)$, which clearly is equal to zero if a solution to the original problem exists, is equivalent to finding a path γ that implements $\hat{U}$. In practice, the multidimensional path is conveniently discretized for instance into polygonal loops, i.e., into loops that have a finite number of vertices between which one interpolates linearly. Then we are effectively searching for the minimum in a subspace of all (continuous) loops and the coordinates of the vertices serve as natural optimization variables. Various numerical algorithms for the minimization are possible, but the so-called polytope search [62] was found to be particularly successful for the problem. Exact methods have been studied also for the solution of a similar problem [63].

The functional evaluations for a given polygonal path may easily be carried out by the discretization of the path and considering the connection coefficients $\mathcal{A}_i$ piecewise constant such that evaluation of U_γ reduce to multiplication of matrix exponentials. That is, for a discretization $\gamma_1, \ldots, \gamma_n$ of the loop γ we may write

$$U_\gamma \approx \exp(-\sum_i \mathcal{A}_i(\gamma_n)\delta\gamma_n^i) \cdots \exp(-\sum_i \mathcal{A}_i(\gamma_1)\delta\gamma_1^i), \tag{25}$$

where $\mathcal{A}_i(\gamma_k)$ stands for the i^{th} connection component evaluated at the discretization point γ_k and $\delta\gamma_k^j$ is the finite difference of the j^{th} parameter component of the k^{th} interval. The number of connection components and thus the bounds on the summation index i depend on the number of controllable parameters. From this discretization it is clear why expressions of the kind appearing in Eqs. (14) and (5) are sometimes called product integrals; letting $n \to \infty$ and $\delta\gamma_k^j \to 0$ renders the approximation in Eq. (25) exact. The matrix exponentials may be either calculated using the Taylor expansion or the Cayley form, see Paper V. More details of the numerics can be found in publications I and II. In general, a realization for an arbitrary N-qubit gate is expected to exist if the number of degrees of freedom in the optimization exceeds the dimensionality of the Lie algebra $u(2^N)$ which is 2^{2N}.

Single-qubit gates

To get some concreteness to the problem we consider as an example a case where the individual qubits are encoded in the twofold degenerate ground state of a three-dimensional Hilbert space. We assume that the Hamiltonian is diagonal at the reference point $\mathbf{q}_0$ where the holonomy loops are based and the ground state energy is set to zero. Then the Hamiltonian at this point may be written simply as

$$\mathcal{H}_{\mathbf{q}_0} = \begin{pmatrix} \epsilon & 0 & 0 \\ 0 & 0 & 0 \\ 0 & 0 & 0 \end{pmatrix}, \tag{26}$$

with $\epsilon > 0$. We then consider the adiabatic isospectral temporal dependence of the Hamiltonian to be of the form $\mathcal{H}_{\mathbf{q}} = W_{\mathbf{q}}\mathcal{H}_{\mathbf{q}_0}W_{\mathbf{q}}^\dagger$, where $W_{\mathbf{q}}$ is a unitary transformation that satisfies $W_{\mathbf{q}_0} = I_3$, where I_3 is the 3×3 identity matrix. All the temporal dependence of the Hamiltonian is encoded in $W_{\mathbf{q}}$ and this dependence is assumed to be adiabatic.

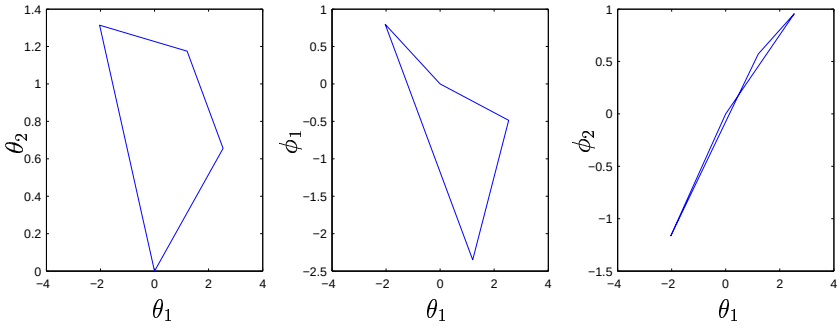

Figure 1. Loop in the parameter space that yields the gate $U = e^i \exp\left(i\frac{\pi}{7}\sigma_z\right) \exp\left(i\frac{1}{3}\sigma_y\right) \exp(i\sigma_z)$. *From Paper I.*

A convenient method to parameterize the unitary transformation $W_{\mathbf{q}}$ is to use the so-called Givens decomposition. It turns out that arbitrary rotations $W_{\mathbf{q}}$ are isomorphic to the complex projective space [64] $\mathbb{C}P^2$. This manifold may be parameterized using the four coordinates denoted θ_i and ϕ_i with $i = 1, 2$ in Papers I and II. The corresponding Wilczek-Zee matrices $\mathcal{A}_{\theta_i}$ and $\mathcal{A}_{\phi_i}$ can be found analytically and this allows one to write any holonomy on a single qubit as

$$U_\gamma = \mathcal{P} \exp\left(- \oint_\gamma \sum_{i=1}^{2} (\mathcal{A}_{\theta_i} d\theta_i + \mathcal{A}_{\phi_i} d\phi_i) \right). \tag{27}$$

The numerical calculations were carried using `Fortran 90` and the `IMSL` library. Figure 1 illustrates an example loop in the four-dimensional $(\theta_1, \theta_2, \phi_1, \phi_2)$-space for realizing a particular unitary operation, namely $U = e^i \exp\left(i\frac{\pi}{7}\sigma_z\right) \exp\left(i\frac{1}{3}\sigma_y\right) \exp(i\sigma_z)$. Here σ_z and σ_x are Pauli matrices and $\mathbf{q}_0 = (0, 0, 0, 0)^T$. Papers I and II report realizations for various other gates. The conclusion regarding single-qubit gates in the present setting is that they can all be found with a sufficient amount of flexibility in the paths.

Two-qubit gates

Two-qubit gates may also be found for HQC. To this end a way of coupling the qubits is desired. We define the two-qubit reference Hamiltonian to be

$$H_{\mathbf{q}_0}^{\text{2-qubit}} = \mathcal{H}_{\mathbf{q}_0} \otimes I_3 + I_3 \otimes \mathcal{H}_{\mathbf{q}_0}. \tag{28}$$

The most general kind of isospectral rotations for this 9-dimensional Hamiltonian is very complicated but we shall consider the product of a purely two-qubit rotation and that of a tensor product of single-qubit rotations, i.e.

$$W_{\mathbf{q}} = W_{\mathbf{q}}^{\text{2-qubit}} (W_{\mathbf{q}}^a \otimes W_{\mathbf{q}}^b), \tag{29}$$

where $W_{\mathbf{q}}^a$ ($W_{\mathbf{q}}^b$) is the single-qubit rotation of the Hamiltonian of the qubit a (b) identical to that used in purely single-qubit operations. We take $W^{\text{2-qubit}}$ to be of the form $W^{\text{2-qubit}} = e^{i\xi|11\rangle\langle 11|}$. Thus the rotations of the two-qubit Hamiltonian are parameterized using the nine parameters $(\theta_i^c, \phi_i^c, \xi)$ with $i = 1, 2$ and $c = a, b$. Arbitrary two-qubit quantum gates may be found within this model, and various examples may be found in papers I and II.

The problem of coupling multiple qubits is difficult in general, but in the case of HQC it is particularly hard due to the stringent requirement of degeneracy. The coupling presented here is merely an example, albeit a convenient one.

Length optimization

The motivation for studying holonomic quantum gates numerically is not just the need to find implementations of arbitrary gates. Namely, it is possible also to optimize with respect to a more general type of an error functional. Paper II discusses the optimization of HQC with respect to the length of the path numerically. Recently, however, also the exact solution of the so-called isoholonomic problem has been provided for an arbitrary k-dimensional unitary gate within a Hilbert space with a dimension larger than $2k$ [65].

3.3 Non-adiabatic Josephson charge-qubit gates

The developments presented above in the context of holonomic quantum computation may easily be generalized also to "ordinary" dynamical quantum computing. The optimization of multiqubit gates for the so-called Josephson charge-qubit model is the topic of publications III, IV and V. The only practical difference in the numerical optimization scheme of the present problem and HQC is the evaluation of the unitary operator. Whereas Eq. (14) was used above, here we utilize Eq. (5). The evaluation of the unitary operator was carried out using parallel programming [66]. The motivation is the same though: It is desired that a more complicated gate could be realized in a single shot without evoking elementary gates. Josephson charge qubits are discussed in detail for instance in Refs. [25,67] and Publication V. For an introduction to Cooper pair tunneling and superconducting circuits see e.g. Refs. [68–70].

Physical model

Consider the Josephson junction circuit shown in Fig. 2. In Fig. 2(a) an individual Cooper pair box is shown. It consists of a small metallic superconducting island (typically aluminum cooled to some 20–50 mK) having sub-micron dimensions coupled to a superconducting lead through a SQUID loop. The SQUID loop consists of Josephson junctions that are, e.g., formed by an oxide layer between superconducting metallic films. Cooper pairs may not be found inside the layer but they can have a finite possibility for tunneling through, provided that the oxide is sufficiently thin and the area of the junction sufficiently large. The state of a Josephson junction may be described by the superconducting phase difference ϕ over it which is just the time-integral of voltage times

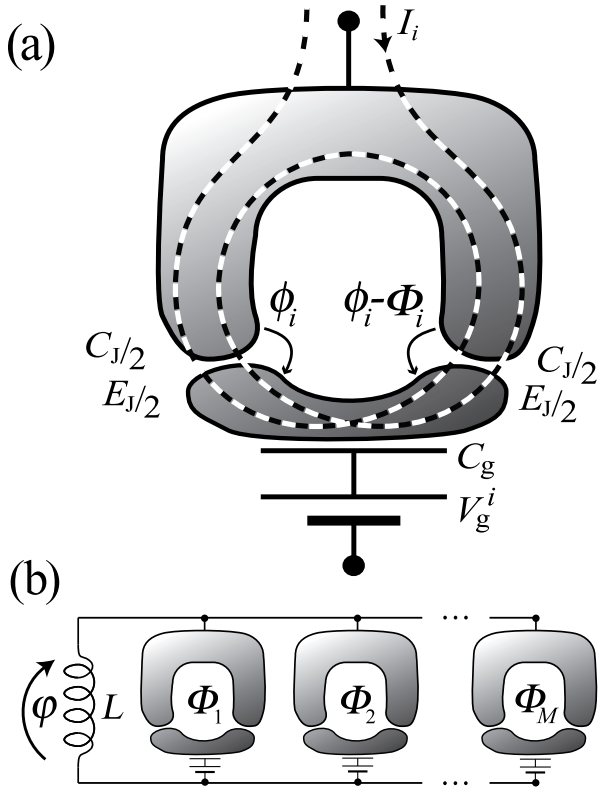

Figure 2. (a) Single Cooper pair box coupled to the environment through a SQUID. (b) Array of Josephson charge qubits coupled inductively.

$2e/\hbar$. The potential energy stored in the junction is $-E_{\rm J}\cos\phi$, where $E_{\rm J}$ is the so-called Josephson energy. Classically, the current flowing through a "large" Josephson junction is $I_{\rm c}\sin\phi$ where I_c is called the critical current and ϕ obeys $\dot{\phi} = 2eV/\hbar$, where V is the voltage. The critical current is related to the Josephson energy via $I_{\rm c} = (2e/\hbar)E_{\rm J}$. SQUIDs are used as tunable Josephson junctions. In the case of identical junctions the Josephson energy term is $-E_{\rm J}\cos(\pi\Phi/\Phi_0)\cos(\phi)$, where $E_{\rm J}/2$ is the Josephson energy of an individual junction, $\Phi_0 = h/2e$ is the flux quantum and Φ is the externally applied flux through the SQUID loop. The normal-state tunneling resistance $R_{\rm T}$ yields the value of $E_{\rm J}$ through the Ambegaokar-Baratoff formula [71] $E_{\rm J} = h\Delta_{\rm BCS}/8e^2R_{\rm T}$, where $\Delta_{\rm BCS}$ is the superconducting gap at zero temperature. A Josephson junction has also a parallel-plate capacitance ($C_{\rm J}/2$ in this case) associated with it, which is typically on the order of fF. The superconducting island is further coupled to a gate voltage $V_{\rm g}$ through a gate capacitance $C_{\rm g}$. These capacitances give rise to a typical charging energy for Cooper pairs $E_{\rm C} = 2e^2/C_\Sigma$, where $C_\Sigma = C_{\rm J} + C_{\rm g}$ is the total capacitance of the island. This charging energy is assumed to be so large that the addition of a single Cooper pair to the island requires more energy than the thermal motion of the environment, roughly speaking, may provide. For charge qubits, we also require that $E_{\rm J} < E_{\rm C}$.

An individual qubit may be manipulated both through the magnetic flux Φ and the gate voltage $V_{\rm g}$. The logical states of the qubit correspond to zero and one extra Cooper pair residing on the island, denoted by $|0\rangle$ and $|1\rangle$ respectively. Since changing the polarization of the island does not induce any tunneling amplitude but, in contrast, changes the relative energy of different charge configurations, the diagonal part of the

two-by-two Hamiltonian for the qubit is controlled through $V_{\rm g}$. However, since the superconducting phase on the island is conjugate to the number of Cooper pairs on the island, it follows that $\cos(\phi)$ gives rise to tunneling and thus the magnetic flux controls the off-diagonal part of the Hamiltonian. Furthermore, Fig. 2(b) illustrates a potential coupling scheme for the charge qubits in which the boxes are fabricated in parallel with an inductance L, possibly realized in practice using a large Josephson junction. The inductor along with the total capacitance of the array of qubits serves as an LC-oscillator whose presence effectively couples the qubits assuming that the frequency of oscillation is much higher than the relevant frequencies of the individual qubits. We may write the Hamiltonian for M qubits (see Paper V and Ref. [25]) as

$$\mathcal{H}_{\rm qb} = \sum_{i=1}^{M} \left[-\frac{B_z^i}{2}\sigma_z^i - \frac{B_x^i}{2}\sigma_x^i \right] - D \sum_{i=1}^{M} \sum_{j=i+1}^{M} B_x^i B_x^j \sigma_y^i \otimes \sigma_y^j \ , \tag{30}$$

where $B_z^i = E_{\rm C}(1-2n_{\rm g}^i)$, $B_x^i = E_{\rm J}(\Phi_i)$ and $D = L(\pi C_{\rm qb}/C_{\rm J}\Phi_0)^2$. We have further denoted $C_{\rm qb} = C_{\rm J}C_{\rm g}/(C_{\rm J}+C_{\rm g})$. The index i refers to the i^{th} qubit. Above $E_{\rm J}(\Phi_i) = E_{\rm J}\cos(\pi\Phi_i/\Phi_0)$ is the effective Josephson energy and $n_{\rm g}^i = C_{\rm g}V_{\rm g}^i$ is the gate charge. It is worthwhile to note that this Hamiltonian is only valid near $n_{\rm g} = 0.5$, i.e. one of the degeneracy points and if $E_{\rm J} \ll E_{\rm C}$. A particularly convenient property of Eq. (30) is that the entire Hamiltonian may be set equal to zero, thereby stopping all temporal evolution. Note that if any two qubits have a non-vanishing tunneling amplitude, they will be automatically coupled. It is easy to construct any single-qubit gate within this model on qubit j by setting $B_x^i = B_z^i = 0$ for $i \neq j$ and by manipulating B_x^j and B_z^j, see Paper V. Using arbitrary one-qubit operations along with almost any nontrivial two-qubit gate [46] one may construct any multiqubit operation. This would not, however, by any means lead to an optimal implementation.

Optimization

In Publication III, the general problem of finding multiqubit gates for the present Hamiltonian is considered. The concept is further developed in Publication IV where particular attention is paid to accelerating algorithms using three-qubit gates. Paper V considers, as an example, the execution of Shor's algorithm on Josephson charge qubits using the optimization method. Just like within HQC, it is possible to associate a loop in the parameter space with every unitary operation. The parameter vector for a k-qubit operation now assumes the form

$$\mathbf{q}(t) = \left[B_z^1(t) \ldots \quad B_z^k(t) \quad B_x^1(t) \quad \ldots \quad B_x^k(t) \right]^T . \tag{31}$$

We may take the origin, where $\mathcal{H}_{\rm qb} = 0$, as the starting point for all quantum-control operations. Then, exactly like in the case of HQC, we may assume that the operations are polygons in the parameter space. Only now the natural parameterization for loops is given by time, and also the speed at which the loops are traversed of course matters. However, we may fix the duration of each edge of the polygon and thus a polygon for k qubits and with $l+1$ vertices has $2l \times k$ degrees of freedom. It is reasonable to require

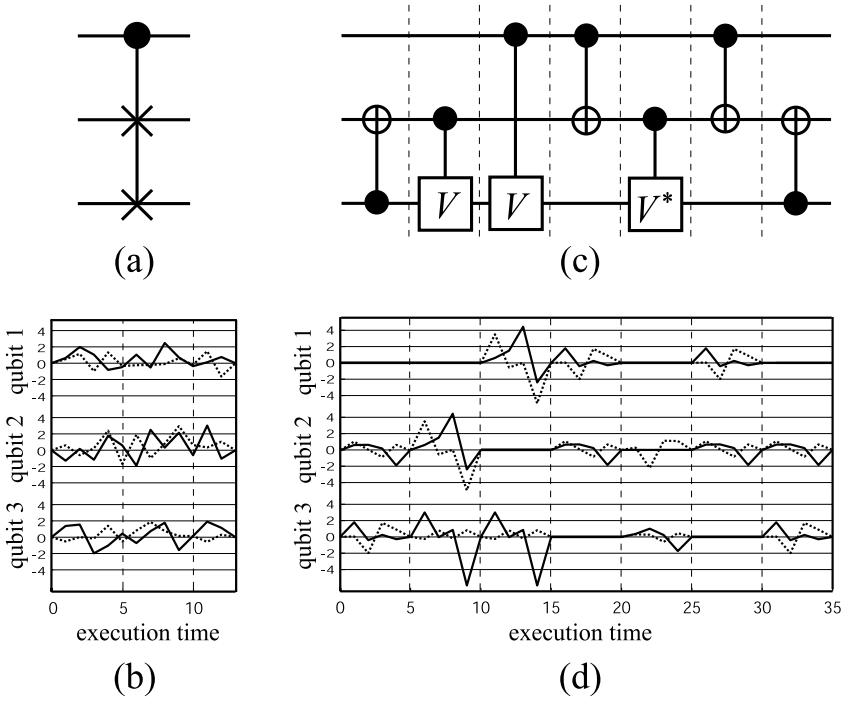

Figure 3. Illustration of the strength of the method in the case of the Fredkin gate. In (a) and (c), the quantum-circuit notation (see text) for the single-shot and decomposed Fredkin gate is shown. Subfigures (b) and (d) show the corresponding parameter pulses. The solid line represents B_z^i while the dashed line represents B_x^i. The resulting direct three-qubit implementation is in this case almost three times faster.

that $2lk \geq 2^{2k} - 1$ in order to achieve[1] the whole $SU(2^k)$. The gates are again found by minimizing $f(\gamma)$ but now the evaluation of U_γ is carried out by discretizing the loop γ into a finite set of points $\gamma_1, \ldots, \gamma_n$ (typically $n = 10^2$–10^4) in the $2k$-dimensional space and since the total time is fixed, we also can fix the time difference Δt between the points and write

$$U_\gamma \approx \exp(-i\mathcal{H}_{\rm qb}(\gamma_n)\Delta t) \ldots \exp(-i\mathcal{H}_{\rm qb}(\gamma_1)\Delta t). \tag{32}$$

It is easy to see from the above expression that one can readily divide the evaluation of the unitary operation into smaller sections of the full loop γ and delegate each subtask to a separate processor. Thus the evaluation of U_γ is almost trivially parallelized, which allows for very efficient optimization. In the case of three-qubit gates, 13 processors were used such that one processor was the master taking care of the optimization routine and the multiplication of the intermediate results was handled by the slaves consisting of the 12 other processors. The length of each linear edge is fixed to one unit and also $D = 1$ as well as $\hbar = 1$. The three-qubit gates require 12 edges and the two-qubit gates call for 5 edges. The results are applicable independent of the sample parameters since rescaling D is possible by simultaneously scaling energy and time.

Figure 3 (Fig. 2 of Paper IV) contains an illustration of the strength of the present

[1]We cannot achieve $U(2^k)$ with the present Hamiltonian since it has been chosen to be traceless, but the global phase is meaningless.

scenario; instead of using the two-qubit gate decomposition of Fig. 3(c) and Fig. 3(d), in which the realization of individual gates has already been optimized, one may search for a minimum of $f(\gamma)$ directly for the whole so-called three-qubit Toffoli gate (see e.g. Ref. [2]). In Fig. 3 as well as in Publications III–V the so-called quantum-circuit notation is used. In this notation, time runs from the left to the right and the horizontal lines represent the history of actions on a particular qubit. In Fig. 3, the qubits are labeled 1, 2 and 3 from top to bottom. A black circle is used to indicate a controlled operation. In Fig. 3(a), for instance, the notation means that a SWAP (denoted by two crosses) is performed between the quantum states of qubits 2 and 3 if the state of the qubit 1 is $|1\rangle$. Otherwise nothing is done. This is in fact the definition of the Toffoli gate. In Fig. 3(c), on the other hand, a sequence of seven operations performing the Toffoli gate in seven substeps is illustrated. The first (leftmost) operation is a controlled-NOT (CNOT) which flips the qubit 2 iff the qubit 3 is $|1\rangle$. The controlled-V operation means that the operation $V = \sqrt{\sigma_x}$ is carried out iff the control qubit is $|1\rangle$. Furthermore, the star in Fig. 3(c) stands for a Hermitean conjugate. A matrix representation can of course be used for any gates provided that an ordering of the subsystems, i.e. the vector presentation, has been fixed, but the quantum circuit notation is in many ways much more informative. For more on this notation see e.g. Ref. [2].

It should be clear from Fig. 3 why the direct implementation is superior. Instead of allowing one qubit to be idle (parameters B_x^i and B_z^i set to zero) we can operate on all the three qubits simultaneously. The resulting single-shot pulse sequence is almost three times faster than the decomposed version. More examples of optimized gates may be found in Publications III–V.

Alternative: Optimal control theory

It is also possible to apply tools from optimal control theory (OCT) in the design of control pulses for Josephson qubits. Figure 4 illustrates a control pulse for the three-qubit Fourier transform that was calculated using an algorithm complementary to ours described recently in Refs. [72, 73] along with a pulse obtained using our method. This method is somewhat different from the method presented in this Thesis and relies on the use of variational calculus. Both methods, OCT and the polytope search, scale exponentially with the number of qubits. Both methods can be parallelized too. The OCT algorithm, however, yields a smooth control pulse, but it would also be possible to use smooth pulses with our method as well. Then the node degrees of freedom would be replaced, for instance, by the coefficients of some basis functions. In both OCT and our approach it is possible to take into account the limitations of a particular experimental situation and design the control pulses accordingly. Thus, the piecewise linear pulses presented in this Thesis should be considered merely as examples. Nevertheless, the philosophy of our method and the OCT in the context of quantum computing is the same; in both cases the use of elementary gates can be avoided and the execution time and errors decreased. Comparing the relative superiority of our method and OCT would call for a separate study and the results would probably depend strongly on the exact form of the Hamiltonian.

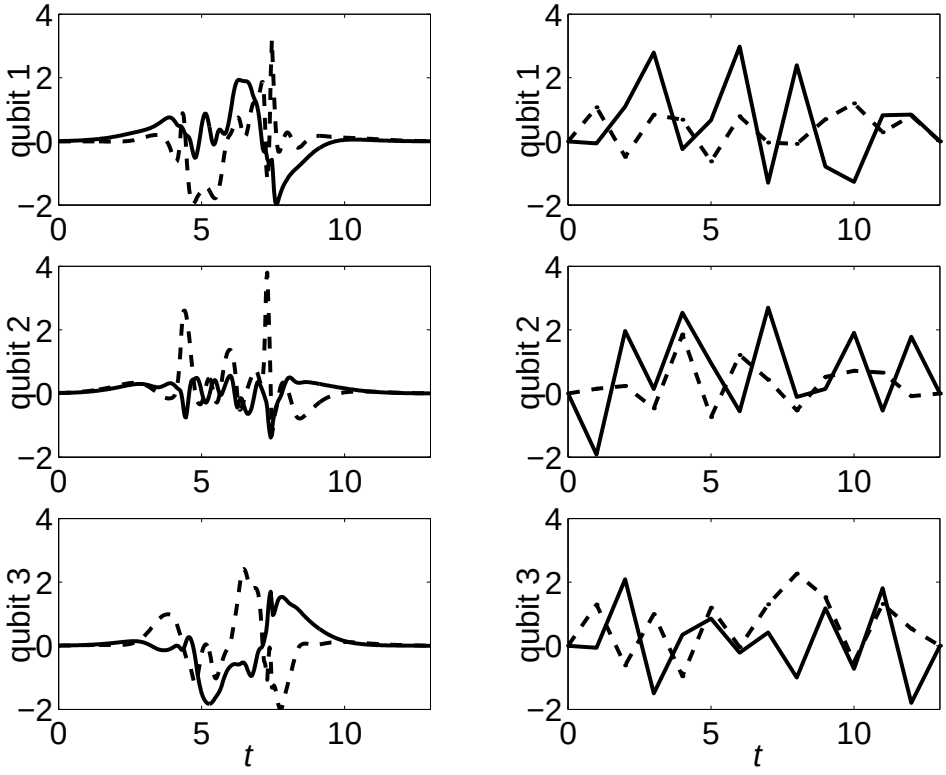

Figure 4. (left) An optimal control theory realization of the quantum Fourier transform for three qubits. The dashed line indicates B_x^i and the solid line represents B_z^i. (right) Piecewise linear realization of the QFT from Paper III.

Example: Factoring 21

Publication V discusses the feasibility of factoring the number 21 using the numerical optimization method developed here using inductively coupled Josephson qubits. The number 21 is arguably the smallest nontrivial number[2] to be factored using Shor's algorithm. Figure 5 of this Paper illustrates the full quantum circuit for the quantum part of the algorithm. As many as 5900 two-qubit gates and 2300 three-qubit gates are involved in the implementation. If only (arbitrary) two-qubit qubit gates were available, then some 16 400 of them would be required. The number of elementary gates would be necessarily orders of magnitude higher, depending on the exact set available. However, in any realistic scenario the use of a limited set of elementary gates is not viable; every measure of cutting down the execution time of the quantum part of the algorithm needs to be taken. Thus even very heavy classical preoptimization is justifiable. Nevertheless, for a superconducting Al sample the runtime of the algorithm would at best be 10^{-6} s. This coincides with the best experimental estimates for the coherence time of a superconducting system [22], though for only a single qubit at a special point. The use of arbitrary two-qubit gates instead of three-qubit gates would increase the runtime by some 40%. The number of required qubits would be 22 with two independent controls per qubit. Clearly this kind of an experiment with the requirement that the tempera-

[2]The first obvious choice would be 15 but in this case the classical preprocessing happens to reveal the answer, see Publication V. Of course $21 = 3 \times 7$, but this is not a triviality of the same kind.

ture of the environment be around tens of mK is not easy and would probably require dedicated low-temperature control circuitry, such as rapid single flux quantum (RSFQ) logic [74,75]. Otherwise at least 44 RF-lines and very complicated pulse generators would be mandatory. Despite the difficulties, factoring 21 on superconducting qubits should be possible with very careful design.

Using a scaling argument we may also comment on the factoring of numbers large enough to break the RSA cryptosystem in the absence of any active coherence preservation method, such as error correction [2, 76]. For instance, breaking the 512-bit RSA would require thousands of qubits and since the runtime scales at best as $n^3 \log n$, where n is the number of bits it takes to represent the number to be factored, we can argue based on the estimates given above that tens of seconds of decoherence time is necessary. The number of independent high-frequency controls would be thousands. Clearly a scalable implementation of a superconducting quantum computer is extremely challenging and far in the future. However, many applications rely on very similar ideas and these are quite reachable even today. One such application is considered in the next Section.

4 Cooper Pair Pumping

In this Section we consider an application of Berry's [31] Abelian geometrical phase to Cooper pair pumping using mesoscopic Josephson junctions. Particular attention is paid to the so-called Cooper pair "sluice" introduced in Paper VI. The idea of operation and the techniques used are very similar to the control of Josephson charge qubits. Actually, a Cooper pair "sluice" in a proper environment could serve as a qubit, since the Hamiltonian presented below offers more than enough possibilities for control. Mastering the flux and voltage control of only a few superconducting qubits, which is being pursued by many groups worldwide, does not necessarily have immediate practical impact in the field of quantum computing. However, spin-offs such the "sluice" may find uses, e.g., in metrology. Some differences between Cooper pair pumping and superconducting qubits exist, though. For instance, superpositions of energetically different states are not pursued and the basic control pulse (pumping cycle) is applied repetitively in contrast to single-shot quantum gates.

As to charge pumps in general, a seven-junction single-electron pump [30] with currents on the order of pA has been demonstrated to be usable as a capacitance standard [77], but the realization of the so-called quantum metrological triangle [78] would require currents on the order of nA. This is beyond single-electron pumps, but Cooper pair pumps could potentially yield currents accurately in the nA range. The use of Surface Acoustic Waves (SAW) to pump electrons is being studied actively as an alternative to ordinary electron pumps, see e.g. Ref. [79]. The engineering of the electromagnetic environment of both electron pumps [80] as well as Cooper pair devices [81] using on-chip resistors has been considered in order to achieve a frequency-locked current source. No metrological Cooper pair pump has been realized yet.

The considered form of the temporal control is not found numerically but rather using analytic physical arguments. In Subsection 4.1, the relationship between Cooper pair pumping and Berry's phase is discussed. Subsection 4.2 discusses the theory of the "sluice". Subsection 4.3, based on the experiments of Publication VII, is the highlight of the present Section.

4.1 Adiabatic Cooper pair pumping and Berry's phase

An adiabatic Cooper pair pump is a chain of Josephson junctions with at least two tunable parameters. For instance the first measured pump of Geerligs et al. [26] had three Josephson junctions in a chain and two voltage gates coupled to the islands in between. A similar structure was also recently measured by Toppari et al. [82]. However, longer chains, including the seven-junction Cooper pair pump of Aumentado et al. [83], have been studied as well. The requirement that at least two parameters are needed is due to the fact that the pumping effect is attributable to a loop in the parameter space. We will make the connection between the pumped charge and Berry's phase clear in simple terms. For a more formal derivation see Ref. [84].

The Cooper pair pump shown in Fig. 5 serves as a generic model that encompasses both the traditional gate-controlled pumps and the flux-assisted pump studied here. For

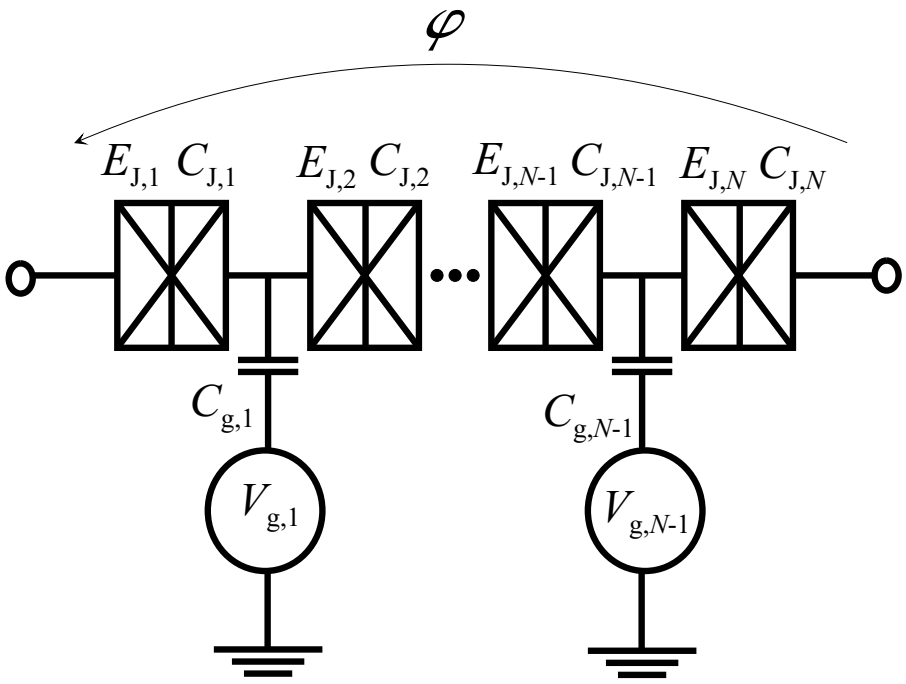

Figure 5. Generic model of a Cooper pair pump.

now, the device is assumed to be phase biased such that the superconducting phase difference over the device is φ. The average current operator for a chain of Josephson junctions is given by

$$\mathcal{I} = \frac{2e}{\hbar}\frac{\partial \mathcal{H}_{\mathrm{pump}}}{\partial \varphi}. \tag{33}$$

Assuming, for simplicity, that $C_{\mathrm{J},j} = C_{\mathrm{J}}$ for all j and that $C_{\mathrm{g},j}/C_{\mathrm{J}} \ll 1$ allows us to write the Hamiltonian for an N-junction pump in the absence of quasiparticles as

$$\begin{aligned}\mathcal{H}_{\mathrm{pump}} = \frac{1}{2}(\hat{\mathbf{n}} - \mathbf{n}_{\mathrm{g}})^{\mathrm{T}}\mathbb{C}^{-1}(\hat{\mathbf{n}} - \mathbf{n}_{\mathrm{g}}) - \sum_{k=2}^{N-1} E_{\mathrm{J},k}\cos(\phi_{k-1} - \phi_k + \varphi/N) \\ - E_{\mathrm{J},1}\cos(\varphi/N - \phi_1) - E_{\mathrm{J},N}\cos(\varphi/N + \phi_{N-1}).\end{aligned} \tag{34}$$

Here $E_{\mathrm{J},k}$ is the Josephson energy of the k^{th} junction and ϕ_k is the superconducting phase on the k^{th} island whereas $\mathbb{C}$ is the three-band capacitance matrix of the junction chain given by

$$\mathbb{C} = \begin{pmatrix} C_{\mathrm{g},1} + 2C_{\mathrm{J}} & -C_{\mathrm{J}} & & \\ -C_{\mathrm{J}} & C_{\mathrm{g}} + 2C_{\mathrm{J}} & -C_{\mathrm{J}} & \\ & \ddots & \ddots & \\ & & -C_{\mathrm{J}} & C_{\mathrm{g},N-1} + 2C_{\mathrm{J}} \end{pmatrix}. \tag{35}$$

Allowing the Josephson energies to be different for each junction, even though the capacitances are equal, anticipates the developments of the next Subsection. The number operators of Cooper pairs $\hat{n}_k$ of each of the islands and the gate charges $n_{\mathrm{g},k} = C_{\mathrm{g},k}V_{\mathrm{g},k}$

are contained in $\hat{\mathbf{n}}$ and $\mathbf{n}_{\mathrm{g}}$, that is

$$\hat{\mathbf{n}} = \begin{pmatrix} \hat{n}_1 \\ \vdots \\ \hat{n}_N \end{pmatrix} \qquad \text{and} \qquad \mathbf{n}_{\mathrm{g}} = \begin{pmatrix} n_{\mathrm{g},1} \\ \vdots \\ n_{\mathrm{g},N} \end{pmatrix}. \tag{36}$$

Now let us assume that the parameters of the system denoted collectively by $\mathbf{q}(t)$ are tuned adiabatically around a cycle γ in the parameter space over the time $t \in [0, t_{\mathrm{cycle}}]$ and that the ground state is non-degenerate. What the parameters are is not important for the derivation. Clearly, the total charge that passes through the device is

$$Q_{\mathrm{tot}} = \int_0^{t_{\mathrm{cycle}}} \langle \psi(t)|\mathcal{I}|\psi(t)\rangle dt, \tag{37}$$

where $|\psi(t)\rangle$ is the state vector of the pump at the time t. Using Eq. (9) of Section 2 with $g = 1$ as well as Eq. (11) allows us to write the state of the pump at time t as

$$|\psi(t)\rangle = e^{i\theta(t)}|0;\mathbf{q}(t)\rangle \tag{38}$$

due to the adiabaticity assumption. Here $|0;\mathbf{q}\rangle$ is the ground-state vector which depends on the control-parameter vector $\mathbf{q}$. The phase $\theta(t)$ has two contributions, namely the dynamical phase

$$\theta_{\mathrm{dyn}}(t) = -\frac{1}{\hbar}\int_0^t \langle 0;\mathbf{q}(\tau)|\mathcal{H}_{\mathrm{pump}}|0;\mathbf{q}(\tau)\rangle d\tau \tag{39}$$

and the geometrical phase

$$\theta_{\mathrm{geom}}(t) = i\int_0^t \langle 0;\mathbf{q}(\tau)|\frac{d}{d\tau}|0;\mathbf{q}(\tau)\rangle d\tau = i\int_{\mathbf{q}(0)}^{\mathbf{q}(t)} \langle 0;\mathbf{q}|\nabla_{\mathbf{q}}|0;\mathbf{q}\rangle \cdot d\mathbf{q}. \tag{40}$$

At time t_{cycle} it holds in particular that

$$\theta_{\mathrm{Berry}} \equiv \theta_{\mathrm{geom}}(t_{\mathrm{cycle}}) = i\oint_\gamma \langle 0;\mathbf{q}|\nabla_{\mathbf{q}}|0;\mathbf{q}\rangle \cdot d\mathbf{q} \tag{41}$$

since at this instant the cycle is full. Now, it is possible to rewrite the integrand in Eq. (37) as

$$\langle \psi(t)|\mathcal{I}|\psi(t)\rangle = \langle \psi(t)|\frac{2e}{\hbar}\frac{\partial \mathcal{H}_{\mathrm{pump}}}{\partial \varphi}|\psi(t)\rangle = \frac{2e}{\hbar}\langle \psi(t)|\left[\frac{\partial}{\partial \varphi}, \mathcal{H}_{\mathrm{pump}}\right]|\psi(t)\rangle. \tag{42}$$

Owing to the Schrödinger equation, we may further write

$$\langle \psi(t)|\mathcal{I}|\psi(t)\rangle = 2ei\frac{d}{dt}\left(\langle \psi(t)|\frac{\partial}{\partial \varphi}|\psi(t)\rangle\right). \tag{43}$$

On the other hand

$$\begin{aligned} \langle \psi(t)|\frac{\partial}{\partial \varphi}|\psi(t)\rangle &= \langle 0;\mathbf{q}(t)|e^{-i\theta(t)}\frac{\partial}{\partial \varphi}e^{i\theta(t)}|0;\mathbf{q}(t)\rangle \\ &= i\frac{\partial \theta(t)}{\partial \varphi}\langle 0;\mathbf{q}(t)|0;\mathbf{q}(t)\rangle + \langle 0;\mathbf{q}(t)|\frac{\partial}{\partial \varphi}|0;\mathbf{q}(t)\rangle \\ &= i\frac{\partial \theta(t)}{\partial \varphi} + \langle 0;\mathbf{q}(t)|\frac{\partial}{\partial \varphi}|0;\mathbf{q}(t)\rangle. \end{aligned} \tag{44}$$

The pumped charge is thus (use $\mathbf{q}(0) = \mathbf{q}(t_{\rm cycle})$ and $\theta(0) = 0$)

$$Q_{\rm tot} = -2e \int_0^{t_{\rm cycle}} \frac{d}{dt}\left(\frac{\partial\theta(t)}{\partial\varphi}\right) dt + \underbrace{\int_0^{t_{\rm cycle}} 2ei\frac{d}{dt}\langle 0;\mathbf{q}(t)|\frac{\partial}{\partial\varphi}|0;\mathbf{q}(t)\rangle dt}_{=0}$$
$$= -2e\frac{\partial}{\partial\varphi}\left(\theta_{\rm dyn}(t_{\rm cycle}) + \theta_{\rm Berry}\right). \tag{45}$$

The total charge transferred is $-2e$ times the derivative of the phase accumulated over one cycle with respect to the global superconducting phase difference. The first part, or the dynamical contribution is

$$Q_{\rm s} = -2e\frac{\partial}{\partial\varphi}\left(\theta_{\rm dyn}(t_{\rm cycle})\right) = \frac{2e}{\hbar}\frac{\partial}{\partial\varphi}\int_0^{t_{\rm cycle}} \langle 0;\mathbf{q}(t)|\mathcal{H}_{\rm pump}|0;\mathbf{q}(t)\rangle dt$$
$$= \int_0^{t_{\rm cycle}} \langle 0;\mathbf{q}(t)|\mathcal{I}|0;\mathbf{q}(t)\rangle dt \tag{46}$$

which is just the "classical" Josephson supercurrent. In pumping applications one tries to suppress the supercurrent altogether. The second contribution is the more nontrivial pumped charge

$$Q_{\rm p} = -2e\frac{\partial}{\partial\varphi}\left(\theta_{\rm Berry}\right) = -2e\frac{\partial}{\partial\varphi}\oint_\gamma i\langle 0;\mathbf{q}(t)|\nabla_{\mathbf{q}}|0;\mathbf{q}(t)\rangle\cdot d\mathbf{q} \tag{47}$$

and as may be seen, this is in close connection with Berry's phase. Thus pumping Cooper pairs may, very naturally, be seen as an observable manifestation of Berry's phase. It is remarkable that Berry's phase of a nondegenerate ground state has observable consequences while for instance in quantum computing either degeneracy (holonomy) or superpositions of energetically different states are required for observable consequences. In quantum computing the loop γ applies a logical operation whereas here it pumps charge.

It is possible to derive from Eq. (47) a more elaborate expression for the pumped charge appearing often in literature. We may write

$$Q_{\rm p} = 2\hbar\,{\rm Im}\left[\sum_{m=1}^{\infty}\oint_\gamma \frac{\langle 0;\mathbf{q}|\mathcal{I}|m;\mathbf{q}\rangle}{\varepsilon_{\mathbf{q},0} - \varepsilon_{\mathbf{q},m}}\langle m;\mathbf{q}|\nabla_{\mathbf{q}}|0;\mathbf{q}\rangle\cdot d\mathbf{q}\right], \tag{48}$$

where $|m;\mathbf{q}\rangle$ is the $m^{\rm th}$ energy eigenstate and $\varepsilon_{\mathbf{q},m}$ is its energy. This is the form found first in Ref. [27] and the equivalence between Eq. (48) and Eq. (47) is demonstrated in Ref. [84].

4.2 Cooper pair "sluice"

The expressions derived above for the pumped charge are quite general and the exact nature of the tunable parameters has not yet been specified. Traditionally, charge pumping through a chain of Josephson junctions is achieved via cyclically manipulating gate voltages in such a manner that the state of the system propagates adiabatically through

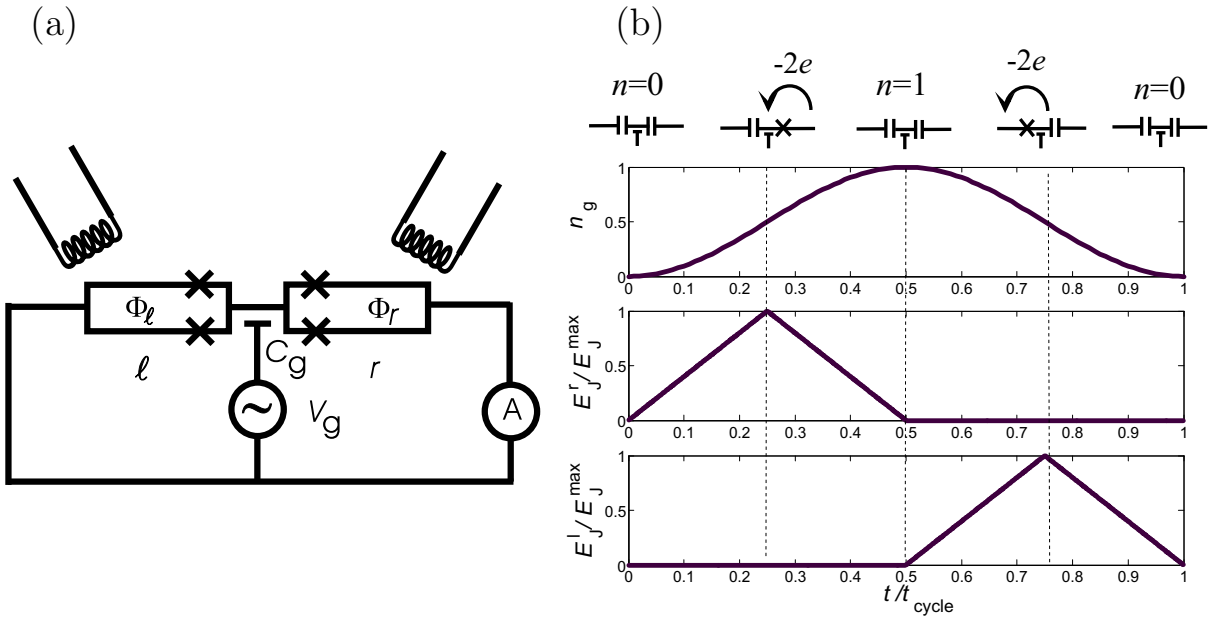

Figure 6. (a) Schematic of the Cooper pair "sluice". (b) Pulse sequence for pumping a single Cooper pair through the sluice. The exact form of the pulses is not crucial as long as synchronization is maintained.

a series of near-eigenstates of charge. For instance, in the three-junction Cooper pair pump [26, 27, 82] one may denote by (Q_1, Q_2) the eigenstate of charge with Q_1 residing on island 1 and Q_2 residing on island 2. Then the gate voltages are manipulated adiabatically such that the cycle $(Q_1, Q_2) : (0, 0) \to (0, 2e) \to (2e, 0) \to (0, 0)$ is almost achieved. However, due to the non-vanishing Josephson coupling, the eigenstate of energy is not an eigenstate of charge. It is impossible to decrease the Josephson energies of the junctions indefinitely without sacrificing the adiabaticity since the smallest excitation energy is proportional to E_J. Stated otherwise, there is a tradeoff between accuracy and adiabaticity. From the point of view of adiabaticity it would be beneficial to increase E_J indefinitely, but in the adiabatic limit there is an error in the pumped charge proportional to E_J such that it would be desirable to make E_J small. These two seemingly contradicting requirements are the reason for considering tunable Josephson junctions, i.e. SQUIDs.

The Cooper pair sluice is a single-island Cooper pair pump. It was introduced and analyzed theoretically in Publication VI. A single island and a single gate voltage are sufficient due to the fact that also the couplings are controlled. A schematic of the device is shown in Fig. 6(a). The Hamiltonian of a homogeneous Cooper pair sluice is explicitly

$$\begin{aligned}\mathcal{H}_\mathrm{sluice} =& E_\mathrm{C}(\hat{n} - n_\mathrm{g})^2 - E_\mathrm{J}^\mathrm{r}\left(\pi\frac{\Phi_\mathrm{r}}{\Phi_0}\right)\cos(\phi + \varphi/2) \\ & - E_\mathrm{J}^\mathrm{l}\left(\pi\frac{\Phi_\mathrm{l}}{\Phi_0}\right)\cos(\varphi/2 - \phi). \end{aligned} \tag{49}$$

Here ϕ is the phase on the island and $\hat{n}$ is the number operator for Cooper pairs. They obey the commutation relation $[\hat{n}, \phi] = i$. The charging energy is given by

$E_{\rm C} = 2e^2/(2C_{\rm J} + C_{\rm g})$ and the gate charge is $n_{\rm g} = C_{\rm g}V_{\rm g}/2e$. Furthermore, $E_{\rm J}^{\rm l}$ and $E_{\rm J}^{\rm r}$ are the effective Josephson energies of the left and right SQUIDs, respectively, which we assume may in principle be set to zero. The flux through the left (right) junction is denoted by $\Phi_{\rm l}$ ($\Phi_{\rm r}$). The parameter vector $\mathbf{q}$ for the present device is given by $\mathbf{q} = (n_{\rm g}, E_{\rm J}^{\rm r}, E_{\rm J}^{\rm l})^{\rm T}$. The pumping of charge is achieved via manipulating the parameters $\mathbf{q}$ adiabatically such that at certain instants the ground state is ideally also exactly an eigenstate of charge. This may be achieved by setting the Josephson couplings to zero. A typical pumping cycle is shown in Fig. 6(b).

For instance, we may assume that initially the ground state is an eigenstate with zero Cooper pairs which we attain e.g. with $E_{\rm J}^{\rm l} = 0$, $E_{\rm J}^{\rm r} = 0$ and $n_{\rm g} = 0$. Then keeping $E_{\rm J}^{\rm r} = 0$ and tuning $n_{\rm g}$ from zero to one and simultaneously opening the left SQUID (first vertical dashed line in Fig. 6(b)) and closing it again (second dashed line) adiabatically increases the number of Cooper pairs on the island by one. Namely, the ground state is after the manipulation still an eigenstate of charge but with one more pair and we have assumed that the system stays at its ground state. The extra Cooper pair must have tunneled through the left SQUID since the right one was closed altogether. Ramping $n_{\rm g}$ from one again back to zero while simultaneously opening (third dashed line) and closing the right SQUID clearly takes us to where we began: The island again has zero Cooper pairs. This time the charge must have flown through the left SQUID. In conclusion, this cycle leads to a pumping of exactly one Cooper pair through the device. Repeating the cycle at the frequency f leads to a DC current $I = 2ef$. Note that the above logic immediately generalizes to the pumping of m Cooper pairs by working between $n_{\rm g} = 0$ and $n_{\rm g} = m$ yielding $I = 2emf$. The crucial assumption is that the temporal evolution is adiabatic. It is worth pointing out explicitly that the above cycle maintains the non-degeneracy of the ground state such that the system indeed is protected against excitations to higher levels.

The imperfections of the sluice have been analyzed in Publication VI. To this end, the sluice was simulated using numerical integration of the Schrödinger equation. This was carried out using the loop shown in Fig. 6(b) as a basis for the time dependence of the Hamiltonian $\mathcal{H}_{\rm sluice}$. Then, just like in the case of quantum algorithms, the time axis was split to a discrete set of points (10^6 or more) that were a distance Δt apart and the Hamiltonian was considered piecewise constant in time. The Hilbert space was truncated to some 10–30 charge states depending on the value of m considered. The state vectors were propagated using

$$|\psi(t + \Delta t)\rangle \approx \exp(-i\mathcal{H}_{\rm sluice}(t + \Delta t/2)\Delta t/\hbar)|\psi(t)\rangle. \tag{50}$$

The quantity of interest, $Q_{\rm P}$ in Eq. (37) was evaluated simply using the trapezoidal rule. Note that the current operator also has a time dependence. The discretization was made fine enough such that increasing the number of points did not change the result.

It was found that the pumping of individual Cooper pairs with an accuracy of 10^{-7} should be possible at currents of some 10 pA. However, increasing m to $m = 10$, would allow pumping of 0.1 nA with the same accuracy. These estimates only take into account the finite operating frequency. The optimal value of m is not known. It was

also found that with sufficient phase averaging errors should not increase. Namely, the leakage supercurrent is proportional to $\sin\varphi$ while the error in the pumped charge $Q_{\rm P}$ is proportional to $\cos\varphi$. The average of both of these under a perfect voltage bias V is clearly zero since then $\varphi = 2eVt/\hbar$.

4.3 Experiments on the "sluice"

Paper VII describes the experiments demonstrating the pumping of Cooper pairs utilizing the idea described above. Figure 7 shows scanning electron micrographs (SEM) of the measured sample as well as a schematic of the measurement setup. The sample was fabricated using standard e-beam lithography and two-angle shadow evaporation. The steps of the fabrication process included spinning a two-layer PMMA/MAA (polymethyl methacrylate/methacrylic acid) and PMMA resist on top of a silicon wafer, drawing the pattern of the device using an electron beam, developing the resist in two different solvents (first in a mixture of 25% MIBK (methyl isobutyl ketone) and 75% IPA (isopropanol) and then in pure IPA) to get an "undercut" and finally evaporating aluminum from two different angles in vacuum with an oxidization step between the layers. The Josephson junctions are thus realized as an Al-AlO_x-Al sandwich. The thicknesses of the Al layers were 30 nm and 50 nm while the thickness of the oxide is a few nm. The extra aluminum was removed in the lift-off done by dipping the chip in acetone. The two different layers can be seen as "shadows" in Fig. 7(b). The sample was then attached to the sample holder of a He^3- He^4 dilution cryostat with a base temperature of 20 mK and electrically connected using Al wire bonds. The two ends of the device were bonded to DC lines in a four-point configuration as shown in Fig. 7(c) while the two input coils and the gate were connected to RF lines with bandwidth up to tens of GHz. The measurement electronics along with the arbitrary waveform generators used for realizing the flux and voltage control were connected to a PC. `Matlab` scripts and `Matlab`'s `Data Acquisition Toolbox` were used to carry out the measurement.

The sample parameters were $C_{\rm g} \approx 0.2$ fF, $E_C/k_{\rm B} \approx 1$ K and $E_{\rm J}/k_{\rm B} \approx 0.5$ K. The estimate of the gate capacitance is based on gate periodicity measurements, that of the charging energy on the measurement of the normal-state conductance at 4.2 K [85] while the estimate of $E_{\rm J}$ is based on the normal-state resistance and the Ambegaokar-Baratoff formula [71], i.e., $E_{\rm J} = h\Delta_{\rm BCS}/8e^2R_{\rm T}$. For the arrangement of the flux pulsing it is important to know the mutual inductances between the input coils and the SQUIDs. The SQUIDs were intentionally designed to have large extensions to get better coupling. The mutual inductances were measured by sweeping the DC current in the two input coils at constant bias voltage and by measuring the current. This allows one to design the flux pulses with proper compensations for the cross-talk, see Publication VII. The relative phases were optimized by sweeping them and maximizing the current. Since we were using commercial waveform generators, we were forced to use frequencies on the order of a few MHz. Luckily, though, we could compensate for the low frequency by increasing the number of pumped charges m, i.e. the gate amplitude.

The measurement of the full current-voltage characteristics was carried out with the

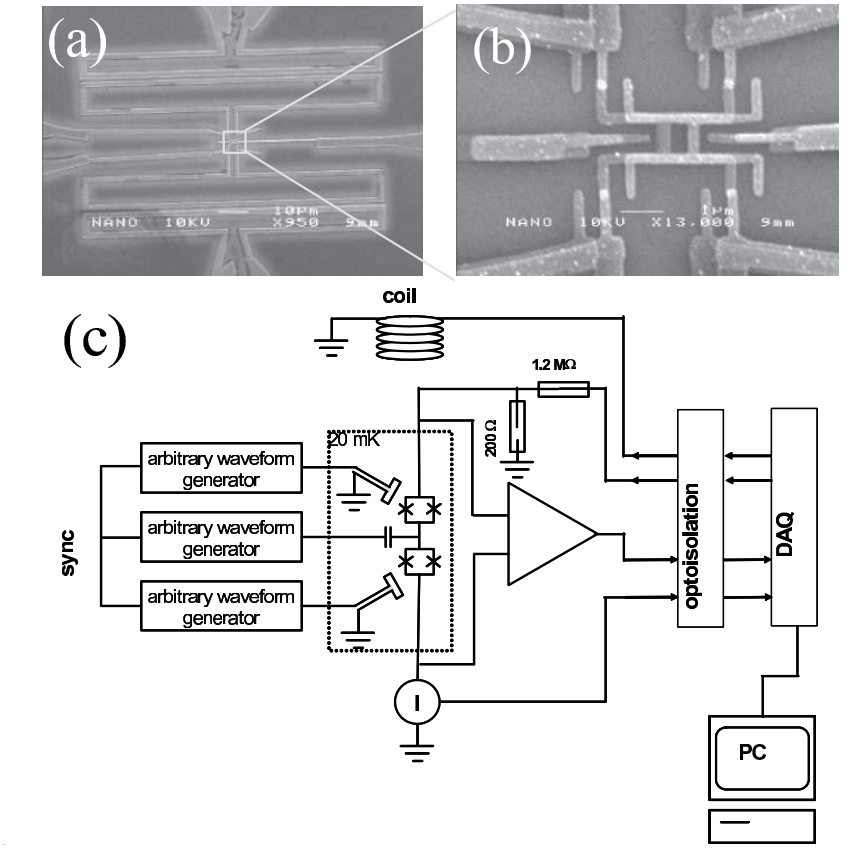

Figure 7. (a) Scanning electron micrograph of the Cooper pair "sluice". The input coils are seen topmost and lowest in the picture while the gate extends to the right. The current flows between the two electrodes on the left. (b) Close-up of the island. The Josephson junctions are the four lighter-shade spots formed in the overlap of the two shadows. (c) Measurement setup.

pumping signal being applied underneath. It was found that despite the manipulation of the Josephson energies, leakage current unfortunately also existed. However, since it was possible to change the direction of the current by shifting the phase of the gate through 180 degrees, it is possible to extract the pumped current from this measurement. Namely, subtracting the IVs with the pumping applied forward and backward from each other should leave us with twice the pumped current. Figure 8 shows full IVs at 3 MHz for different gate amplitudes with pumping in both directions along with the aforementioned differences ΔI vs. voltage. It is seen that the difference in the current nicely obeys the expected pumping behavior. In order to serve as a practical current pump the leakage should be taken care of, e.g., by improved voltage biasing and/or improving the closing of the SQUIDs.

The most convincing evidence of the pumping along with the fact that the above phase shift procedure works, is found by gradually increasing the gate amplitude and then measuring the current at a constant voltage bias. The results are shown in Fig. 9. The quantity that we studied was ΔI in this measurement too. The amplitude was increased such that the low level of the gate $V_{\rm g}^{\rm lo}$ was fixed and the high level $V_{\rm g}^{\rm hi}$ was swept. This

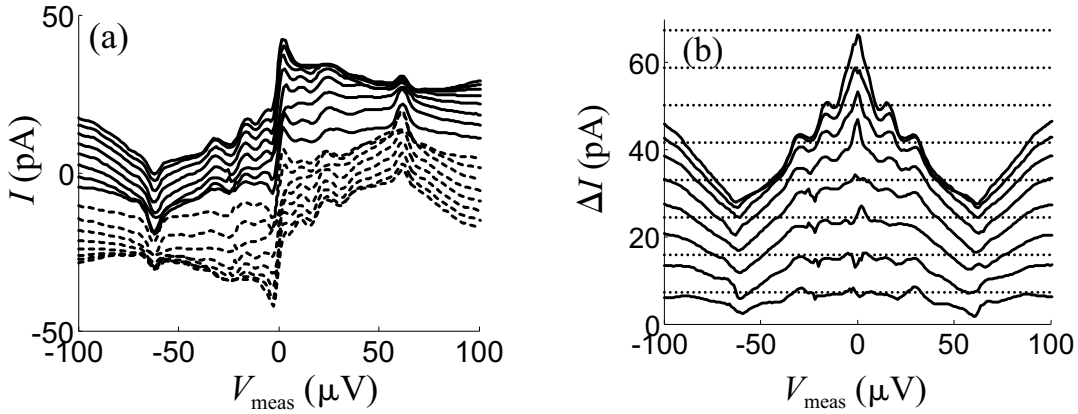

Figure 8. (a) IVs for pumping forward (solid) and backward (dashed). Here m ranges between 4 and 34. (b) Differences ΔI in the IVs (see text). Horizontal dotted lines indicate the expected levels of current. Here $V_{\rm meas}$ is the measured value of voltage.

should result in $2e$-periodic staircase in the pumped current with the step heights[3] equal to $4ef$. However, due to quasiparticle poisoning faster than the measurement time scale but slower than the pumping, the measured behavior was e-periodic with $2ef$ steps. This is interpreted to be because we actually measure the average of two $2e$-periodic staircases shifted by e with respect to each other. Figure 9(b) also shows the high gate amplitude behavior of ΔI and it is seen that up to amplitudes of $10e$ the agreement with the expected behavior is good. Fig. 9(c) illustrates the least-squares fitted slopes to the linear regime of Figs. 9(a–b). The agreement with theory is seen to be good with a few percent error.

To conclude, we have demonstrated in practice the original idea of Publication VI for pumping Cooper pairs with tunable Josephson junctions, i.e. SQUIDs. The experimental evidence is convincing enough to show that the idea for pumping works, although several non-idealities still exist. Possible solutions for cutting down the leakage include fabricating an on-chip capacitor much larger than the junction capacitance parallel with the pump, considering a more complicated design for the SQUIDs (see Fig. 1(b) of Publication VI) and maybe even using a longer array. Lengthening the array would, though, inevitably complicate the control. The capacitance, however, would better conserve the energy of the pump since then the so-called P(E)-curve would be peaked close to the zero of energy, see e.g. Ref. [70]. The quasiparticle poisoning is not necessarily a problem even from the application point of view, if the quasiparticle current is small enough. Namely, our measurements indicate that the net quasiparticle flow is negligible but, instead, the quasiparticles jump randomly on and off the island with no preferred direction. That is, the flow of current is mostly due to Cooper pairs. The quasiparticles in the present measurement are thus probably of the non-equilibrium type reported in Ref. [86]. There the reported time scale of quasiparticle poisoning for a superconducting SET was 10 μs. In Ref. [87] the relevant time-scale was 10^{-2} s but in a somewhat different setup. These figures support our time scale argument, since the integration time for our measurement

[3]Recall that ΔI should be twice the pumped current.

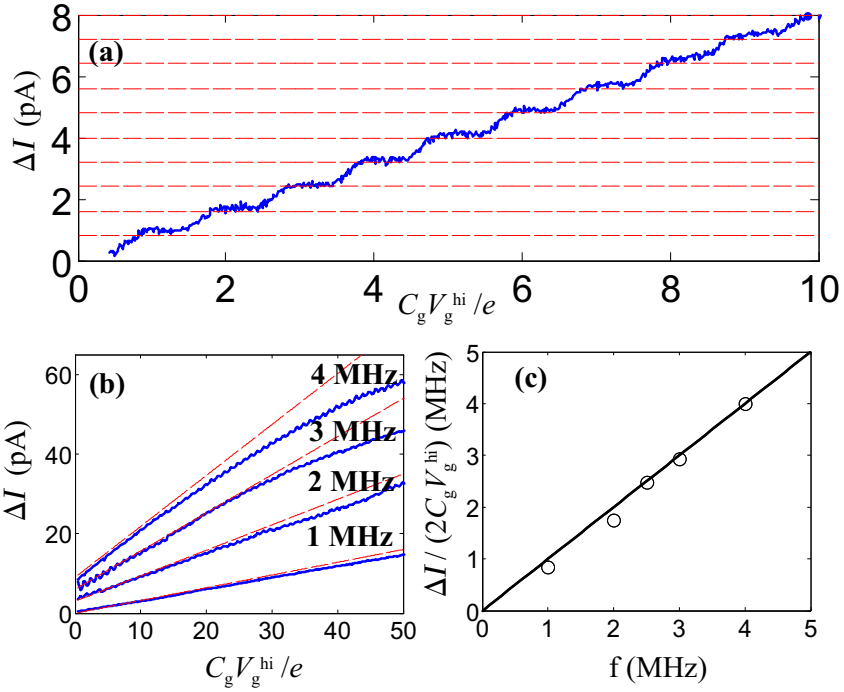

Figure 9. (a) Difference ΔI in the current for forward and backward pumping at 2.5 MHz against the high level of the gate signal V_g^{hi} with the low level at zero. The dashed lines are drawn at $2ef$ intervals. (b) Large gate amplitude behavior of ΔI at a few frequencies. The dashed lines show the expected gate dependence, i.e. their slope is $2ef$. The curves are offset for clarity. (c) Fitted slopes to the data of the previous plots up to $V_g C_g/e = 10$ are shown by circles. The solid line indicates the expected behavior. The voltage bias point was around 10 μV in all the above plots.

was on the order of 0.1 s and the pumping time smaller than 1 μs. We could not, however, experimentally determine the characteristic time for quasiparticles in the present setup.

5 Conclusions

In this Overview we have discussed different aspects of the controlled evolution of quantum systems, both geometrical and dynamical. Particular attention was paid to nanoscale Josephson junction circuits. The two applications that were considered in detail included quantum computing and quantum charge pumping. Let us briefly summarize the conclusion of the Publications included in this Thesis:

In Publications I–II, a realization independent numerical method of finding arbitrary holonomic quantum gates was studied. It was shown that holonomy loops realizing any one and two-qubit unitary operation for the studied three-state model can be found easily. Moreover, it was shown that the length of the loop could be reduced by numerical optimization.

In Publications III–V, the optimization method was generalized to dynamical quantum computing. The physical system studied was the inductively coupled Josephson charge qubit array, although the method could easily be generalized to other systems. The algorithm was parallelized and shown to be capable of finding single-shot realizations for up to three-qubit gates. Publication III introduced the method while Publication IV concentrated on accelerating quantum algorithms using three-qubit gates. The more extended Publication V discussed the requirements of performing Shor's algorithm on the inductively coupled charge-qubit array. It was found that factoring 21, arguably the simplest "non-trivial" composite integer, would require 22 qubits and microsecond coherence times which is on the same order as the best reported coherence times in superconducting circuits. However, it was found, that breaking for instance the 512-bit RSA would require thousands of qubits working co-operatively and tens of seconds in terms of coherence time. All the estimates were based on the assumption that arbitrary three-qubit gates are available in single-shot form. The use of elementary gates would prolong the runtime severely. The conclusion regarding Publications I-V is that even though no change in the complexity of the algorithm is obtained via numerical optimization, the stringent limits set by short decoherence times makes it well worthwhile to try and reduce the runtime even by a numerical factor. Optimization may well result in cutting down the runtime by orders of magnitude opposed to elementary-gate logic inspired by classical computers.

In Publication VI, an application of Berry's geometrical phase in a superconducting circuit was discussed. There a novel Cooper pair pump, the "sluice", consisting of just one superconducting island connected to leads via SQUID loops and utilizing both flux and voltage control was introduced. It was shown that the device can potentially reach metrological accuracy. In Publication VII, the experimental results of the device were reported. It was found that the pumped current increases in clear steps with the increasing gate amplitude and changes direction under a 180-degree phase shift of the gate, even though quasiparticle poisoning and leakage were present. Many suggestions for improving the device were given. The "sluice" was found to be a promising candidate for a practical current pump. The clear benefit of the "sluice" is that it is simple with just three control parameters and it would allow for higher operating frequencies. One

may further argue that solving the practical challenges in its control is much easier than building even a simple working quantum computer. It could, therefore, find use as a great test bench for the control techniques of superconducting qubits.

References

[1] P. W. Shor, *Algorithms for quantum computation: discrete logarithms and factoring*, in *Proceedings, 35th Annual Symposium on Foundations of Computer Science*, IEEE Computer Society Press, Los Alamitos, CA, (1994).

[2] M. A. Nielsen and I.L. Chuang, *Quantum computation and quantum information*, Cambridge University Press, Cambridge (2000).

[3] M. Hirvensalo, *Quantum computing*, Springer, Berlin (2001).

[4] J. Gruska, *Quantum computing*, McGraw–Hill, New York (1999).

[5] A. Galindo and M. A. Martín-Delgado, *Information and computation: Classical and quantum aspects*, Rev. Mod. Phys. **74**, 347 (2002).

[6] N. Gisin, G. Ribordy, W. Tittel, and H. Zbinden, *Quantum cryptography*, Rev. Mod. Phys. **74**, 145 (2002).

[7] L. M. K. Vandersypen and I. L. Chuang, *NMR techniques for quantum control*, quant-ph/0404064 (2004).

[8] S. A. Rice and M. Zhao, *Optimal control of molecular dynamics*, Wiley, New York (2000).

[9] L. M. K. Vandersypen, M. Steffen, G. Breyta, C. S. Yannoni, M. H. Sherwood, and I.L. Chuang, *Experimental realization of Shor's quantum factoring algorithm using magnetic resonance*, Nature **414**, 883 (2001).

[10] A. Shnirman, G. Schön, and Z. Hermon, *Quantum meanipulations with small Josephson junctions*, Phys. Rev. Lett. **79**, 2371 (1997).

[11] Y. Nakamura, Yu. A. Pashkin, and J. S. Tsai, *Coherent control of macroscopic quantum states in a single-Cooper-pair box*, Nature **398**, 786 (1999).

[12] Y. Nakamura, Yu. A. Pashkin, and J. S. Tsai, *Rabi oscillations in a Josephson-junction charge two-level system*, Phys. Rev. Lett. **87**, 246601 (2002).

[13] Y. Nakamura, Yu. A. Pashkin, T. Yamamoto, and J. S. Tsai, *Charge echo in a Cooper-pair box*, Phys. Rev. Lett. **88**, 047901 (2002).

[14] Yu. A. Pashkin, T. Yamamoto, O. Astafiev, Y. Nakamura, D. V. Averin and J. S. Tsai, *Quantum oscillations in two coupled charge qubits*, Nature **421**, 823 (2003).

[15] T. Yamamoto, Yu. A. Pashkin, O. Astafiev, Y. Nakamura, and J. S. Tsai, *Demonstration of conditional gate operation using superconducting charge qubits*, Nature **425**, 941 (2003).

[16] J. E. Mooij, T. P. Orlando, L. Levitov, L. Tian, C. H. van der Wal, and S. Lloyd, *Josephson persistent-current qubit*, Science **285**, 1036 (1999).

[17] T. P. Orlando, J. E. Mooij, L. Tian, C. H. van der Wal, L. Levitov, S. Lloyd, and J. J. Mazo, *Superconducting persistent-current qubit*, Phys. Rev. B **60**, 15398 (1999).

[18] C. H. van der Wal, A. C. J. ter Haar, F. K. Wilhelm, R. N. Schouten, C. J. P. M. Harmans, T. P. Orlando, S. Lloyd, and J. E. Mooij, *Quantum superposition of macroscopic persistent-current states*, Science **290**, 773 (2000).

[19] I. Chiorescu, Y. Nakamura, C. J. P. M. Harmans, and J. E. Mooij, *Coherent quantum dynamics of a superconducting flux qubit*, Science **299**, 1869 (2003).

[20] Y. Yu, S. Han, X. Chu, S. Chu, and Z. Wang, *Coherent temporal oscillations of macroscopic quantum states in a Josephson junction*, Science **296**, 889 (2002).

[21] J. M. Martinis, S. Nam, J. Aumentado, and C. Urbina, *Rabi oscillations in a large Josephson-junction qubit*, Phys. Rev. Lett. **89**, 117901 (2002).

[22] D. Vion, A. Aassime, A. Cottet, P. Joyez, H. Pothier, C. Urbina, D. Esteve, and M. H. Devoret, *Manipulating the quantum state of an electrical circuit*, Science **296**, 886 (2002).

[23] J. Claudon, F. Balestro, F. W. J. Hekking and O. Buisson, *Coherent oscillations in a superconducting multi-level quantum system*, cond-mat/0405430 (2004).

[24] M. V. Feigel'man, L. B. Ioffe, V. B. Geshkenbein, P. Dayal, and G. Blatter, *Superconducting tetrahedral quantum bits*, Phys. Rev. Lett. **92**, 098301 (2004).

[25] Yu. Makhlin, G. Schön, and A. Shnirman, *Quantum-state engineering with Josephson-junction devices*, Rev. Mod. Phys. **73**, 357 (2001).

[26] L. J. Geerligs, S. M. Verbrugh, P. Hadley, J. E. Mooij, H. Pothier, P. Lafarge, C. Urbina, D. Esteve, and M. H. Devoret, *Single Cooper pair pump*, Z. Phys. B: Condens. Matter **85**, 349 (1991).

[27] J. P. Pekola, J. J. Toppari, M. Aunola, M. T. Savolainen, and D. V. Averin, *Adiabatic transport of Cooper pairs in arrays of Josephson junctions*, Phys. Rev. B **60**, R9931 (1999).

[28] R. Fazio, F. W. J. Hekking, and J. P. Pekola, *Measurement of coherent charge transfer in an adiabatic Cooper-pair pump*, Phys. Rev. B **68**, 054510 (2003).

[29] P. Zanardi and M. Rasetti, *Holonomic quantum computation*, Phys. Lett. A. **264**, 94–99, 1999.

[30] M. W. Keller, J. M. Martinis, N. M. Zimmerman, and A. H. Steinbach, *Accuracy of electron counting using a 7-junction electron pump*, Appl. Phys. Lett. **69**, 1804 (1996).

[31] M. Berry, *Quantal phase factors accompanying adiabatic changes*, Proc. R. Soc. Lond. A **392**, 45 (1984).

[32] F. Wilczek and A. Zee, *Appearance of gauge structure in simple dynamical systems*, Phys. Rev. Lett. **52**, 2111 (1984).

[33] W. H. Zurek, *Decoherence, einselection, and the quantum origins of the classical*, Rev. Mod. Phys. **75**, 715 (2003).

[34] A. O. Caldeira and A. J. Leggett, *Path integral approach to quantum Brownian motion*, Physica A, **121**, 587 (1983).

[35] R. W. Simmonds, K. M. Lang, D. A. Hite, D. P. Pappas, and J. M. Martinis, *Decoherence in Josephson qubits from junction resonances*, cond-mat/0402470 (2004).

[36] J. M. Martinis, S. Nam, J. Aumentado, K. M. Lang, and C. Urbina, *Decoherence of a superconducting qubit from bias noise*, Phys. Rev. B **67**, 094510 (2003)

[37] E. Paladino, L. Faoro, G. Falci, and R. Fazio, *Decoherence and 1/f noise in Josephson qubits*, Phys. Rev. Lett. **88**, 228304 (2002).

[38] J. P. Pekola and J. J. Toppari, *Decoherence in circuits of small Josephson junctions*, Phys. Rev. B **64**, 172509 (2001).

[39] M. J. Storcz and F. K. Wilhelm, *Decoherence and gate performance of coupled solid-state qubits*, Phys. Rev. A **67**, 042319 (2003).

[40] L. E. Ballentine, *Quantum mechanics*, World Scientific, Singapore (1998).

[41] A. Zee, *Non-Abelian gauge structure in nuclear quadrupole resonance*, Phys. Rev. A **38**, 1 (1988).

[42] A. Einstein, B. Podolsky, and N. Rosen, *Can quantum-mechanical description of reality be considered complete?*, Phys. Rev. **47**, 777 (1935).

[43] M. Riebe, H. Häffner, C. F. Roos, W. Hänsel, J. Benhelm, G. P. T. Lancaster, T. W. Körber, C. Becher, F. Schmidt-Kaler, D. F. V. James, and R. Blatt, *Deterministic quantum teleportation with atoms*, Nature **429**, 734 (2004).

[44] M. D. Barrett, J. Chiaverini, T. Schaetz, J. Britton, W. M. Itano, J. D. Jost, E. Knill, C. Langer, D. Leibfried, R. Ozeri, and D. J. Wineland, *Deterministic quantum teleportation of atomic qubits*, Nature **429**, 737 (2004).

[45] L. K. Grover, *Quantum mechanics helps in searching for a needle in a haystack*, Phys. Rev. Lett. **79**, 325 (1997).

[46] A. Barenco, C. H. Bennett, R. Cleve, D. P. DiVincenzo, N. Margolus, P. Shor, T. Sleator, J. A. Smolin, and H. Weinfurter, *Elementary gates for quantum computation*, Phys. Rev. A **52**, 3457 (1995).

[47] J. J. Vartiainen, M. Möttönen, and M. M. Salomaa, *Efficient Decomposition of Quantum Gates*, Phys. Rev. Lett. **92**, 177902 (2004).

[48] M. Möttönen, J. J. Vartiainen, V. Bergholm, and M. M. Salomaa, *Universal quantum computation*, quant-ph/0404089 (2004).

[49] D. P. DiVincenzo, *The physical implementation of quantum computation*, Fortscr. Phys. **48**, 771 (2000).

[50] S. Oh, *Errors due to finite rise and fall times of pulses in superconducting qubits*, Phys. Rev. B **65**, 144526 (2002).

[51] M. Nakahara, Y. Kondo, K. Hata, and S. Tanimura, *Demonstrating quantum algorithm acceleration with NMR quantum computer*, quant-ph/0405040 (2004).

[52] J. Pachos, P. Zanardi, and M. Rasetti, *Non-Abelian Berry connections for quantum computation*, Phys. Rev. A **61**, 010305(R) (1999).

[53] D. Ellinas and J. Pachos, *Universal quantum computation by holonomic and nonlocal gates with imperfections*, Phys. Rev. A. **64**, 022310 (2001).

[54] J. Pachos and P. Zanardi, *Quantum holonomies for quantum computing*, Int. J. Mod. Phys. **15**, 1257 (2001).

[55] K. Fujii, *Mathematical foundations of holonomic quantum computer*, Rep. Math. Phys. **48**, 75 (2001).

[56] L. Faoro, J. Siewert, and R. Fazio, *Non-Abelian holonomies, charge pumping, and quantum computation with Josephson junctions*, Phys. Rev. Lett. **90**, 028301 (2003).

[57] M. S. Choi, *Geometric quantum computation on solid-state qubits*, J. Phys.: Condens. Matter **15**, 7823 (2003).

[58] M. Cholascinski, *Quantum holonomies with Josephson-junction devices*, cond-mat/0401087 (2004).

[59] J. Pachos and S. Chountasis, *Optical holonomic quantum computer*, Phys. Rev. A. **62**, 052318 (2000).

[60] P. Solinas, P. Zanardi, N. Zanghi, and F. Rossi, *Holonomic quantum gates: A semiconductor-based implementation*, Phys. Rev A **67**, 062315 (2003).

[61] G. Falci, R. Fazio, G. M. Palma, J. Siewert, and V. Vedral, *Detection of geometric phases in superconducting circuits*, Nature **407**, 355 (2000).

[62] J. C. Lagarias, J. A. Reeds, M. H. Wright, and P. E. Wright, *Convergence properties of the Nelder-Mead simplex algorithm in low dimensions*, SIAM J. Optim. **9**, 112 (1998).

[63] S. Tanimura, D. Hayashi, and M. Nakahara, *Exact solution of holonomic quantum computation*, Phys. Lett. A **325**, 199 (2004).

[64] M. Nakahara, *Geometry, topology and physics*, IOP Publishing Ltd. (1990).

[65] S. Tanimura, M. Nakahara, and D. Hayashi, *Exact solutions of the isoholonomic problem and the optimal control problem in holonomic quantum computation*, quant-ph/0406038 (2004).

[66] G. R. Andrews, *Foundations of multithreaded, parallel, and distributed programming*, Addison-Wesley, Reading (2000).

[67] J. Q. You, J. S. Tsai, and F. Nori, *Scalable quantum computing with Josephson charge qubits*, Phys. Rev. Lett. **89**, 197902 (2002).

[68] M. Tinkham, *Introduction to superconductivity, 2nd ed.*, McGraw-Hill, New York (1996).

[69] M. H. Devoret, *Quantum fluctuations in electrical circuits*, Quantum Fluctuations, eds.: S. Reymaud, E. Giacobino, and J. Zinn-Justin, Elsevier Science, B.V. (1997).

[70] G. L. Ingold and Yu. V. Nazarov, *Charge tunneling rates in ultrasmall junctions*, in *Single Charge Tunneling* edited by H. Grabert and M. H. Devoret, Plenum Press, New York (1992).

[71] V. Ambegaokar and A. Baratoff, *Tunneling between superconductors*, Phys. Rev. Lett. **10**, 486 (1963).

[72] J. P. Palao and R. Kosloff, *Quantum computing by an optimal control algorithm for unitary transformations*, Phys. Rev. Lett. **89**, 188301 (2002).

[73] J. P. Palao and R. Kosloff, *Optimal control theory for unitary transformations*, Phys. Rev. A **68**, 062308 (2003).

[74] V. K. Semenov and D. V. Averin, *SFQ control circuits for Josephson junction qubits*, IEEE Trans. Appl. Super. **13**, 960 (2003).

[75] D. S. Crankshaw, J. L. Habif, X. Zhou, T. P. Orlando, M. J. Feldman, and M. F. Bocko, *An RSFQ variable duty cycle oscillator for driving a superconductive qubit*, IEEE Trans. Appl. Super. **13**, 966 (2003).

[76] P. W. Shor, *Scheme for reducing decoherence in quantum computer memory*, Phys. Rev. A **52**, R2493 (1995).

[77] M. W. Keller, A. L. Eichenberger, J. M. Martinis, and N. M. Zimmerman, *A capacitance standard based on counting electrons*, Science **285**, 1706 (1999).

[78] K. K. Likharev and A. B. Zorin, *Theory of the Bloch-wave oscillations in small Josephson junction*, J. Low Temp. Phys. **59**, 347 (1985).

[79] J. Cunningham, V. I. Talyanskii, J. M. Shilton, M. Pepper, M. Y. Simmons, and D. A. Ritchie, *Single-electron acoustic charge transport by two counterpropagating surface acoustic wave beams*, Phys. Rev. B **60**, 4850 (1999).

[80] S. V. Lotkhov, S. A. Bogoslovsky, A. B. Zorin, and J. Niemeyer, *Operation of a three-junction single-electron pump with on-chip resistors*, Appl. Phys. Lett. **78**, 946 (2001).

[81] A. B. Zorin, S. V. Lotkhov, S. A. Bogoslovsky, and J. Niemeyer, *Radio-frequency-driven motion of single Cooper pairs across the superconducting single-electron transistor with dissipative environment*, cond-mat/0105211 (2001).

[82] J. J. Toppari, J. M. Kivioja, J. P. Pekola, and M. T. Savolainen, *Turnstile behaviour of the Cooper pair pump*, J. Low Temp. Phys. **136**, 57 (2004).

[83] J. Aumentado, M. W. Keller, and J. M. Martinis, *A seven junction Cooper pair pump*, Physica E **18**, 37 (2003).

[84] M. Aunola and J. J. Toppari, *Connecting Berry's phase and the pumped charge in a Cooper pair pump*, Phys. Rev. B **68**, 020502 (2003).

[85] J. Pekola, K. P. Hirvi, J. P. Kauppinen, and M. A. Paalanen, *Thermometry by arrays of tunnel junctions*, Phys. Rev. Lett. **73**, 2903 (1994).

[86] J. Aumentado, M. W. Keller, J. M. Martinis, and M. H. Devoret, *Nonequilibrium quasiparticles and 2e periodicity in single-Cooper-pair transistors*, Phys. Rev. Lett. **92**, 066802 (2004).

[87] J. Männik and J. E. Lukens, *Effect of measurement on the periodicity of the Coulomb staircase of a superconducting box*, Phys. Rev. Lett. **92**, 057004 (2004).

Reprinted with permission from the publisher.
In: Physical Review 2003. Vol. A 67, pp. 012319-1–10.

Realization of arbitrary gates in holonomic quantum computation

Antti O. Niskanen, Mikio Nakahara,* and Martti M. Salomaa
Materials Physics Laboratory, Helsinki University of Technology, POB 2200 (Technical Physics), FIN-02015 HUT, Finland
(Received 29 August 2002; published 29 January 2003)

Among the many proposals for the realization of a quantum computer, holonomic quantum computation is distinguished from the rest as it is geometrical in nature and thus expected to be robust against decoherence. Here we analyze the realization of various quantum gates by solving the inverse problem: Given a unitary matrix, we develop a formalism by which we find loops in the parameter space generating this matrix as a holonomy. We demonstrate that such a one-qubit gate as the Hadamard gate and such two-qubit gates as the controlled-NOT gate and the SWAP gate, and the discrete Fourier transformation can be obtained with a single loop.

DOI: 10.1103/PhysRevA.67.012319 PACS number(s): 03.67.Lx, 03.65.Vf, 02.60.Pn

I. INTRODUCTION

Quantum computing is an emerging scientific discipline, in which the merging and mutual cross fertilization of two of the most important developments in physical science and information technology of the past century—quantum mechanics and computing—has resulted in an extraordinarily rapid rate of progress of interdisciplinary nature. Interesting problems to address in this context include fundamental questions as to what are the ultimate physical limits of computation and communication. For introductions to quantum computing and quantum information processing see, e.g., Refs. [1–3].

Holonomic quantum computation (HQC) was first suggested by Zanardi and Rasetti in Ref. [4]. The concept has been further developed in Refs. [5–9]. The suggestion is very intriguing itself; quantum-logical operations are achieved by driving a degenerate system around adiabatic loops in the parameter manifold. The resulting gates are a generalization of the celebrated Berry phase [10] to encompass a degenerate system. These are, in fact, non-Abelian holonomies. Due to the geometric nature of these gates, quantum information processing is expected to be fault tolerant. For instance, the issue of timing and the lack of spontaneous decay are definite strengths of HQC. Here we study the construction of holonomic quantum logic gates numerically via solving a certain inverse problem. Namely, we find the loop $\hat{\gamma}$ corresponding to the desired unitary operator $\hat{U}$ by solving a high-dimensional optimization task.

The paper is organized as follows: In Sec. II, we present the physical and mathematical background underlying our approach. Sections III, IV, and V comprise the main part of the present paper. Loop parametrizations for one- and two-qubit gates are presented in Sec. III. The numerical method is introduced in Sec. IV. Then the optimal realization of a unitary gate as a holonomy associated with a loop in the parameter space is investigated numerically in Sec. V. Section VI discusses the results.

II. HAMILTONIAN AND HOLONOMY

Here we first review the concept of non-Abelian holonomy to establish notation conventions. Let us consider a family of Hamiltonians $\{H_\lambda\}$. The point λ, continuously parametrizing the Hamiltonian, is an element of a manifold $\mathcal{M}$ called the control manifold and the local coordinate of λ is denoted by $\lambda^i (1 \leqslant i \leqslant m = \dim \mathcal{M})$. It is assumed that there exists only a finite number of eigenvalues $\varepsilon_k(\lambda)(1 \leqslant k \leqslant R)$ for an arbitrary $\lambda \in \mathcal{M}$ and that no level crossings occur. Suppose the nth eigenvalue $\varepsilon_n(\lambda)$ is g_n-fold degenerate for any $\lambda \in \mathcal{M}$ and $\Sigma_{n=1}^{R} g_n = N$. The degenerate subspace at λ is denoted by $\mathcal{H}_n(\lambda)$. Accordingly, the Hamiltonian is expressed as a $N \times N$ matrix. The orthonormal basis vectors of $\mathcal{H}_n(\lambda)$ are denoted by $\{|n\alpha;\lambda\rangle\}$

$$H_\lambda |n\alpha;\lambda\rangle = \varepsilon_n(\lambda)|n\alpha;\lambda\rangle, \quad \langle n\alpha;\lambda|m\beta;\lambda\rangle = \delta_{mn}\delta_{\alpha\beta}.$$

Note that there are $U(g_n)$ degrees of freedom in the choice of the basis vectors $\{|n\alpha;\lambda\rangle\}$.

Let us now assume that the parameter λ is changed adiabatically. We will be concerned with a particular subspace, say the ground state $\mathcal{H}_1(\lambda)$, and we will drop the index n to simplify the notation. Suppose the initial state at $t=0$ is an eigenstate $|\psi_\alpha(0)\rangle = |\alpha;\lambda(0)\rangle$ with the energy $\varepsilon = 0$ possibly through shifting the zero point of the energy. In fact, we are not interested in the dynamical phase at all and hence assume that the eigenvalue in this subspace vanishes for any $\lambda \in \mathcal{M}$. The Schrödinger equation is

$$i\frac{d}{dt}|\psi_\alpha(t)\rangle = H_{\lambda(t)}|\psi_\alpha(t)\rangle, \tag{1}$$

whose solution may be assumed to take the form

$$|\psi_\alpha(t)\rangle = \sum_{\beta=1}^{g} |\beta;\lambda(t)\rangle U_{\beta\alpha}(t). \tag{2}$$

The unitarity of the matrix $U_{\beta\alpha}(t)$ follows from the normalization of $|\psi_\alpha(t)\rangle$. By substituting Eq. (2) into Eq. (1), one finds that $U_{\beta\alpha}$ satisfies

*Also at Department of Physics, Kinki University, Higashi-Osaka 577-8502, Japan.

1050-2947/2003/67(1)/012319(10)/$20.00

$$\dot{U}_{\beta\alpha}(t)=-\sum_{\gamma}\left\langle \beta;\lambda(t)\left|\frac{d}{dt}\right|\gamma;\lambda(t)\right\rangle U_{\gamma\alpha}. \tag{3}$$

The formal solution may be expressed as

$$\begin{aligned}U(t)&=\mathcal{T}\exp\left(-\int_0^t A(\tau)d\tau\right)\\&=I-\int_0^t A(\tau)d\tau+\int_0^t d\tau\int_0^\tau d\tau' A(\tau)A(\tau')+\cdots,\end{aligned} \tag{4}$$

where $\mathcal{T}$ is the time-ordering operator and

$$A_{\beta\alpha}(t)=\left\langle \beta;\lambda(t)\left|\frac{d}{dt}\right|\alpha;\lambda(t)\right\rangle.$$

Let us introduce the Lie-algebra-valued connection

$$\mathcal{A}_{i,\beta\alpha}=\left\langle \beta;\lambda(t)\left|\frac{\partial}{\partial\lambda^i}\right|\alpha;\lambda(t)\right\rangle \tag{5}$$

through which $U(t)$ is expressed as

$$U(t)=\mathcal{P}\exp\left(-\int_{\lambda(0)}^{\lambda(t)}\mathcal{A}_i d\lambda^i\right), \tag{6}$$

where $\mathcal{P}$ is the path-ordering operator. Note that $\mathcal{A}_i$ is anti-Hermitian, $\mathcal{A}_i^\dagger=-\mathcal{A}_i$.

Suppose the path $\lambda(t)$ is a loop $\gamma(t)$ in $\mathcal{M}$ such that $\gamma(0)=\gamma(T)=\lambda_0$. Then it is found that after traversing γ, one ends up with the state

$$|\psi_\alpha(T)\rangle=\sum_{\beta=1}^{g}|\psi_\beta(0)\rangle U_{\beta\alpha}(T), \tag{7}$$

where the definition $|\psi_\beta(0)\rangle=|\beta;\lambda_0\rangle$ has been used. The unitary matrix

$$U_\gamma\equiv U(T)=\mathcal{P}\exp\left(-\oint_\gamma \mathcal{A}_i d\gamma^i\right) \tag{8}$$

is called the holonomy associated with the loop $\gamma(t)$. Note that U_γ is independent of the parametrization of the path, but only depends upon its geometric image in $\mathcal{M}$ [11,12].

The space of all the loops based at λ_0 is denoted by

$$L_{\lambda_0}(\mathcal{M})=\{\gamma:[0,T]\to\mathcal{M}|\,\gamma(0)=\gamma(T)=\lambda_0\}. \tag{9}$$

The set of the holonomy

$$\mathrm{Hol}(\mathcal{A})=\{U_\gamma|\,\gamma\in L_{\lambda_0}(\mathcal{M})\} \tag{10}$$

has a group structure [13] and is called the holonomy group. It is clear that $\mathrm{Hol}(\mathcal{A})\subset U(g)$. The connection $\mathcal{A}$ is called irreducible when $\mathrm{Hol}(\mathcal{A})=U(g)$.

III. THREE-STATE MODEL AND QUANTUM-GATE CONSTRUCTION

A. One-qubit gates

To make things tractable, we employ a simple model Hamiltonian called the three-state model as the basic building block for our strategy. This is a three-dimensional (3D) Hamiltonian with the matrix form

$$H_{\lambda_0}=\epsilon|2\rangle\langle 2|=\begin{pmatrix}\epsilon&0&0\\0&0&0\\0&0&0\end{pmatrix}. \tag{11}$$

The first column (row) of the matrix refers to the auxiliary state $|2\rangle$ with the energy $\epsilon>0$, while the second and the third columns (rows) refer to the vectors $|0\rangle$ and $|1\rangle$, respectively, with vanishing energy. The qubit consists of the last two vectors.

The control manifold of the Hamiltonian (11) is the complex projective space $\mathbb{C}P^2$. This is seen most directly as follows: The most general form of the isospectral deformation of the Hamiltonian is of the form $H_\gamma\equiv W_\gamma H_{\lambda_0}W_\gamma^\dagger$, where $W_\gamma\in\mathrm{U}(3)$. Note, however, that not all the elements of U(3) are independent. It is clear that H_γ is independent of the overall phase of W_γ, which reduces the number of degrees of freedom from U(3) to $\mathrm{U}(3)/\mathrm{U}(1)=\mathrm{SU}(3)$. Moreover, any element of SU(3) may be decomposed into a product of three SU(2) matrices as follows:

$$W_\gamma=\underbrace{\begin{pmatrix}\bar\beta_1&\bar\alpha_1&0\\-\alpha_1&\beta_1&0\\0&0&1\end{pmatrix}}_{U_1}\underbrace{\begin{pmatrix}\bar\beta_2&0&\bar\alpha_2\\0&1&0\\-\alpha_2&0&\beta_2\end{pmatrix}}_{U_2}\underbrace{\begin{pmatrix}1&0&0\\0&\bar\beta_3&\bar\alpha_3\\0&-\alpha_3&\beta_3\end{pmatrix}}_{U_3}, \tag{12}$$

which is know as the Givens decomposition. Here $\alpha_j=e^{i\phi_j}\sin\theta_j$ and $\beta_j=e^{i\psi_j}\cos\theta_j$. It is clear that H_γ is independent of U_3 since $[H_{\lambda_0},\mathrm{U}_3]=0$. This further reduces the physical degrees of freedom to $\mathrm{SU}(3)/\mathrm{SU}(2)\cong S^5$. The product U_1U_2 contains six parameters, while S^5 is five dimensional; there must be one redundant parameter in U_1U_2. This parameter is easily found out by writing the product explicitly. The result depends only on the combination $\phi_2-\psi_2$ and not on individual parameters. Accordingly, we may redefine ϕ_2 as $\phi_2-\psi_2$ to eliminate ψ_2. Furthermore, after this redefinition we find that the Hamiltonian depends only

on $\phi_1-\psi_1$ and $\phi_2-\psi_1$ and hence ψ_1 may also be subsumed by redefining ϕ_1 and ϕ_2, which reduces the independent degrees of freedom down to $\mathbb{C}P^2\cong S^5/S^1$.

Let $[z^1,z^2,z^3]$ be the homogeneous coordinate of $\mathbb{C}P^2$ and $(1,\xi_1,\xi_2)$ be the corresponding inhomogeneous coordinate, where $\xi_1=z^2/z^1,\xi^2=z^3/z^1$ in the coordinate neighborhood with $z^1\neq 0$. If we write $\xi_k=r_k e^{i\varphi_k}$, the above correspondence, i.e. the embedding of $\mathbb{C}P^2$ into U(3), is explicitly given by $\theta_k=\tan^{-1}r_k$ and $\phi_k=\varphi_k$.

The connection coefficients are easily calculated in the present model and are given by

$$\mathcal{A}_{\theta_1}=\begin{pmatrix} 0 & -\sin\theta_2 e^{-i(\phi_2-\phi_1)} \\ \sin\theta_2 e^{i(\phi_2-\phi_1)} & 0 \end{pmatrix}, \tag{13}$$

$$\mathcal{A}_{\theta_2}=\begin{pmatrix} 0 & 0 \\ 0 & 0 \end{pmatrix}, \tag{14}$$

$$\mathcal{A}_{\phi_1}=\begin{pmatrix} -i\sin^2\theta_1 & -\frac{i}{2}\sin 2\theta_1\sin\theta_2 e^{i(\phi_1-\phi_2)} \\ -\frac{i}{2}\sin 2\theta_1\sin\theta_2 e^{i(\phi_2-\phi_1)} & i\sin^2\theta_2\sin^2\theta_1 \end{pmatrix}, \tag{15}$$

$$\mathcal{A}_{\phi_2}=\begin{pmatrix} 0 & 0 \\ 0 & -i\sin^2\theta_2 \end{pmatrix}, \tag{16}$$

where the first column (row) refers to $|0\rangle$, while the second one refers to $|1\rangle$. Using these connection coefficients, it is possible to evaluate the holonomy associated with a loop γ as

$$U_\gamma=\mathcal{P}\exp\Big(-\oint_\gamma(\mathcal{A}_{\theta_1}d\theta_1+\mathcal{A}_{\theta_2}d\theta_2 + \mathcal{A}_{\phi_1}d\phi_1+\mathcal{A}_{\phi_2}d\phi_2)\Big). \tag{17}$$

Now our task is to find a loop that yields a given unitary matrix as its holonomy.

B. Two-qubit gates

Let us consider a two-qubit reference Hamiltonian

$$H^{2\text{-qubit}}_{\lambda_0}=H^a_{\lambda_0}\otimes I_3+I_3\otimes H^b_{\lambda_0}, \tag{18}$$

where $H^{a,b}_\lambda$ are three-state Hamiltonians and I_3 is the 3×3 unit matrix. Generalization to an arbitrary N-qubit system is obvious. The Hamiltonian scales as 3^N, instead of the 2^N in the present model. It is also possible to consider a model with g-degenerate eigenstates with one auxiliary state having finite energy. This model, however, has a difficulty in realizing an entangled state, without which the full computational power of a quantum computer is impossible.

We want to maintain the multipartite structure of the system in constructing the holonomy. For this purpose, we separate the unitary transformation into a product of single-qubit transformations $(W^a_\gamma\otimes W^b_\gamma)$ and a purely two-qubit rotation $W^{2\text{-qubit}}_\gamma$ which cannot be reduced into a tensor product of single-qubit transformations. Therefore, we write the isospectral deformation for a given loop γ as

$$H^{2\text{-qubit}}_\gamma=W^{2\text{-qubit}}_\gamma(W^a_\gamma\otimes W^b_\gamma)H^{2\text{-qubit}}_{\lambda_0}(W^a_\gamma\otimes W^b_\gamma)^\dagger W^{2\text{-qubit}\dagger}_\gamma. \tag{19}$$

The advantage of expressing the unitary matrix in this form is easily verified when we write down the connection coefficients for the one-qubit coordinates. Namely, the two-qubit transformation does not affect the one-qubit transformation at all;

$$\mathcal{A}_{i,\alpha\beta}=\left\langle \alpha;\lambda\left| W^\dagger_\gamma\frac{\partial}{\partial\gamma^i}W_\gamma\right|\beta;\lambda\right\rangle = \left\langle \alpha;\lambda\left|(W^a_\gamma\otimes W^b_\gamma)^\dagger\frac{\partial}{\partial\gamma^i}(W^a_\gamma\otimes W^b_\gamma)\right|\beta;\lambda\right\rangle,$$

where γ^i denotes a one-qubit coordinate.

There is a large number of possible choices for $W^{2\text{-qubit}}_\gamma$, depending on the physical realization of the present scenario. To keep our analysis as concrete as possible, we have made the simplest choice

$$W^{2\text{-qubit}}_\gamma=W_\xi\equiv e^{i\xi|11\rangle\langle 11|} \tag{20}$$

for our two-qubit unitary rotation. Let

$$H'_\gamma = H^a_\gamma \otimes I_3 + I_3 \otimes H^b_\gamma$$

$$= \begin{pmatrix}
h^a_{11}+h^b_{11} & h^b_{12} & h^b_{13} & h^a_{12} & 0 & 0 & h^a_{13} & 0 & 0 \\
h^b_{21} & h^a_{11}+h^b_{22} & h^b_{23} & 0 & h^a_{12} & 0 & 0 & h^a_{13} & 0 \\
h^b_{31} & h^b_{32} & h^a_{11}+h^b_{33} & 0 & 0 & h^a_{12} & 0 & 0 & h^b_{13} \\
h^a_{21} & 0 & 0 & h^a_{22}+h^b_{11} & h^b_{12} & h^b_{13} & h^a_{23} & 0 & 0 \\
0 & h^a_{21} & 0 & h^b_{21} & h^a_{22}+h^b_{22} & h^b_{23} & 0 & h^a_{23} & 0 \\
0 & 0 & h^a_{21} & h^b_{31} & h^b_{32} & h^a_{22}+h^b_{33} & 0 & 0 & h^a_{23} \\
h^a_{31} & 0 & 0 & h^a_{32} & 0 & 0 & h^a_{33}+h^b_{11} & h^b_{12} & h^b_{13} \\
0 & h^a_{31} & 0 & 0 & h^a_{32} & 0 & h^b_{21} & h^a_{33}+h^b_{22} & h^b_{23} \\
0 & 0 & h^a_{31} & 0 & 0 & h^a_{32} & h^b_{31} & h^b_{32} & h^a_{33}+h^b_{33}
\end{pmatrix}$$

be a two-qubit Hamiltonian before W_ξ is applied. Then after the application of W_ξ to H'_γ, we have the full Hamiltonian

$$H^{2\text{-qubit}}_\gamma = W_\xi H'_\gamma W^\dagger_\xi = \begin{pmatrix}
h^a_{11}+h^b_{11} & h^b_{12} & h^b_{13} & h^a_{12} & 0 & 0 & h^a_{13} & 0 & 0 \\
h^b_{21} & h^a_{11}+h^b_{22} & h^b_{23} & 0 & h^a_{12} & 0 & 0 & h^a_{13} & 0 \\
h^b_{31} & h^b_{32} & h^a_{11}+h^b_{33} & 0 & 0 & h^a_{12} & 0 & 0 & h^b_{13}e^{-i\xi} \\
h^a_{21} & 0 & 0 & h^a_{22}+h^b_{11} & h^b_{12} & h^b_{13} & h^a_{23} & 0 & 0 \\
0 & h^a_{21} & 0 & h^b_{21} & h^a_{22}+h^b_{22} & h^b_{23} & 0 & h^a_{23} & 0 \\
0 & 0 & h^a_{21} & h^b_{31} & h^b_{32} & h^a_{22}+h^b_{33} & 0 & 0 & h^a_{23}e^{-i\xi} \\
h^a_{31} & 0 & 0 & h^a_{32} & 0 & 0 & h^a_{33}+h^b_{11} & h^b_{12} & h^b_{13}e^{-i\xi} \\
0 & h^a_{31} & 0 & 0 & h^a_{32} & 0 & h^b_{21} & h^a_{33}+h^b_{22} & h^b_{23}e^{-i\xi} \\
0 & 0 & h^a_{31}e^{i\xi} & 0 & 0 & h^a_{32}e^{i\xi} & h^b_{31}e^{i\xi} & h^b_{32}e^{i\xi} & h^a_{33}+h^b_{33}
\end{pmatrix}. \tag{21}$$

As for the connection, we find

$$\mathcal{A}_\xi = \begin{pmatrix}
0 & 0 & 0 & 0 \\
0 & 0 & 0 & 0 \\
0 & 0 & 0 & 0 \\
0 & 0 & 0 & i\cos^2\theta^a_2 \cos^2\theta^b_2
\end{pmatrix}, \tag{22}$$

where the columns and rows are ordered with respect to the basis $\{|00\rangle,|01\rangle,|10\rangle,|11\rangle\}$. It should be apparent from the above analysis that we can construct an arbitrary controlled phase-shift gate with the help of a loop in the (θ^2_a,ξ) or (θ^2_b,ξ) space. Accordingly, this gives the controlled-NOT gate with one-qubit operations, as shown below.

C. Some examples

Before we proceed to present the numerical prescription to construct arbitrary one- and two-qubit gates in the following section, it is instructive to first work out some important examples whose loop can be constructed analytically. In particular, we will show that all the gates required for the proof of universality may be obtained within the present three-state model.

The first example is the $\pi/8$ gate,

$$U_{\pi/8} = \begin{pmatrix} 1 & 0 \\ 0 & e^{i\pi/8} \end{pmatrix}. \tag{23}$$

By inspecting the connection coefficients in Eqs. (13)–(16), we easily find that the loop presented by the sequence

$$(\theta_2,\phi_2): (0,0) \rightarrow (\pi/2,0) \rightarrow (\pi/2,\pi/8) \rightarrow (0,\pi/8) \rightarrow (0,0) \tag{24}$$

yields the desired gate. Note that the loop is in the (θ_2,ϕ_2) plane and all the other parameters are fixed at zero. Explicitly, we verify that

$$\begin{aligned} U_{\pi/8} &= \exp\left(\frac{\pi}{8}\mathcal{A}_{\phi_2}\Big|_{\theta_2=0}\right)\exp\left(\frac{\pi}{2}\mathcal{A}_{\theta_2}\Big|_{\phi_2=\pi/8}\right) \\ &\quad\times\exp\left(-\frac{\pi}{8}\mathcal{A}_{\phi_2}\Big|_{\theta_2=\pi/2}\right)\exp\left(-\frac{\pi}{2}\mathcal{A}_{\theta_2}\Big|_{\phi_2=0}\right) \\ &= \exp\left(-\frac{\pi}{8}\mathcal{A}_{\phi_2}\Big|_{\theta_2=\pi/2}\right). \end{aligned} \tag{25}$$

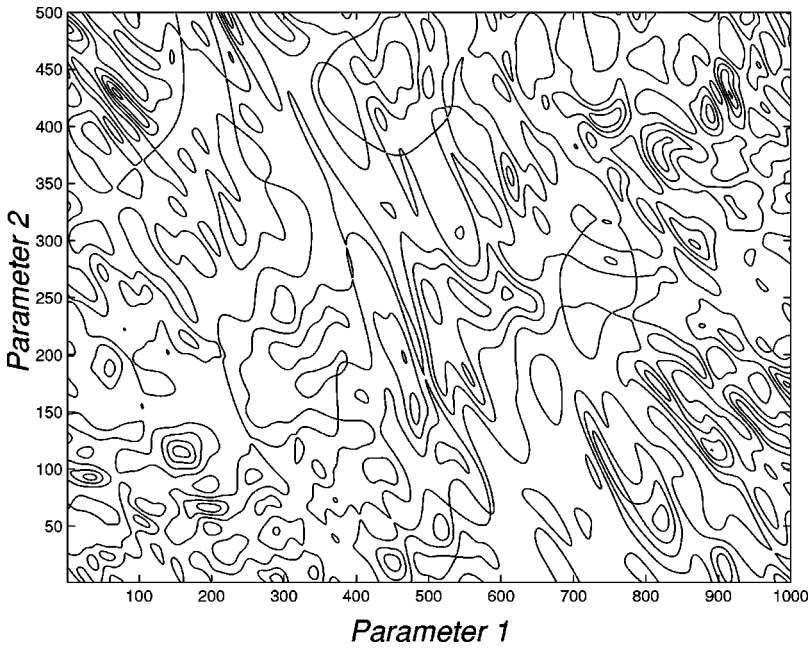

FIG. 1. Objective function landscape in 2D. Parameter 1 interpolates between the two known minima as described in the text, whereas parameter 2 represents a randomly chosen perpendicular direction.

The next example is the Hadamard gate

$$H=\frac{1}{\sqrt{2}}\begin{pmatrix}1 & 1\\ 1 & -1\end{pmatrix}. \tag{26}$$

Instead of constructing H directly, we will rather use the decomposition

$$H=e^{-i\pi/2}\exp\left(i\frac{\pi}{2}\sigma_z\right)\exp\left(i\frac{\pi}{4}\sigma_y\right).$$

It is easy to verify that the holonomy associated with the loop

$$(\theta_2,\theta_1):(0,0)\rightarrow(\pi/2,0)\rightarrow(\pi/2,\beta)\rightarrow(0,\beta)\rightarrow(0,0) \tag{27}$$

is $\exp(i\beta\sigma_y)$, while that associated with the loop

$$\begin{aligned}(\theta_1,\theta_2,\phi_1):(0,0,0)&\rightarrow(\pi/2,0,0)\rightarrow(\pi/2,\pi/2,0)\\ &\rightarrow(\pi/2,\pi/2,\alpha)\rightarrow(\pi/2,0,\alpha)\\ &\rightarrow(0,0,\alpha)\rightarrow(0,0,0)\end{aligned} \tag{28}$$

is $\exp(i\alpha\sigma_z)$. Here again, the rest of the parameters are fixed at zero. Finally, we construct the phase-shift gate $e^{i\delta}$, which is produced by a sequence of two loops. First, we construct a gate similar to the δ-shift gate using (cf. the $\pi/8$-shift gate)

$$(\theta_1,\phi_1):(0,0)\rightarrow(\pi/2,0)\rightarrow(\pi/2,\delta)\rightarrow(0,\delta)\rightarrow(0,0). \tag{29}$$

This loop followed by the similar loop in the (θ_2,ϕ_2) space yields the $e^{i\delta}$ gate as

$$\begin{aligned}(\theta_1,\phi_1,\theta_2,\phi_2):(0,0,0,0)&\rightarrow(0,0,\pi/2,0)\rightarrow(0,0,\pi/2,\delta)\\ &\rightarrow(0,0,0,\delta)\rightarrow(0,0,0,0)\\ &\rightarrow(\pi/2,0,0,0)\rightarrow(\pi/2,\delta,0,0)\\ &\rightarrow(0,\delta,0,0)\rightarrow(0,0,0,0).\end{aligned} \tag{30}$$

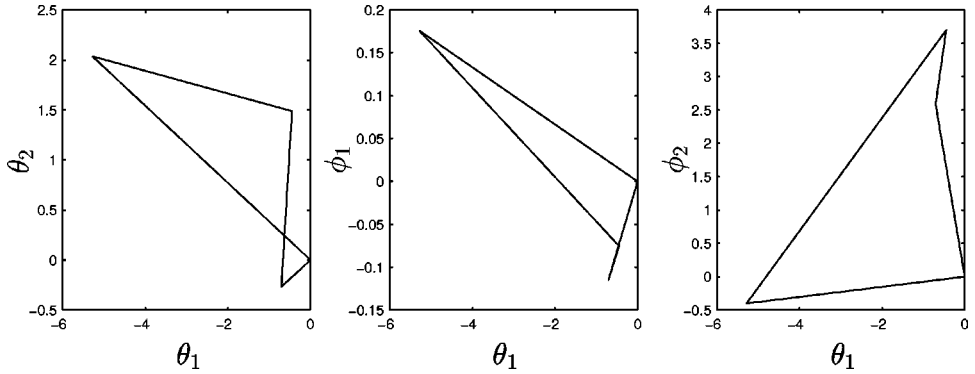

FIG. 2. Loop in parameter space that gives the Hadamard gate (in dimensionless units).

TABLE I. Loop of Fig. 2 numerically in dimensionless units.

Node	θ_1	θ_2	ϕ_1	ϕ_2
Begin	0	0	0	0
1	−5.28	2.04	0.18	−0.40
2	−0.44	1.49	−0.08	3.70
3	−0.70	−0.27	−0.11	2.59
End	0	0	0	0

TABLE II. Loop of Fig. 3 numerically in dimensionless units.

Node	θ_1	θ_2	ϕ_1	ϕ_2
Begin	0	0	0	0
1	−2.03	1.31	0.80	−1.16
2	1.21	1.18	−2.35	0.57
3	2.54	0.66	−0.49	0.96
End	0	0	0	0

Finally, the controlled-phase gate $U(\Theta)=\exp(i\Theta|11\rangle\langle 11|)$ can be written as

$$(\theta_2^a,\xi):(0,0)\rightarrow(\pi/2,0)\rightarrow(\pi/2,\Theta)\rightarrow(0,\Theta)\rightarrow(0,0). \tag{31}$$

IV. NUMERICAL METHOD

Now we adopt a systematic approach to actually construct the arbitrary quantum gates. The arbitrary one- and two-qubit gates are constructed in a three-state model, that is, in a way the simplest possible realization for HQC, while still maintaining the tensor-product structure necessary for exponential speed up. It has not been shown previously how to construct the CNOT, let alone the two-qubit Fourier transform in a single loop. Hence, we resort to numerical methods. Since it is extremely difficult to see which single loop results in a given unitary operator, our approach will be that of variational calculus.

We convert the inverse problem, i.e., which loop corresponds to a given unitary operator, to an optimization problem. The problem of finding the unitary operator for a given loop is straightforward. Keeping the basepoint of the holonomy loop fixed, we let the midpoints vary. Owing to the 2π periodicity, the loops can end either in the origin or at any point that is modulo (2π).

The space of all possible loops is denoted by $\mathcal{V}$. We shall restrict the variational task to the space of polygonal paths $\mathcal{V}_k$, where k is the number of vertices in the path excluding the basepoint. Naturally, we have $\mathcal{V}_k\subset\mathcal{V}$ such that we are not guaranteed to find the best possible solution among all the loops, but provided that we use a good optimization method, we may expect to find the best solution in the limited space $\mathcal{V}_k$. Since the dimension of the variational space increases with k, one is forced to use as low a k as possible. For instance, for one-qubit gates, the dimension is $4k$. In the case of two-qubit gates, the dimension is $9k$. Low k appears to be desirable for experimental reasons as well.

Formally, the optimization problem is to find a $\tilde{\gamma}$, such that

$$f(\gamma)=\|\hat{U}-U_\gamma\|_F \tag{32}$$

is minimized over all $\gamma\in\mathcal{V}_k$. We naturally hope the minimum value to be zero. Here $\|\cdot\|_F$ is the so-called Frobenius trace norm defined by $\|A\|_F=\sqrt{\mathrm{Tr}(A^\dagger A)}$. We could employ the well-known conjugate-gradient method to solve the task at hand, but this method, or any other derivative-based method, is not expected to perform well in the present problem due to the complicated structure of the objective function. Hence we will use the robust polytope algorithm [14].

We have plotted a sample 2D section of the optimization space in Fig. 1. The axes represent two orthogonal directions in the optimization space of a certain two-qubit gate. The x axis was obtained by interpolating between two known minima, whereas the y axis was chosen randomly. One can readily verify from the figure that the optimization task is indeed extremely hard.

The calculation of the holonomy requires evaluating the ordered product in Eq. (8). The method used in the numerical algorithm is to simply write the ordered product in a finite-difference approximation by considering the connection components as being constant over a small difference in the parameters $\delta\gamma_i$, i.e.,

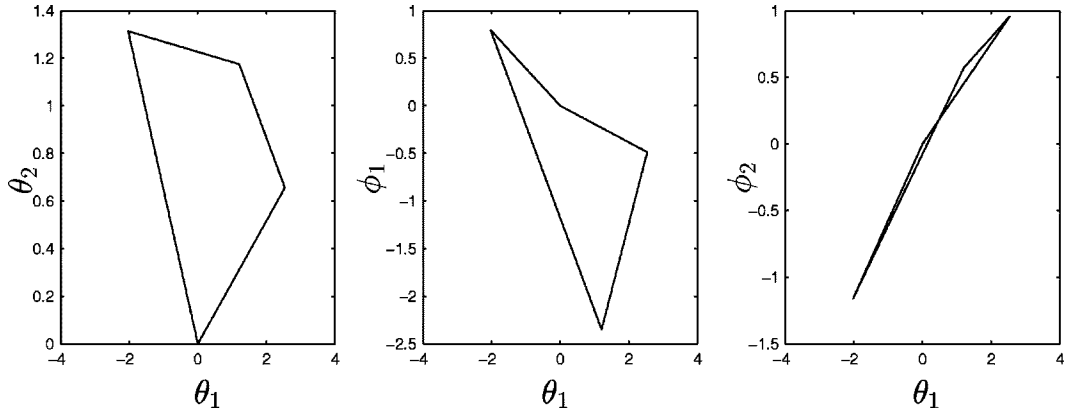

FIG. 3. Loop in parameter space that yields the gate $U=e^i\exp[i(\pi/7)\sigma_z]\exp[i(1/3)\sigma_y]\exp i\sigma_z$ (dimensionless units).

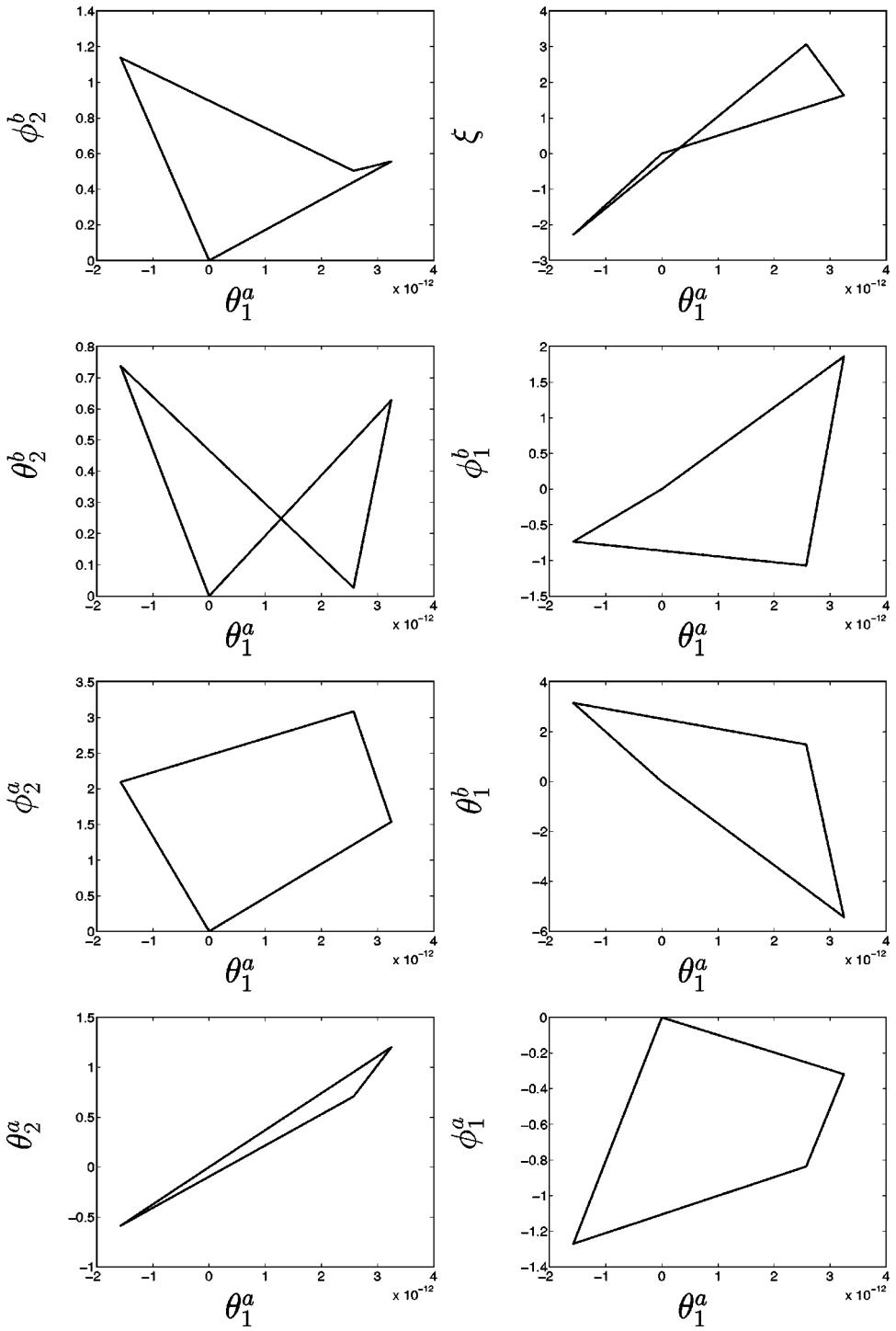

FIG. 4. Loop in parameter space that gives the controlled-NOT gate. Here $\gamma_{\mathrm{CNOT}} \in \mathcal{V}_3$ and the error is below 10^{-13} (dimensionless units).

$$U_\gamma \approx \exp(-\mathcal{A}_i(\gamma_n)\,\delta\gamma_n^i)\cdots\exp(-\mathcal{A}_i(\gamma_1)\,\delta\gamma_1^i). \quad (33)$$

Throughout the study we used 200 discretization points per edge, i.e., $n = 200\times(k+1)$.

V. RESULTS

First, we attempted to find a loop that yields the Hadamard gate. Using a random initial configuration, we obtained the results that are plotted in Fig. 2. The error function $f(\gamma)$ had a value smaller than 10^{-8} at the numerical optimum. The plot represents all the possible projections on two perpendicular axes (the horizontal axis is always θ_1) in the four-dimensional space. Note that this optimization was carried out in $\mathcal{V}_3$, meaning that there are three vertices other than the reference point. The results do not take advantage of the 2π periodicity. We have also included the data points in Table I. It is impressive that such a simple control loop yields the gate. Furthermore, this is just one implementation of the Hadamard gate. It is possible to find many different ones.

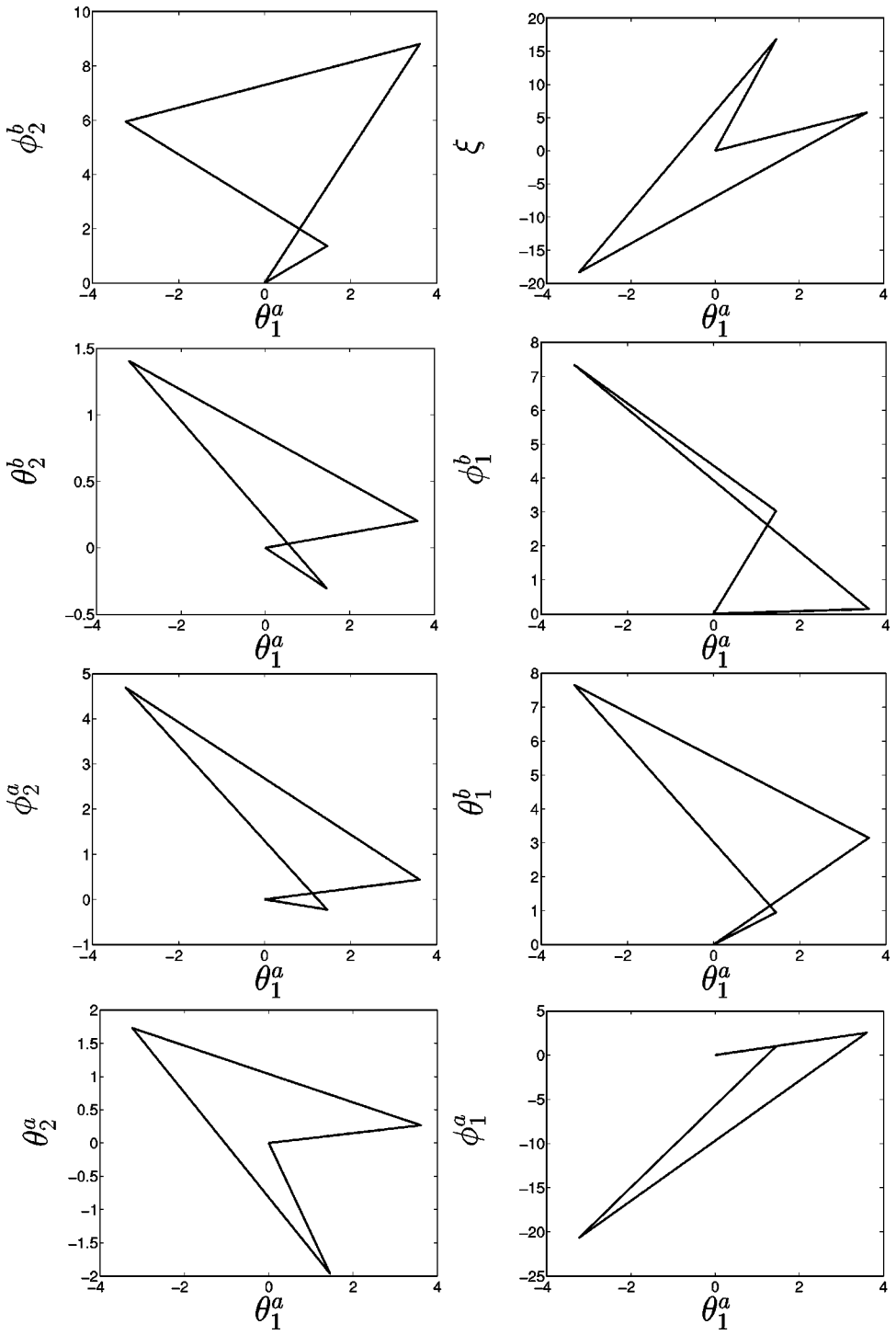

FIG. 5. Loop in parameter space which realizes the SWAP gate. Here the error is below 10^{-13}. In this case, the variational space is $\mathcal{V}_5$ (in dimensionless units).

Another example of one-qubit gates is given in Fig. 3 and in Table II. The gate that we tried to implement was now chosen arbitrarily to be $U = e^i \exp[i(\pi/7)\sigma_z]\exp[i(1/3)\sigma_y]\exp i\sigma_z$. Again, the error was well below 10^{-8} at the optimum. We argue that our method is capable of finding any one-qubit gate. These results are not very enlightening as such, but should nevertheless clearly prove the strength of the technique.

We also found several implementations for two-qubit gates. Figure 4 presents the loop $\gamma_{\mathrm{CNOT}} \in \mathcal{V}_3$ that produces the CNOT. We observe, however, that again the minimization resulted in an accurate solution. The minimization landscape is just as rough in the case of two qubits. Now, of course, the dimension of $\mathcal{V}_3$ is 24.

We also found an implementation of the SWAP gate given in Fig. 5.

Finally, it is interesting to observe that even the two-qubit quantum Fourier transform can be performed easily. The resulting loop is presented in Fig. 6. It is remarkable that such a simple single loop yields a two-qubit quantum Fourier transform. We used only three vertices, but were still able to

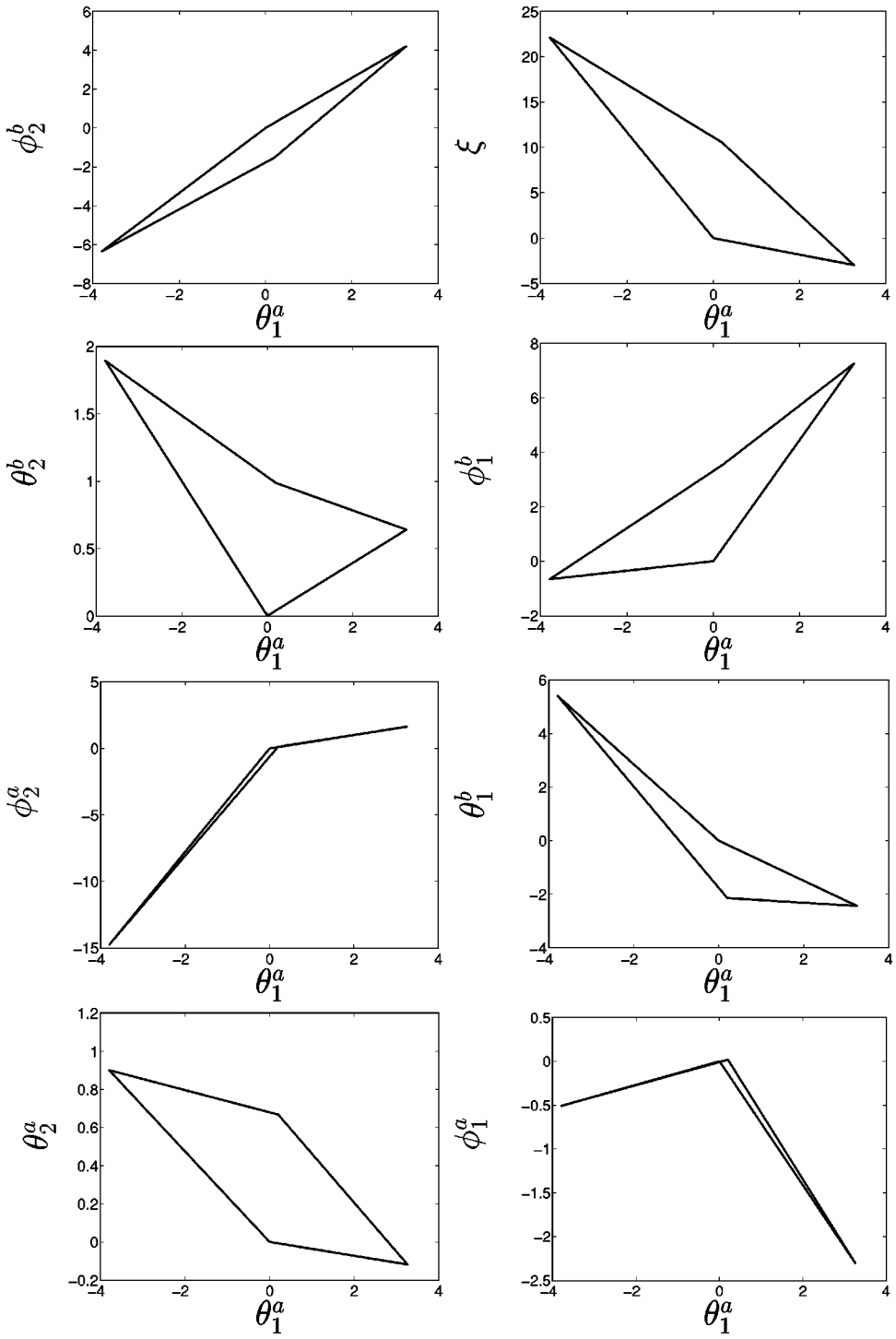

FIG. 6. Loop γ_{Fourier}. The error is below 10^{-13} (dimensionless units).

find an acceptable solution. We argue that the error can be made arbitrarily small for any two-qubit gate.

VI. DISCUSSION

The realization of arbitrary one- and two-qubit gates in the context of holonomic quantum computation has been demonstrated. By restricting the loops in the control manifold within a polygon with *k* vertices, it becomes possible to cast the realization problem to a finite-dimensional variational problem. We have shown explicitly that some useful two-qubit gates are realized by a single loop.

A possible improvement of the present scenario would be to minimize the length of the path realizing a given gate. This can be carried out by introducing an appropriate penalty or barrier function and the Fubini-Study metric in the control manifold $\mathbb{C}P^2$. This optimization program is under progress and will be reported elsewhere.

ACKNOWLEDGMENTS

A.O.N. would like to thank the Research Foundation of Helsinki University of Technology and the Graduate School

in Technical Physics for financial support; M.N. thanks the Helsinki University of Technology for financial support, and he is also grateful for partial support of a Grant-in-Aid from the Ministry of Education, Culture, Sports, Science, and Technology, Japan (Project Nos. 14540346 and 13135215); M.M.S. acknowledges the Academy of Finland for a Research Grant in Theoretical Materials Physics.

---

[1] J. Gruska, *Quantum Computing* (McGraw-Hill, New York, 1999).
[2] M.A. Nielsen and I.L. Chuang, *Quantum Computation and Quantum Information* (Cambridge University Press, Cambridge, 2000).
[3] A. Galindo and M.A. Martin-Delgado, Rev. Mod. Phys. **74**, 347 (2002).
[4] P. Zanardi and M. Rasetti, Phys. Lett. A **264**, 94 (1999).
[5] K. Fujii, Rep. Math. Phys. **48**, 75 (2001).
[6] D. Ellinas and J. Pachos, Phys. Rev. A **64**, 022310 (2001).
[7] J. Pachos, P. Zanardi, and M. Rasetti, Phys. Rev. A **61**, 010305(R) (1999).
[8] J. Pachos and P. Zanardi, Int. J. Mod. Phys. B **15**, 1257 (2001).
[9] J. Pachos and S. Chountasis, Phys. Rev. A **62**, 052318 (2000).
[10] M. Berry, Proc. R. Soc. London, Ser. A **392**, 45 (1984).
[11] A. Zee, Phys. Rev. A **38**, 1 (1988).
[12] F. Wilczek and A. Zee, Phys. Rev. Lett. **52**, 2111 (1984).
[13] M. Nakahara, *Geometry, Topology and Physics* (IOP, Bristol, 1990).
[14] J.C. Lagarias, J.A. Reeds, M.H. Wright, and P.E. Wright, SIAM J. Optim. **9**, 112 (1998).

Reprinted with permission from the publisher.
In: Quantum Information and Computation 2002.
Vol. 2, Special, pp. 560–577.

OPTIMAL HOLONOMIC QUANTUM GATES

ANTTI O. NISKANEN
Materials Physics Laboratory, Helsinki University of Technology,
P. O. Box 2200 (Technical Physics), FIN-02015 HUT, Finland

MIKIO NAKAHARA*
Department of Physics, Kinki University
Higashi-Osaka 577-8502, Japan

MARTTI M. SALOMAA
Materials Physics Laboratory, Helsinki University of Technology,
P. O. Box 2200 (Technical Physics), FIN-02015 HUT, Finland

Received September 30, 2002

We study the construction of holonomy loops numerically in a realization-independent model of holonomic quantum computation. The aim is twofold. First, we present our technique of finding the suitable loop in the control manifold for any one-qubit and two-qubit unitary gates. Second, we develop the formalism further and add a penalty term for the length of the loop, thereby aiming to minimize the execution time for the quantum computation. Our method provides a general means by which holonomy loops can be realized in an experimental setup. Since holonomic quantum computation is adiabatic, optimizing with respect to the length of the loop may prove crucial.

Keywords: quantum geometric and topological computations, numerical optimization

Communicated by: R Cleve

1. Introduction

We study the implementation of a quantum computer numerically using so-called non-Abelian holonomies. Holonomic quantum computation (HQC) was suggested by Zanardi and Rasetti in Ref. [1] and further developed, e.g., in Refs. [2, 3, 4, 5, 6, 7, 8]. In order to build a working quantum computer of N qubits, one has to be able to produce any unitary operations in $U(2^N)$, i.e. time-evolutions, on the qubits. In holonomic quantum computation, these operations are achieved by selecting a degenerate qubit system and allowing for an adiabatic time-development that does not change the degeneracy structure. Even though the Hamiltonian in this subspace is completely trivial, it turns out that a non-Abelian and irreducible gauge potential appears, using which any unitary evolution can be carried out. As the word holonomy itself suggests, we drive the system around loops in the control-parameter space (or

*Also at the Materials Physics Laboratory, Helsinki University of Technology, P. O. Box 2200 (Technical Physics), FIN-02015 HUT, Finland.

manifold) and after each loop there is a nontrivial change in the state of the system. This is a generalization of the famous Berry phase [9] to a degenerate system.

This paper is organized as follows. In Section 2 we first review the concept of non-Abelian holonomy. Then in Section 3 we introduce our realization-independent model. Namely, we consider the general setting for non-Abelian holonomy and unitary gate construction in a three-state system. This part applies to a much wider class of research topics in modern physics than just quantum computation. Many physical systems may be suitable for the actual implementation of this model. Section 4 is the main part of the work. There we first consider the generic algorithm for numerically finding implementations of holonomic quantum gates. We have previously studied the computational construction of holonomic quantum gates in Ref. [10]. There we limited our attention, however, to the solution of the inversion problem itself; we showed that one can numerically find a holonomy loop corresponding to a desired gate. Here we further extend the concept to actually optimizing with respect to the length of the path. We find some new and more efficient implementations of holonomic quantum gates. Because holonomic quantum computation is adiabatic and hence time-consuming, it is important to optimize the construction of quantum gates. We argue that our optimization method could also be extended to dynamical quantum computation. Section 5 is devoted to discussion.

2. Non-Abelian Holonomy

We briefly outline the concept of non-Abelian holonomy associated with adiabatic change of control parameters. This is necessary not only to establish notation conventions but also to rectify certain confusion appearing in the literature on the definition of the holonomy operator. The concept was first introduced by Wilczek and Zee in Ref. [11]. Other excellent references are Zee [12] and Mostafazadeh [13].

Let us consider a family of Hamiltonians $\{H_\lambda\}$ parameterized by $\lambda \in M$, where M is a manifold called the control manifold. The local coordinate of λ is denoted by λ^i $(1 \le i \le m = \dim M)$. We assume that there are only a finite number of eigenvalues $\varepsilon_k(\lambda)$ $(1 \le k \le R)$ for an arbitrary point λ of M and that no level crossings take place through all of M. The eigenvalue $\varepsilon_k(\lambda)$ is assumed to be g_k-fold degenerate independently of λ. This degenerate subspace will be denoted by $\mathcal{H}_k(\lambda)$. Then the Hamiltonian is expressed as an $N \times N$ hermitian matrix, where $N = \sum_{k=1}^{R} g_k$.

Let us denote the orthonormal basis vectors of $\mathcal{H}_k(\lambda)$ as $\{|k\alpha;\lambda\rangle\}$;

$$H_\lambda |k\alpha;\lambda\rangle = \varepsilon_k(\lambda)|k\alpha;\lambda\rangle, \qquad \langle j\alpha;\lambda|k\beta;\lambda\rangle = \delta_{jk}\delta_{\alpha\beta}. \tag{1}$$

Note that there are $U(g_k)$ degrees of freedom in choosing the set of basis vectors $\{|k\alpha;\lambda\rangle\}$.

Suppose the control parameter λ is varied continuously over M. It is assumed that the variation is so slow that the adiabaticity condition is fulfilled, i.e., transitions between the different energy levels are negligible. We will be concerned with a particular subspace, the ground state $\mathcal{H}_1$, for example. We will drop the index $k = 1$ hereafter to simplify the notation. Let us take a basis vector $|\alpha;\lambda(0)\rangle$ at $t = 0$ and study how the state develops as a function of time. We may assume that $\varepsilon(\lambda) = 0$ for any $\lambda \in M$, possibly after first readjusting the

zero-point of the energy. Now our task is to solve the Schrödinger equation

$$i\frac{d}{dt}|\psi_\alpha(t)\rangle = H_{\lambda(t)}|\psi_\alpha(t)\rangle \tag{2}$$

with the initial condition $|\psi_\alpha(0)\rangle = |\alpha;\lambda(0)\rangle$. It follows from the adiabaticity condition that the solution of the above equation may always be expanded in the form

$$|\psi_\alpha(t)\rangle = \sum_{\beta=1}^{g} |\beta;\lambda(t)\rangle U_{\beta\alpha}(t). \tag{3}$$

The unitarity of the matrix $U_{\beta\alpha}$ follows from the condition $\langle\psi_\beta(t)|\psi_\alpha(t)\rangle = \delta_{\beta\alpha}$. By substituting Eq. (3) into Eq. (2), we find that

$$\dot{U}_{\alpha\beta} = -\sum_{\gamma=1}^{g} \left\langle \beta;\lambda(t) \left| \frac{d}{dt} \right| \gamma;\lambda(t) \right\rangle U_{\gamma\alpha}. \tag{4}$$

The formal solution of the above equation is readily obtained as

$$\begin{aligned} U(t) &= \mathcal{T}\exp\left(-\int_0^t A(\tau)d\tau\right) \\ &= I - \int_0^t A(\tau)d\tau + \int_0^t d\tau \int_0^\tau d\tau' A(\tau)A(\tau') + \ldots \end{aligned} \tag{5}$$

where $\mathcal{T}$ is the time-ordering operator and

$$A_{\beta\alpha}(t) = \left\langle \beta;\lambda(t) \left| \frac{d}{dt} \right| \alpha;\lambda(t) \right\rangle. \tag{6}$$

Let us define the Lie-algebra-valued connection one-form

$$\mathcal{A}_{\beta\alpha} = \left\langle \beta;\lambda(t) \left| \frac{\partial}{\partial\lambda^i} \right| \alpha;\lambda(t) \right\rangle d\lambda^i \tag{7}$$

by which $U(t)$ may be expressed as

$$U(t) = \mathcal{P}\exp\left(-\int_{\lambda(0)}^{\lambda(t)} \mathcal{A}\right), \tag{8}$$

where $\mathcal{P}$ is the path-ordering operator. Note that $\mathcal{A}$ is anti-Hermitian; $\mathcal{A}^\dagger = -\mathcal{A}$.

Suppose that the path $\lambda(t)$ is a loop $\gamma(t)$ $(0 \le t \le T)$ in M, such that $\gamma(0) = \gamma(T) = \lambda_0$. Then it is found after traversing the loop γ that the resulting state is

$$|\psi_\alpha(T)\rangle = \sum_{\beta=1}^{g} |\beta;\lambda_0\rangle U_{\beta\alpha}(T). \tag{9}$$

The unitary matrix

$$U_\gamma \equiv U(T) = \mathcal{P}\exp\left(-\oint_\gamma \mathcal{A}\right) \tag{10}$$

is called the holonomy associated with the loop γ. It is clear that U_γ is independent of the parameterization for the loop but only depends on the geometric image of the loop in M.

Suppose the initial state is a superposition

$$|\psi(0)\rangle = \sum_{\alpha=1}^{g} c_\alpha(\text{in})|\alpha;\lambda_0\rangle.$$

Then the linearity of the Schrödinger equation leads to the final state

$$\begin{aligned} |\psi(T)\rangle &\equiv \sum_{\beta=1}^{g} c_\beta(\text{out})|\beta;\lambda_0\rangle \\ &= \sum_{\beta=1}^{g} |\beta;\lambda_0\rangle U_{\beta\alpha}(T)c_\alpha(\text{in}) \end{aligned} \tag{11}$$

which implies that $c_\beta(\text{out}) = \sum_\alpha U_{\beta\alpha}(T)c_\alpha(\text{in})$. Thus, we confirm that U is indeed the matrix representation of the time-evolution operator with the standard ordering of indices. In this context, it is crucial that the summation in Eq. (3) goes over the first index β.

The space of all the loops based at λ_0 is denoted as

$$L_{\lambda_0}(M) = \{\gamma : [0,T] \to M | \gamma(0) = \gamma(T) = \lambda_0\}. \tag{12}$$

The set of the holonomy

$$\text{Hol}(\mathcal{A};\lambda_0) = \{U_\gamma |\ \gamma \in L_{\lambda_0}(M)\} \tag{13}$$

has a group structure and is called the holonomy group. The product is just an ordinary matrix product. It is easily seen that $\text{Hol}(\mathcal{A};\lambda_0)$ is isomorphic to $\text{Hol}(\mathcal{A};\lambda_1)$ for any $\lambda_0, \lambda_1 \in M$ if M is arcwise-connected. It is clear that $\text{Hol}(\mathcal{A}) \subset U(g)$ since $U(g)$ is the maximal possible group in $\mathbb{C}^g$, which preserves the norm of a vector. The connection $\mathcal{A}$ is called irreducible if $\text{Hol}(\mathcal{A}) = U(g)$. We assume that our control manifold is always arcwise-connected and we omit the explicit quotation of the base point from now on.

3. Three-State Model and Quantum-Gate Construction

3.1. *One-qubit gates*

To realize the idea outlined in the previous section, we employ a simple model Hamiltonian called the three-state model as the basic building block for our strategy. This is a 3-dimensional Hamiltonian defined by

$$H_{\lambda_0} = \epsilon|2\rangle\langle 2| = \begin{pmatrix} \epsilon & 0 & 0 \\ 0 & 0 & 0 \\ 0 & 0 & 0 \end{pmatrix} \tag{14}$$

at the base point $\lambda_0 \in M$. The first column (row) of the matrix refers to the auxiliary state $|2\rangle$ with an energy $\epsilon > 0$ while the second and the third columns (rows) refer to the vectors $|0\rangle$ and $|1\rangle$, respectively, having vanishing energy. The computational subspace (qubit) consists of

the last two vectors. In spite of the fact that the qubit operation takes place in this subspace, the auxiliary state $|2\rangle$ is necessary since the Hamiltonian trivially vanishes otherwise.

The control manifold M of the Hamiltonian (14) is the complex projective space $\mathbb{C}P^2 = U(3)/(U(2)\times U(1))$. This is seen most directly as follows: The most general form of the isospectral deformation of the Hamiltonian is of the form $H_\gamma \equiv W_\gamma H_{\lambda_0} W_\gamma^\dagger$, where $W_\gamma \in U(3)$. Note, however, that not all the elements of $U(3)$ are independent. It is clear that H_γ is independent of the overall phase of W_γ, which reduces the degrees of freedom from $U(3)$ to $U(3)/U(1) \cong SU(3)$. Moreover, any element of $SU(3)$ may be decomposed into a product of three $SU(2)$ matrices as follows

$$W_\gamma = \underbrace{\begin{pmatrix} \bar\beta_1 & \bar\alpha_1 & 0 \\ -\alpha_1 & \beta_1 & 0 \\ 0 & 0 & 1 \end{pmatrix}}_{U_1} \underbrace{\begin{pmatrix} \bar\beta_2 & 0 & \bar\alpha_2 \\ 0 & 1 & 0 \\ -\alpha_2 & 0 & \beta_2 \end{pmatrix}}_{U_2} \underbrace{\begin{pmatrix} 1 & 0 & 0 \\ 0 & \bar\beta_3 & \bar\alpha_3 \\ 0 & -\alpha_3 & \beta_3 \end{pmatrix}}_{U_3}, \tag{15}$$

where the α_j and the β_j satify the relation $|\alpha_j|^2 + |\beta_j|^2 = 1$. This decompostion is know as the Givens decomposition. We put $\alpha_j = e^{i\phi_j}\sin\theta_j$ and $\beta_j = e^{i\psi_j}\cos\theta_j$. It is clear that H_γ is independent of U_3 since $U_3 H_{\lambda_0} U_3^\dagger = H_{\lambda_0}$. This further reduces the physical degrees of freedom to $SU(3)/SU(2) \cong S^5$. This is not the end of the story, however, since $\mathbb{C}P^2$ is real four-dimensional and we have to get rid of a phase from S^5. Accordingly, we have to "gauge away" two redundant parameters in the product U_1U_2 which contains altogether six parameters. These redundancies are easily identified by writing the product out explicitly. The result depends only on the combination $\phi_2 - \psi_2$ and not on individual parameters. Accordingly, we may redefine ϕ_2 as $\phi_2 - \psi_2$ to eliminate ψ_2. Furthermore, after this redefinition we find that the Hamiltonian depends only on $\phi_1 - \psi_1$ and $\phi_2 - \psi_1$ and hence ψ_1 may also be subsumed by redefining ϕ_1 and ϕ_2, which reduces the independent degrees of freedom down to $\mathbb{C}P^2 \cong S^5/S^1$.

Let $[z^1, z^2, z^3]$ be the homogeneous coordinate of $\mathbb{C}P^2$ and $(1, \xi_1, \xi_2)$ be the corresponding inhomogeneous coordinate, where $\xi_1 = z^2/z^1, \xi^2 = z^3/z^1$ in the coordinate neighborhood with $z^1 \neq 0$. If we write $\xi_k = r_k e^{i\varphi_k}$ the above correspondence, i.e. the embedding of $\mathbb{C}P^2$ into $U(3)$, is explicitly given by $\theta_k = \tan^{-1} r_k$ and $\phi_k = \varphi_k$.

The connection coefficients are easily calculated in the present model and are given by

$$\mathcal{A}_{\theta_1} = \begin{pmatrix} 0 & -\sin\theta_2 e^{-i(\phi_2-\phi_1)} \\ \sin\theta_2 e^{i(\phi_2-\phi_1)} & 0 \end{pmatrix}, \tag{16}$$

$$\mathcal{A}_{\theta_2} = \begin{pmatrix} 0 & 0 \\ 0 & 0 \end{pmatrix}, \tag{17}$$

$$\mathcal{A}_{\phi_1} = \begin{pmatrix} -i\sin^2\theta_1 & -\frac{i}{2}\sin 2\theta_1 \sin\theta_2 e^{i(\phi_1-\phi_2)} \\ -\frac{i}{2}\sin 2\theta_1 \sin\theta_2 e^{i(\phi_2-\phi_1)} & i\sin^2\theta_2 \sin^2\theta_1 \end{pmatrix}, \tag{18}$$

$$\mathcal{A}_{\phi_2} = \begin{pmatrix} 0 & 0 \\ 0 & -i\sin^2\theta_2 \end{pmatrix}, \tag{19}$$

where the first column (row) refers to $|0\rangle$ while the second one refers to $|1\rangle$. Using these connection coefficients, it is possible to evaluate the holonomy associated with a loop γ as

$$U_\gamma = \mathcal{P}\exp\left(-\oint_\gamma (\mathcal{A}_{\theta_1}d\theta_1 + \mathcal{A}_{\theta_2}d\theta_2 + \mathcal{A}_{\phi_1}d\phi_1 + \mathcal{A}_{\phi_2}d\phi_2)\right). \tag{20}$$

Now our task is to find a loop that yields a given unitary matrix as its holonomy.

3.2. *Two-qubit gates*

Let us next consider a two-qubit reference Hamiltonian

$$H_{\lambda_0}^{\text{2-qubit}} = H_{\lambda_0}^a \otimes I_3 + I_3 \otimes H_{\lambda_0}^b, \tag{21}$$

where $H_\lambda^{a,b}$ are three-state Hamiltonians and I_3 is the 3×3 unit matrix. Generalization to an arbitrary N-qubit system is obvious. The Hamiltonian scales as 3^N, instead of the 2^N in the present model.

We want to preserve the multipartite structure of the system in constructing the holonomy. For this purpose, we separate the unitary transformation into a tensor product of single-qubit transformations $(W_\gamma^a \otimes W_\gamma^b)$ and a purely two-qubit rotation $W_\gamma^{\text{2-qubit}}$ which cannot be reduced into a tensor product of single-qubit transformations. Therefore, we write the isospectral deformation for a given loop γ as

$$H_\gamma^{\text{2-qubit}} = W_\gamma^{\text{2-qubit}}(W_\gamma^a \otimes W_\gamma^b)H_{\lambda_0}^{\text{2-qubit}}(W_\gamma^a \otimes W_\gamma^b)^\dagger W_\gamma^{\text{2-qubit}\dagger}. \tag{22}$$

The advantage of expressing the unitary matrix in this form is easily verified when we write down the connection coefficients for the one-qubit coordinates. Namely, the two-qubit transformation does not affect the one-qubit transformation at all;

$$\begin{aligned}\mathcal{A}_{i,\alpha\beta} &= \left\langle \alpha;\lambda \left| W_\gamma^\dagger \frac{\partial}{\partial\gamma^i} W_\gamma \right| \beta;\lambda \right\rangle \\ &= \left\langle \alpha;\lambda \left| (W_\gamma^a \otimes W_\gamma^b)^\dagger \frac{\partial}{\partial\gamma^i}(W_\gamma^a \otimes W_\gamma^b) \right| \beta;\lambda \right\rangle,\end{aligned}$$

where γ^i denotes a one-qubit coordinate.

There is a large number of possible choices for $W_\gamma^{\text{2-qubit}}$, depending on the physical realization of the present scenario. To keep our analysis as concrete as possible, we have made the simplest choice

$$W_\gamma^{\text{2-qubit}} = W_\xi \equiv e^{i\xi|11\rangle\langle 11|} \tag{23}$$

for our two-qubit unitary rotation. Let

$$\begin{aligned}H_\gamma' &= H_\gamma^a \otimes I_3 + I_3 \otimes H_\gamma^b \\ &= \begin{pmatrix}
h_{11}^a+h_{11}^b & h_{12}^b & h_{13}^b & h_{12}^a & 0 & 0 & h_{13}^a & 0 & 0 \\
h_{21}^b & h_{11}^a+h_{22}^b & h_{23}^b & 0 & h_{12}^a & 0 & 0 & h_{13}^a & 0 \\
h_{31}^b & h_{32}^b & h_{11}^a+h_{33}^b & 0 & 0 & h_{12}^a & 0 & 0 & h_{13}^b \\
h_{21}^a & 0 & 0 & h_{22}^a+h_{11}^b & h_{12}^b & h_{13}^b & h_{23}^a & 0 & 0 \\
0 & h_{21}^a & 0 & h_{21}^b & h_{22}^a+h_{22}^b & h_{23}^b & 0 & h_{23}^a & 0 \\
0 & 0 & h_{21}^a & h_{31}^b & h_{32}^b & h_{22}^a+h_{33}^b & 0 & 0 & h_{23}^a \\
h_{31}^a & 0 & 0 & h_{32}^a & 0 & 0 & h_{33}^a+h_{11}^b & h_{12}^b & h_{13}^b \\
0 & h_{31}^a & 0 & 0 & h_{32}^a & 0 & h_{21}^b & h_{33}^a+h_{22}^b & h_{23}^b \\
0 & 0 & h_{31}^a & 0 & 0 & h_{32}^a & h_{31}^b & h_{32}^b & h_{33}^a+h_{33}^b
\end{pmatrix}.\end{aligned}$$

be a two-qubit Hamiltonian before W_ξ is applied. Then after the application of W_ξ to H'_γ we obtain for the full Hamiltonian

$$\begin{aligned} H_\gamma^{\text{2-qubit}} &= W_\xi H'_\gamma W_\xi^\dagger \\ &= \begin{pmatrix} h_{11}^a+h_{11}^b & h_{12}^b & h_{13}^b & h_{12}^a & 0 & 0 & h_{13}^a & 0 & 0 \\ h_{21}^b & h_{11}^a+h_{22}^b & h_{23}^b & 0 & h_{12}^a & 0 & 0 & h_{13}^a & 0 \\ h_{31}^b & h_{32}^b & h_{11}^a+h_{33}^b & 0 & 0 & h_{12}^a & 0 & 0 & h_{13}^b e^{-i\xi} \\ h_{21}^a & 0 & 0 & h_{22}^a+h_{11}^b & h_{12}^b & h_{13}^b & h_{23}^a & 0 & 0 \\ 0 & h_{21}^a & 0 & h_{21}^b & h_{22}^a+h_{22}^b & h_{23}^b & 0 & h_{23}^a & 0 \\ 0 & 0 & h_{21}^a & h_{31}^b & h_{32}^b & h_{22}^a+h_{33}^b & 0 & 0 & h_{23}^a e^{-i\xi} \\ h_{31}^a & 0 & 0 & h_{32}^a & 0 & 0 & h_{33}^a+h_{11}^b & h_{12}^b & h_{13}^b e^{-i\xi} \\ 0 & h_{31}^a & 0 & 0 & h_{32}^a & 0 & h_{21}^b & h_{33}^a+h_{22}^b & h_{23}^b e^{-i\xi} \\ 0 & 0 & h_{31}^a e^{i\xi} & 0 & 0 & h_{32}^a e^{i\xi} & h_{31}^b e^{i\xi} & h_{32}^b e^{i\xi} & h_{33}^a+h_{33}^b \end{pmatrix}. \end{aligned} \tag{24}$$

As for the connection, we find

$$\mathcal{A}_\xi = \begin{pmatrix} 0 & 0 & 0 & 0 \\ 0 & 0 & 0 & 0 \\ 0 & 0 & 0 & 0 \\ 0 & 0 & 0 & i\cos^2\theta_2^a \cos^2\theta_2^b \end{pmatrix} \tag{25}$$

where the rows and columns are ordered with respect to the basis $\{|00\rangle, |01\rangle, |10\rangle, |11\rangle\}$. It should be apparent from the above analysis that we can construct an arbitrary controlled phase-shift gate with the help of a loop in the (θ_a^2, ξ)- or (θ_b^2, ξ)-space. Accordingly, this yields the CNOT gate with one-qubit operations, as shown below.

3.3. *Some Examples*

Prior to proceeding to present in the next section the numerical prescription to construct arbitrary one- and two-qubit gates, it is instructive to first work out some important examples whose loop can be constructed analytically. In particular, we will show that all the gates required for the proof of universality may be obtained within the present three-state model.

The first example is the $\pi/8$-gate,

$$U_{\pi/8} = \begin{pmatrix} 1 & 0 \\ 0 & e^{i\pi/8} \end{pmatrix}. \tag{26}$$

By inspecting the connection coefficients in Eqs. (16–19), we easily find that the loop

$$(\theta_2, \phi_2) \quad : \quad (0,0) \to (\pi/2, 0) \to (\pi/2, \pi/8) \to (0, \pi/8) \to (0,0). \tag{27}$$

yields the desired gate. Note that the loop is in the (θ_2, ϕ_2)-plane and that all the other parameters are fixed at zero. Explicitly, we verify that

$$\begin{aligned} U_{\pi/8} &= \exp\left(\frac{\pi}{8}\,\mathcal{A}_{\phi_2}|_{\theta_2=0}\right) \exp\left(\frac{\pi}{2}\,\mathcal{A}_{\theta_2}|_{\phi_2=\pi/8}\right) \\ &\quad \times \exp\left(-\frac{\pi}{8}\,\mathcal{A}_{\phi_2}|_{\theta_2=\pi/2}\right) \exp\left(-\frac{\pi}{2}\,\mathcal{A}_{\theta_2}|_{\phi_2=0}\right) \\ &= \exp\left(-\frac{\pi}{8}\,\mathcal{A}_{\phi_2}|_{\theta_2=\pi/2}\right). \end{aligned} \tag{28}$$

The next example is the Hadamard gate

$$H = \frac{1}{\sqrt{2}} \begin{pmatrix} 1 & 1 \\ 1 & -1 \end{pmatrix}. \tag{29}$$

Instead of constructing H directly, we will rather choose to use the decomposition

$$H = e^{-i\pi/2} \exp\left(i\frac{\pi}{2}\sigma_z\right) \exp\left(i\frac{\pi}{4}\sigma_y\right).$$

It is easy to verify that the holonomy associated with the loop

$$(\theta_2, \theta_1) \quad : \quad (0,0) \to (\pi/2, 0) \to (\pi/2, \beta) \to (0, \beta) \to (0,0) \tag{30}$$

is $\exp(i\beta\sigma_y)$, while that associated with the loop

$$\begin{aligned} (\theta_1, \theta_2, \phi_1) \quad : \quad & (0,0,0) \to (\pi/2, 0, 0) \to (\pi/2, \pi/2, 0) \to (\pi/2, \pi/2, \alpha) \\ & \to (\pi/2, 0, \alpha) \to (0, 0, \alpha) \to (0,0,0) \end{aligned} \tag{31}$$

is $\exp(i\alpha\sigma_z)$. Here again, the rest of the parameters are fixed at zero. Finally, we construct the phase-shift gate $e^{i\delta}$, which is produced by a sequence of two loops. First we construct a gate similar to the δ-shift gate using (cf., the $\pi/8$-shift gate)

$$(\theta_1, \phi_1) \quad : \quad (0,0) \to (\pi/2, 0) \to (\pi/2, \delta) \to (0, \delta) \to (0,0). \tag{32}$$

This loop followed by the similar loop in the (θ_2, ϕ_2)-space yields the $e^{i\delta}$-gate as

$$\begin{aligned} & (\theta_1, \phi_1, \theta_2, \phi_2) : (0,0,0,0) \to (0,0,\pi/2,0) \to (0,0,\pi/2,\delta) \to (0,0,0,\delta) \\ & \to (0,0,0,0) \to (\pi/2,0,0,0) \to (\pi/2,\delta,0,0) \to (0,\delta,0,0) \to (0,0,0,0). \end{aligned} \tag{33}$$

Finally, the controlled-phase gate $U(\Theta) = \exp(i\Theta|11\rangle\langle 11|)$ can be implemented with the loop

$$(\theta_2^a, \xi) \quad : \quad (0,0) \to (\pi/2, 0) \to (\pi/2, \Theta) \to (0, \Theta) \to (0,0). \tag{34}$$

4. Numerical Results

4.1. *Loop-Finding Algorithm*

In this Section we numerically study the construction of holonomic quantum gates for the three-state model. The three-state model is in a way the simplest possible model for holonomic quantum computing while still maintaining the tensor-product structure which is necessary for exponential speed-up. We have previously shown [10] how to solve the inverse problem of finding loops corresponding to desired quantum-logic gates. We have presented several example solutions for various one- and two-qubit gates. We demonstrated, e.g., how to construct the Hadamard gate, the CNOT, the SWAP, and the two-qubit Fourier transform in a single loop. We concluded that our three-state model is capable of universal quantum computing.

Here we will extend the scenario by adding a penalty term for the length of the path. We will also introduce and test a method for optimizing with respect to the length directly but

with a penalty term arising due to excess deviation from the desired gate. In this manner one may efficiently combine loops. Even though these measures will not result in a change in the quantum-computational complexity, it may be possible to significantly reduce the multipliers in front of the highest-order terms in the expression for the CPU execution time. In other words, the big-O notation is the same, but nevertheless, much of the computation time may be saved.

First we review our basic algorithm and show some new example gates. Namely, each loop γ in the parameter space corresponds to a gate U_γ. We wish to solve the inverse problem; We look for a $\hat{\gamma}$ that corresponds to $\hat{U}$. We further restrict ourselves to the space of all polygonal loops. If $\mathcal{V}$ is the space of all possible loops with the given base point, then $\mathcal{V}_k$ will be the space of all those polygonal loops that have k vertices in addition to the base point. Here of course $\mathcal{V}_k \subset \mathcal{V}$. This problem can be formulated as an optimization problem. One needs to find $\hat{\gamma}$ such that

$$f(\gamma) = \|\hat{U} - U_\gamma\|_F \tag{35}$$

is minimized over all $\gamma \in \mathcal{V}_k$ We aim at the minimum value to be zero. Here $\|\cdot\|_F$ denotes the Frobenius norm defined as $\|A\|_F = \sqrt{\mathrm{Tr}\,(A^\dagger A)}$.

For one-qubit gates, the dimension is $4k$ whereas in the case of two-qubit gates the dimension is $9k$. We used the polytope algorithm [15] to solve this problem. The reason for employing this method is the extremely complicated structure of the objective function. In Fig. 1 we have plotted a 2D section of the function values. This figure was obtained by using the line joining two known minima of a certain one-qubit gate along with a randomly chosen perpendicular direction. Thus derivative-based methods are not expected to perform well.

The calculation of the holonomy requires evaluating the ordered product in Eq. (10). The method used in the numerical algorithm is to simply write the ordered product in a finite-difference approximation by considering the connection components as being constant over a small difference in the parameters $\delta\gamma_i$.

For instance, we attempted to find a loop corresponding to the Hadamard gate. We have previously given a different implementation of this gate [10]. The resulting loop is illustrated in Fig. 2. Note that this optimization was carried out in $\mathcal{V}_3$ meaning that there are three vertices other than the reference point. We have taken the origin to be this reference point. The length of this example loop is 12.01 in the Euclidean approximation. To give an example of a two-qubit gate, we have included in Fig. 3 a loop that yields the well-known two-qubit quantum version of the Fourier transform. This loop is again different from the example solutions of Ref. [10]. Thus one is convinced that the solution is by no means unique. For instance, the solution depends strongly on the initial configuration of the polytope algorithm. Hence, there is ample motivation to search for shorter loops.

To show more clearly the power of our technique, we have plotted in Fig. 4 the error as a function of function evaluations for three independent runs. The attempted logical operation was the Hadamard gate. We see that the convergence seems to be exponential. Moreover, a few hundred evaluations of $f(\gamma)$ is enough to achieve an error as low as 10^{-8}. We argue that one can achieve arbitrarily small errors by running the algorithm long enough. Numerical rounding errors will, though, complicate things slightly. It is important from the experimental point of view just to achieve low enough errors.

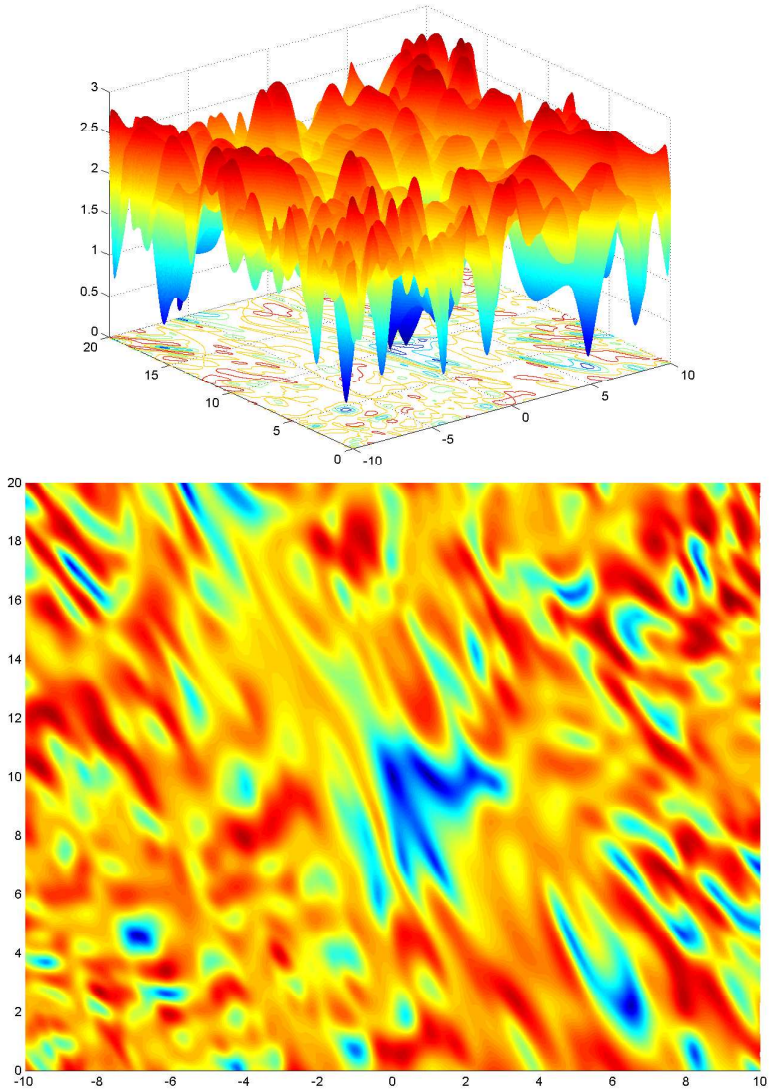

Fig. 1. 2D cross-section of the 12-dimensional objective function.

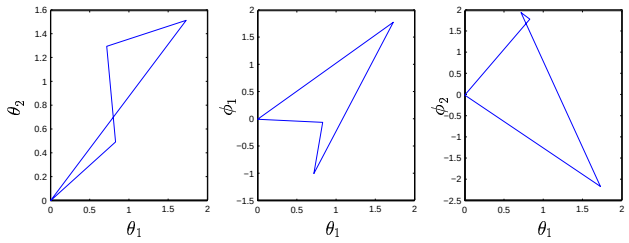

Fig. 2. Loop in the parameter space that implements the Hadamard gate with $L(\gamma_H) = 12.01$.

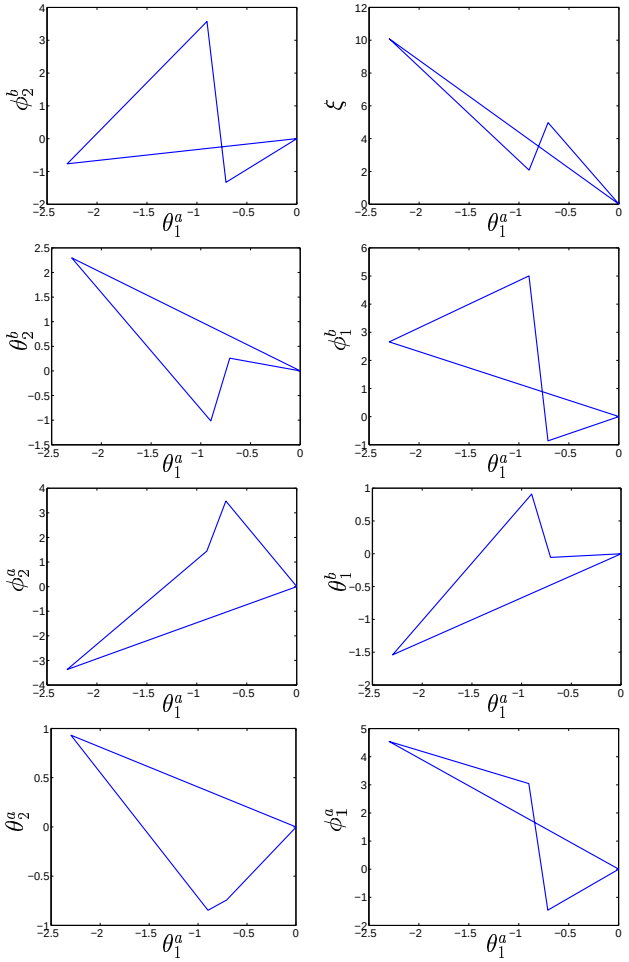

Fig. 3. Loop γ_{Fourier} in the parameter space that gives the two-qubit Fourier gate. Here $L(\gamma_{\text{Fourier}}) = 63.35$. The error was below 10^{-13}.

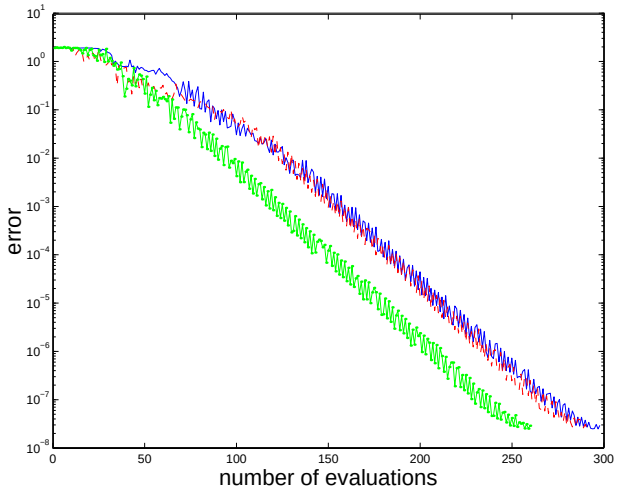

Fig. 4. Error as a function of iterations for the Hadamard gate.

4.2. *Length-Penalty Optimization*

We now proceed to develop the formalism for reducing the length of the loops. We tried adding a penalty term to the objective function see, e.g., Ref. [14]. This function is defined as

$$P(\gamma) = \begin{cases} 0, & \text{if } L(\gamma) < L_{\max} \\ \nu L(\gamma)^p, & \text{otherwise} \end{cases} \tag{36}$$

where $L(\gamma)$ is the length of the path γ; here p and ν are adjustable parameters. Note that the length need not be Euclidean. Our numerical experiments below will, though, use the Euclidean approximation. To be strict, however, we would have to relate the four parameters of our Givens decomposition to the base manifold $\mathbb{C}P^2$ of the bundle $U(3)$ in the case of one-qubit gates. Then we would employ the $\mathbb{C}P^2$ metric to evaluate the length of the loop in the optimization algorithm. Hence the lengths of the loops here should be interpreted with caution. Moreover, since HQC is purely geometrical, the operation should be independent of how fast the loop is traversed. Note, however, that a shorter loop may be traversed more quickly without spoiling the adiabaticity requirement.

It should be clear from the structure of Eq. (36) that the penalty functions are designed to have built-in constraints. In the allowed region, i.e., where the length does not exceed $L_{\max}$, the problem is unchanged. There will be a rapidly growing penalty term elsewhere. From the point of view of the optimization algorithm, short loops are preferred.

Figure 5 illustrates another example solution to the problem of finding a two-qubit Fourier gate but this time with the restriction $L_{\max} = 40$. We have chosen a penalty function with the parameters $p = 2$ and $\nu = 1000$. The solution tends to be on the surface $L(\gamma) = L_{\max}$, at least for short $L_{\max}$. This may be interpreted to originate from the scarcity of the minima for short loops. Tests show that adjusting the maximum length upwards does not result in a solution

very near to the boundary but rather a solution is found in the middle of the volume. One is inclined to deduce from all this that the number of solutions to the minimization problem is huge. This particular loop is shorter than our earlier construction, but not much. However, our first example in Fig. 3 had a loop length of 63.35, such that a remarkable improvement has been achieved.

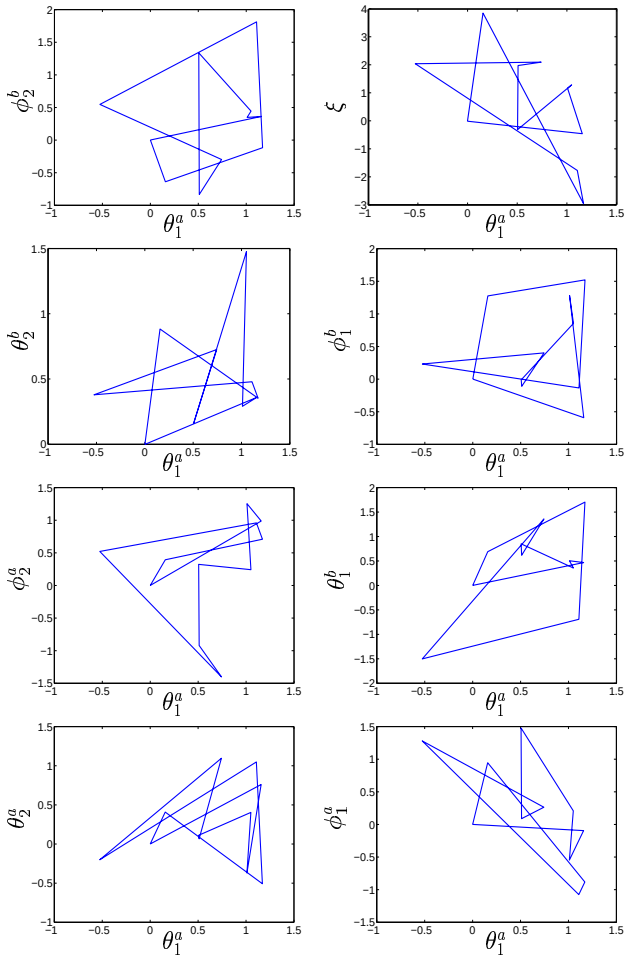

Fig. 5. Length-optimized loop for the quantum Fourier transform in $\mathcal{V}_{10}$. Here $L(\gamma_{\text{Fourier}}) \approx 39.96$ and the error is below 10^{-13} with 200 discretization points per edge.

A more impressive reduction of length may be seen in Fig. 6. We have previously shown [10] an implementation of the SWAP gate that had a length of 107.85. The gate given below has a length of just 29.99. We managed to cut off a major redundant portion of the path.

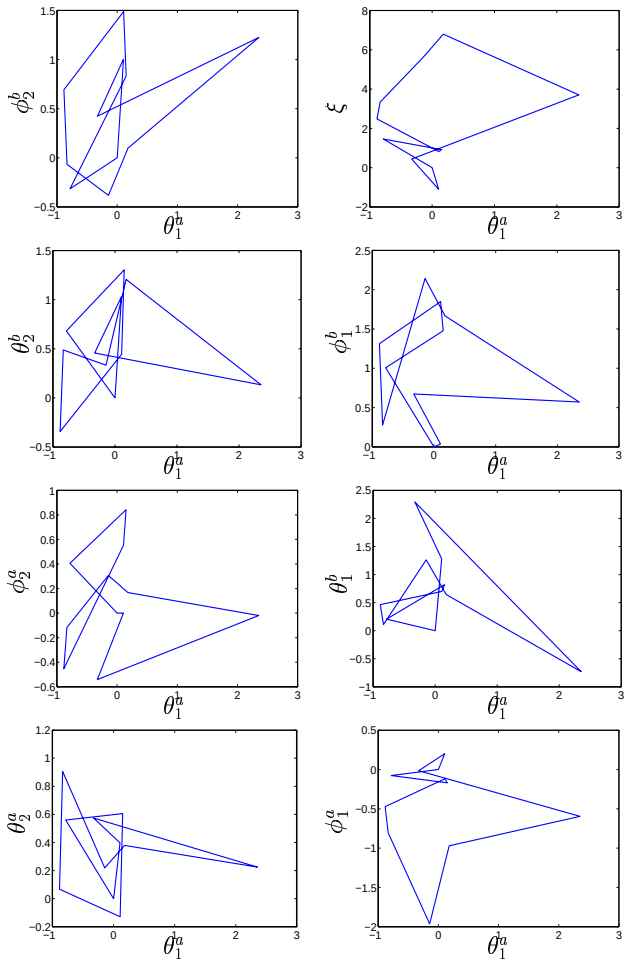

Fig. 6. Length-optimized loop for SWAP in $\mathcal{V}_{10}$. Here $L(\gamma_{\mathrm{SWAP}}) \approx 29.99$ and the error is below 10^{-13} with 200 discretization points per edge. The loop presented in Ref. [10] had a length of 107.85.

4.3. *Error-Penalty Optimization*

We can take the concept of length-penalty optimization one step further. Once we know some loop that produces the desired gate, we may switch the roles of the length of the loop and that of the error. Namely, we assign a penalty function that penalizes for excess error while the main contribution comes from the length. In this manner we can try to make increasingly improved loops that yield the very same quantum gate. That is, we minimize the function

$$F(\gamma) = L(\gamma) + P_2(\gamma) \tag{37}$$

where the penalty term is this time given by

$$P_2(\gamma) = \begin{cases} 0, & \text{if } f(\gamma) < \varepsilon_{\max} \\ \nu f(\gamma)^p, & \text{otherwise.} \end{cases} \tag{38}$$

Here $f(\gamma)$ is the error just as previously. This elaboration of the penalty-function technique proves quite powerful.

A good example of the technique is given by the CNOT gate which we may easily perform analytically. We take an implementation of the CNOT

$$\begin{aligned} (\theta_2^a, \theta_2^b, \theta_1^b, \xi) = & (0,0,0,0) && \to (0,\pi/2,0,0) && \to (0,\pi/2,\pi/4,0) && \to \\ & (0,0,\pi/4,0) && \to (0,0,0,0) && \to (\pi/2,0,0,0) && \to \\ & (\pi/2,0,0,\pi) && \to (0,0,0,\pi) && \to (0,0,0,0) && \to \\ & (0,\pi/2,0,0) && \to (0,\pi/2,-\pi/4,0) && \to (0,0,-\pi/4,0) && \to \\ & (0,0,0,0)\,. \end{aligned} \tag{39}$$

as the initial guess of the optimization task where the vertices are joined linearly. This loop is naturally in $\mathcal{V}_{11}$ but we also add an extra vertex in the middle of each edge such that the loop is more flexible and therefore belongs to $\mathcal{V}_{23}$. The resulting loop after error-penalty minimization is shown in Fig. 7. This figure, as well as all the figures in this section, was obtained by first using poor accuracy and then by minimizing further with improving accuracy starting from the initial guess thus obtained. The starting length was 18.8496 and as can be seen from the length of this loop 14.03, the solution has improved considerably. This is just one example of the power of our technique. Due to the success of the method we are yet more convinced that the acceptable solutions are extremely dense in parameter space.

The use of the Euclidean metric is particularly well motivated in the context of error-penalty optimization. Of course, the underlying physical setting might suggest using a specialized metric that would relate some experimental "cost" to certain areas of the base manifold. For example, it is not clear which shape of the manifold one should choose, analogously to the situation between ellipsoids and spheres. In the present scenario we have two objectives: a low error and a short path. If there emerges a redundant contribution adding to the length from some part of the manifold where the parameterization is not one-to-one, this excess length can be removed without affecting the solution. Since we are also aiming at reducing the Euclidean length, any redundant contributions tend to disappear in practice due to the minimization algorithm. An analogy is provided by the unit ball S^2; if one were to do a

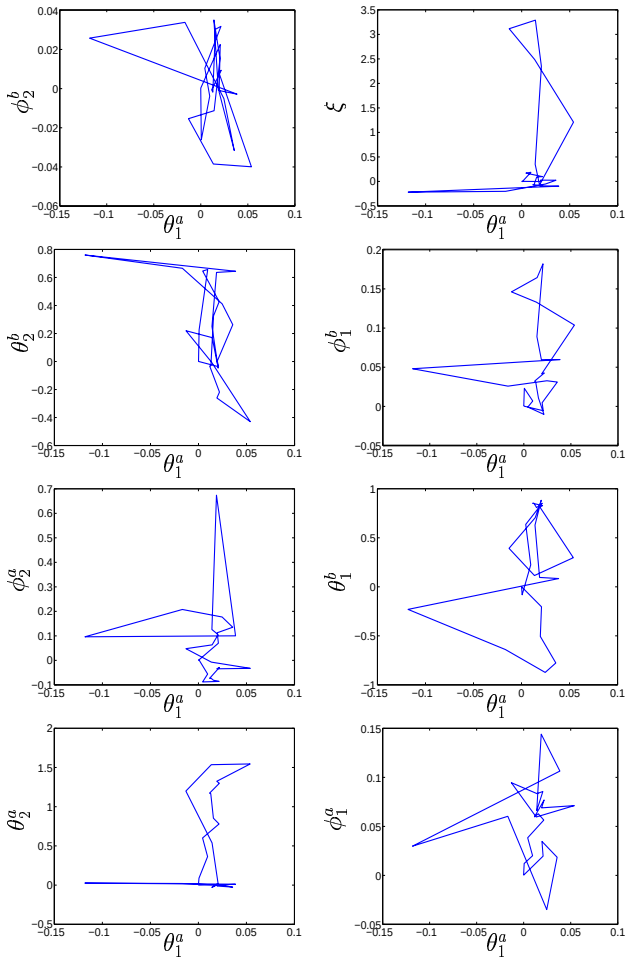

Fig. 7. Result of the error-penalty minimization of an initially known CNOT loop in $\mathcal{V}_{23}$. Here $L(\gamma_{\mathrm{CNOT}}) \approx 14.03$. The original loop was in $\mathcal{V}_{11}$, had a length of 18.85 and actually consisted of three individual loops.

2π turn on one of the poles, there would be an Euclidean contribution that would have no meaning. This excess length would disappear in the minimization process, though.

5. Discussion

We have numerically studied the construction of holonomic quantum gates. Our method is capable of finding the loop in the parameter space corresponding to any one- or two-qubit gate in a three-state model. It seems reasonable that the method would also work in other models. The optimization task is too difficult for derivative-based methods as can be seen in the pictures we have presented. The polytope algorithm has, however, proved useful in this task. Moreover, our previous calculations prove the three-state model that we have presented capable of universal HQC. We discussed example solutions for the Hadamard gate and the two-qubit Fourier transform without length considerations. It is easy to construct a set of universal gates for the model analytically. Numerical results are, though, far superior since they realize a given unitary matrix with a shorter single loop.

In the present paper we have developed a method for minimizing with respect to the length of the loop, thus making the implementation of these holonomies as quick as possible. We have first investigated adding a penalty term for excess length and then experimented swapping the roles of the length and the error. Provided that one already knows some implementation of a desired gate, this latter technique can be used to combine loops in an efficient manner. The results that we have obtained appear promising. The main result is that the optimization problem can be solved even though the landscape is quite rough. For one- and two-qubit gates a regular PC suffices.

It must be emphasized that it certainly is desirable for the loop to have the shortest possible length to achieve fast operation speed without sacrificing the adiabaticity. As a preliminary to our optimization scheme, we neglected the underlying metric of $\mathbb{C}P^2 \simeq U(3)/U(2)\times U(1)$ and pretended as if we were working in a manifold with an Euclidean metric. We demonstrated that our scheme works reliably. We are currently engaged in a more ambitious program with the $\mathbb{C}P^2$ metric properly taken into account. We believe that our optimization method could also be extended to more conventional quantum-computing schemes. Then, however, time would appear explicitly in the minimization.

A few remarks are in order about our method. The fact that the optimization landscape is rough does not imply that HQC would be sensitive to errors. Namely, physical errors do not just move one vertex but rather there are deviations all along the path. To which degree this causes errors would constitute a separate study. Furthermore, increasing the number of vertices does not result in an improved accuracy: For one-qubit gates it is enough to have $2^2 = 4$ independent parameters and for two-qubit gates $4^2 = 16$ parameters. This is because $U(2^N)$ is parameterized by 2^{2N} real parameters. Recall that the number of optimization variables is either $4k$ or $9k$. With $k = 1$ one cannot, however, obtain a non-trivial holonomy. More vertices might mean less length, though.

The speed-up must be considered in terms of the adiabatic time. Short loops can always be traversed slowly but they may also be traversed more quickly. It is important to reduce the operation time to fight the effect of decoherence. Thus the optimization of quantum gates is a very well motivated task.

We wish to point out that all the rotations in $\mathbb{C}P^2$ are available with a construction using

superconducting nanostructures [17].

Acknowledgments

AON would like to thank the Research Foundation of Helsinki University of Technology and the Graduate School in Technical Physics for financial support; MN thanks the Helsinki University of Technology for a Visiting Professorship and he is also grateful for partial support of Grant-in-Aid from the Ministry of Education, Culture, Sports, Science, and Technology, Japan (Project Nos. 14540346 and 13135215); MMS acknowledges the Academy of Finland for a Research Grant in Theoretical Materials Physics.

Note added in proof: It was brought to our attention that the minimization of the loop length for a given holonomy has become known as the "isoholonomic problem", named in analogy with the "isoperimetric problem" in which the area surrounded by a loop with fixed length is maximized. See, e.g., R. Montgomery, "Isoholonomic problems and some applications", Commun. Math. Phys. **128**, 565–592 (1990). In Montgomery's paper, this minimization problem is written in the form of a differential equation. In our approach, however, this does not work since there occur too many local minima. Therefore, we consider our minimization algorithm a far more practical scheme.

References

1. P. Zanardi and M. Rasetti, *Holonomic quantum computation*, Phys. Lett. A **264**, 94-99, 1999.
2. K. Fujii, *Mathematical foundations of holonomic quantum computer*, Rep. Math. Phys. **48**, 75-82, 2001.
3. J. Pachos and S. Chountasis, *Optical holonomic quantum computer*, Phys. Rev. A **62**, 052318, 2000.
4. D. Ellinas and J. Pachos, *Universal quantum computation by holonomic and nonlocal gates with imperfections*, Phys. Rev. A **64**, 022310, 2001.
5. J. Pachos, P. Zanardi and M. Rasetti, *Non-Abelian Berry connections for quantum computation*, Phys. Rev. A **61**, 010305(R), 1999.
6. J. Pachos, P. Zanardi, *Quantum holonomies for quantum computing*, Int. J. Mod. Phys. B **15**, 1257-1285, 2001.
7. M.-S. Choi, *Geometric Quantum Computation on Solid-State Qubits*, LANL e-print, quant-ph/0111019, 2001.
8. L. Faoro, J. Siewert and R. Fazio *Non-Abelian phases, pumping and quantum computation with Josephson Qubits*, LANL e-print, cond-mat/0202217, 2002.
9. M. Berry, *Quantal phase factors accompanying adiabatic changes*, Proc. R. Soc. Lond. A **392**, 45-57, 1984.
10. A. O. Niskanen, M. Nakahara, and M. M. Salomaa, *Realization of arbitrary gates in holonomic quantum computation*, Phys. Rev. A, in print (2002); quant-ph/0209015.
11. F. Wilczek and A. Zee, *Appearance of gauge structure in Simple Dynamical Systems*, Phys. Rev. Lett. **52**, 2111-2114, 1984.
12. A. Zee, *Non-Abelian gauge structure in nuclear quadrupole resonance*, Phys. Rev. A **38**, 1-6, 1988.
13. A. Mostafazadeh, *Generalized Adiabatic Product Expansion: A nonperturbative method of solving time-dependent Schroedinger equation*, J. Math. Phys. **40**, 3311-3326, 1999.
14. M. S. Bazaraa, H. D. Sherali, C. M. Shetty, *Nonlinear Programming, Theory and Algorithms*, John Wiley and Sons, 1993.
15. *http://pangea.stanford.edu/~baris/professional/theorypolytope.html*
16. M. Nakahara, *Geometry, Topology and Physics*, IOP Publishing Ltd., 1990.
17. A. O. Niskanen, M. Nakahara, and M. M. Salomaa, to be published.

Reprinted with permission from the publisher.
In: Physical Review Letters 2003. Vol. 90,
No. 19, pp. 197901-1–4.

Optimal Multiqubit Operations for Josephson Charge Qubits

Antti O. Niskanen,* Juha J. Vartiainen,† and Martti M. Salomaa
Materials Physics Laboratory, Helsinki University of Technology, POB 2200 (Technical Physics), FIN-02015 HUT, Espoo, Finland
(Received 6 February 2003; published 13 May 2003)

We introduce a method for finding the required control parameters for a quantum computer that yields the desired quantum algorithm without invoking elementary gates. We concentrate on the Josephson charge-qubit model, but the scenario is readily extended to other physical realizations. Our strategy is to numerically find any desired double- or triple-qubit gate. The motivation is the need to significantly accelerate quantum algorithms in order to fight decoherence.

DOI: 10.1103/PhysRevLett.90.197901 PACS numbers: 03.67.Pp, 03.67.Lx, 03.75.Lm, 74.50.+r

Quantum computing algorithms are realized through unitary operators that result from the temporal evolution of the quantum system under consideration. Typically, these are achieved with a sequence of universal gates [1] which act analogously to the elementary gates of digital computers. Quantum computers hold the promise of exponential speedup with respect to classical computers owing to the massive parallelism arising from the superposition of quantum bits, qubits; for introductions to quantum computing and quantum information processing, see Ref. [2]. Several physical implementations of quantum computing have been suggested; in particular, quantum computing with Cooper pairs [3].

Superconducting circuits [4] feature controlled fabrication and scalability [5]; their drawback is that the leads inevitably couple the qubit to the environment, thereby introducing decoherence [6]. In a superconductor, the number of the Cooper pairs and the phase of the wave function constitute conjugate variables. The majority of investigations has focused either on the charge regime where the number of Cooper pairs is well defined [7], or on the flux regime where the phase is well defined [8]. Qubits utilizing current-driven large Josephson junctions have been tested experimentally [9]. Decisive experimental progress [10] demonstrated that it is possible to realize 10^4 elementary quantum gates with Josephson-junction qubits. Here we consider Josephson charge qubits.

In this Letter we propose a method to construct arbitrary two- or three-qubit quantum gates by solving the optimization problem of control parameters for a Josephson charge-qubit register. We show that it is possible to numerically find the required control-parameter sequences even for nontrivial three-qubit gates without employing elementary gates. Recently, it has been suggested [11] how to solve a similar problem in the context of holonomic quantum computation [12], where time does not appear as an explicit parameter. Here, the time evolution arises through the Schrödinger equation.

The motivation underlying the investigation of this approach is the need to overcome effects of decoherence. The implementation of a quantum algorithm which is composed of elementary gates is rarely optimal in execution time since the majority of qubits is most of the time inactive; see Fig. 1. The decomposition into elementary gates works extremely well with classical digital computers. However, in the context of quantum computing the number of consecutive operations is strictly limited by the short time window set by interactions with the environment. It is therefore of prime importance to concentrate on the implementations of quantum algorithms [13–15]. We consider the construction of quantum algorithms out of larger building blocks. Whereas careful design and manufacturing can significantly increase the decoherence time, our scenario can serve to reduce the number of the operations needed.

The Josephson charge qubit utilizes the number degree of freedom of a nanoscale Josephson-junction circuit. The states of the qubit correspond to either zero or one extra Cooper pair residing on the superconducting island, usually denoted by $|0\rangle$ and $|1\rangle$, respectively. The Cooper pairs can tunnel coherently to a superconducting electrode. The charging energy of the qubit can be tuned with the help of an external gate voltage, whereas tunneling between the states is controlled with the help of an external magnetic flux.

The explicit single-qubit Hamiltonian for the qubit i is

$$H^i_{\text{single}} = -\frac{1}{2}B^i_z\sigma_z - \frac{1}{2}B^i_x\sigma_x, \tag{1}$$

where the standard notation for Pauli matrices has been utilized. Here B^i_z is a tunable parameter which depends

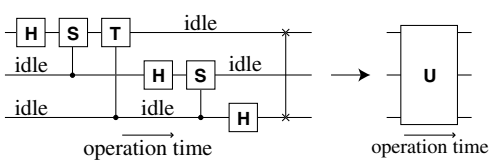

FIG. 1. Instead of implementing the three-qubit quantum Fourier transform with the help of elementary gates, we determine a gate that performs the entire three-qubit operation with a single control loop. Note that idle time is avoided.

on the gate voltage, while B_x^i can be controlled with the help of a flux through the SQUID. Note that setting $B_z^i = B_x^i = 0$ results in degeneracy. At the degeneracy point, there will be no change in the physical state of the system. In the case of single-qubit gates, it is easy to see from this model that any rotation in SU(2) can be performed on the qubits. Note that U(2) is not available since the Hamiltonian is traceless. In general, we cannot achieve U(2^N) for N qubits since the Hamiltonian of the entire quantum register turns out to be traceless. However, the global phase factor is not physical since it corresponds to a redefinition of the zero level of energy.

Qubits can be coupled by connecting them in parallel to an inductor; see Fig. 2. This scenario has the benefit of allowing for a longer decoherence time and that of being tunable. The resulting coupling term in the Hamiltonian between the qubits i and j is then of the form [4]

$$H_{\text{coupling}} = -CB_x^i B_x^j \sigma_y \otimes \sigma_y, \tag{2}$$

where C is a positive parameter depending on the capacitances of the qubits and also on the inductance. It follows from Eqs. (1) and (2) that one can apply nontrivial two-qubit operations by simultaneously turning on the SQUIDs of the two qubits, although the σ_x term will be turned on as well. All the other qubits must have their SQUIDs turned off. On the other hand, one-qubit σ_x operations require that all but one SQUID is turned on. By turning off a SQUID we mean applying a half flux quantum through it. Note that in the present context it is actually impossible to perform independent operations on any two subsets of the quantum register due to the inductive coupling. Since one must also take into account the decoherence mechanism, it is not practical to let most qubits reside at their degeneracy point. The question arises whether it would rather prove more efficient to try and find some scheme of finding larger quantum operations, instead of using elementary gates.

To tackle the challenge posed above, we concentrate on finding quantum gates numerically. The structure of the Josephson-qubit Hamiltonian is such that it is not immediately transparent how one would actually construct even the basic controlled-NOT gate. We accomplish this by considering loops $\gamma(t)$ in the control-parameter space spanned by $\{B_x^j(t)\}$ and $\{B_z^j(t)\}$. Therefore, the function

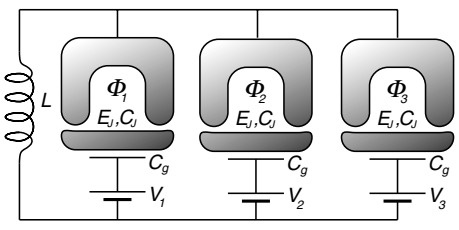

FIG. 2. Schematic illustration of three Josephson charge qubits with inductive coupling. The adjustable parameters include the gate voltages V_i and the enclosed fluxes Φ_i.

$\gamma(t)$ is of the vector form

$$\gamma(t) = [B_z^1(t) \cdots B_z^N(t)\ B_x^1(t) \cdots B_x^N(t)]^T, \tag{3}$$

where we have assumed a register of N qubits. The temporal evolution induces the unitary operator

$$U = \mathcal{T} \exp\left(-i \int_{\gamma(t)} H(\gamma(t)) dt \right), \tag{4}$$

where $\mathcal{T}$ stands for the time-ordering operator and we choose $\hbar = 1$. The integration is performed along the path formed by $\gamma(t)$ where the loop starts at the origin, i.e., at the degeneracy point. We will restrict the path to a special class of loops, which form polygons in the parameter space. Thus the parameters vary in time at a piecewise constant speed, and none of the parameters is turned on or off instantaneously. We further set the time spent in traversing each edge of the polygon equal to unity. This limitation could be relaxed, in which case the length of each edge in time would be an additional free parameter. We also set $C = 1$ in Eq. (2). This can be achieved by properly fabricating the inductor, but we have every reason to believe that the algorithm will work for other choices of C as well. Hence, in order to evaluate Eq. (4) one needs only to specify the coordinates of the vertices of the polygon, which we denote collectively as X_γ. Numerically, it is easy to evaluate the unitary operator in a stable manner by further dividing the loop $\gamma(t)$ into tiny intervals that take the time Δt to traverse. If γ_i denotes all the values of the parameters in the midpoint of the ith interval, and m is the number of such intervals, then we find to a good approximation

$$U_{X_\gamma} \approx \exp(-iH(\gamma_m)\Delta t) \cdots \exp(-iH(\gamma_1)\Delta t). \tag{5}$$

We now proceed to transform the problem of finding the desired unitary operator into an optimization task. Namely, any $\hat{U}$ can be found as the solution of the problem of minimizing the error functional

$$f(X_\gamma) = \|\hat{U} - U_{X_\gamma}\|_F \tag{6}$$

over all possible values of X_γ. Here $\|\cdot\|_F$ is the Frobenius trace norm defined as $\|A\|_F = \sqrt{\text{Tr}(A^\dagger A)}$. The number of adjustable vertices of the polygon ν is kept fixed from the beginning. One needs to have enough vertices to parametrize the unitary group SU(2^N). The dimension of this group is $2^{2N} - 1$ and there are $2N$ parameters for each vertex. Thus, we must have $2N\nu \geq 2^{2N} - 1$. We use $\nu = 12$ for the three-qubit gates and $\nu = 4$ for the two-qubit gates. Within this formulation the method of finding the desired gates is similar to the recently introduced method of finding holonomic quantum gates [11]. Thus we again expect the minimization landscape to be rough and we apply the robust polytope algorithm [16] for the minimization.

We concentrate on finding two- and three-qubit gates, since one-qubit gates can be trivially constructed with the

help of Euler angles. A larger quantum gate could be performed by factoring it into two- and three-qubit operations, and the implementation for these could be found numerically. It seems that quantum operations for four, five, or more qubits could be found with the same method, assuming that sufficient computing resources are available. However, even in the case of three-qubit gates the optimization task becomes challenging and we need to use parallel programming. In the parallel three-qubit program, since the function evaluations of $f(X_\gamma)$ require a major part of the computation, we distribute the workload such that each processor calculates the contribution of a single edge of the polygon. In addition, one processor handles the minimization routine.

Let us turn to the results. First, we attempt to construct a gate equivalent to the controlled-NOT, namely,

$$U = \exp\left(i\frac{\pi}{4}\right)\begin{bmatrix} 1 & 0 & 0 & 0 \\ 0 & 1 & 0 & 0 \\ 0 & 0 & 0 & 1 \\ 0 & 0 & 1 & 0 \end{bmatrix}. \tag{7}$$

The phase factor is needed in order for the gate to belong to SU(4). It is already hard to see from the form of the Hamiltonian how this gate would be carried out in the present setting. Figure 3 illustrates an implementation of this gate that has been obtained by minimizing the error function in Eq. (6); the error is negligible. This example clearly illustrates the potential of our method.

As a second example, we construct the two-qubit quantum Fourier transform (QFT). The QFT (see, e.g., Ref. [2]) is given in the case of two qubits by

$$F_2 = \frac{1}{2}\begin{bmatrix} 1 & 1 & 1 & 1 \\ 1 & i & -1 & -i \\ 1 & -1 & 1 & -1 \\ 1 & -i & -1 & i \end{bmatrix}. \tag{8}$$

Furthermore, we need to multiply this by $\exp(i\frac{\pi}{8})$ in order to find a gate that belongs to SU(4). Figure 4 shows the resulting loop that has been found with the help of the algorithm. In general, the optimization task for two-qubit gates can be performed quite easily with the help of personal computers. However, finding three-qubit gates is already quite time consuming. It proves worth the extra effort to do this, though.

The three-qubit quantum Fourier transform is [2]

$$F_3 = \frac{1}{\sqrt{8}}\begin{bmatrix} 1 & 1 & 1 & 1 & 1 & 1 & 1 & 1 \\ 1 & \omega & \omega^2 & \omega^3 & \omega^4 & \omega^5 & \omega^6 & \omega^7 \\ 1 & \omega^2 & \omega^4 & \omega^6 & 1 & \omega^2 & \omega^4 & \omega^6 \\ 1 & \omega^3 & \omega^6 & \omega & \omega^4 & \omega^7 & \omega^2 & \omega^5 \\ 1 & \omega^4 & 1 & \omega^4 & 1 & \omega^4 & 1 & \omega^4 \\ 1 & \omega^5 & \omega^2 & \omega^7 & \omega^4 & \omega^1 & \omega^6 & \omega^3 \\ 1 & \omega^6 & \omega^4 & \omega^2 & 1 & \omega^6 & \omega^4 & \omega^2 \\ 1 & \omega^7 & \omega^6 & \omega^5 & \omega^4 & \omega^3 & \omega^2 & \omega \end{bmatrix}, \tag{9}$$

where $\omega = \exp(i\frac{\pi}{4})$. Since $\det(F_3) = i$ we must set $\hat{U} = \exp(-i\frac{\pi}{16})F_3$ such that $\hat{U} \in \mathrm{SU}(8)$. As an evidence of the success of the three-qubit algorithm, we have in Fig. 5 plotted the implementation of the three-qubit Fourier transform. We conclude from these three examples that it is possible to find far more powerful optimal implementations of multiqubit quantum gates with the help of the minimization scheme [17].

To further assess the strength of the technique, we compare the number of steps that are required to carry out the three-qubit Fourier transform using only two-qubit gates with the number of steps required when using the full three-qubit implementation of Fig. 5. The two-qubit implementation [18] requires effectively four gates;

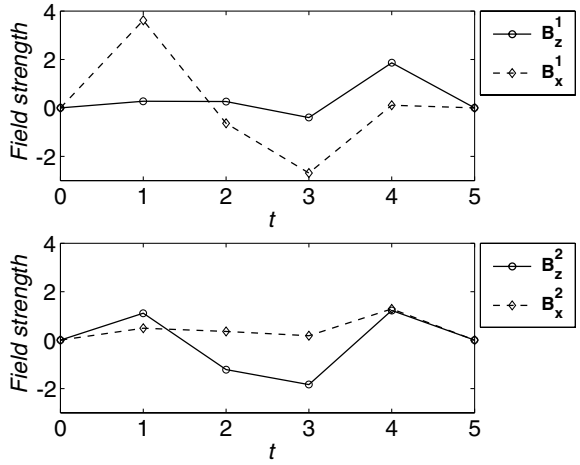

FIG. 3. Control-parameter sequences as functions of time that yield the gate in Eq. (7) which is equivalent to the controlled-NOT. The relative error is on the order of 10^{-11} and 100 discretization points per edge were used.

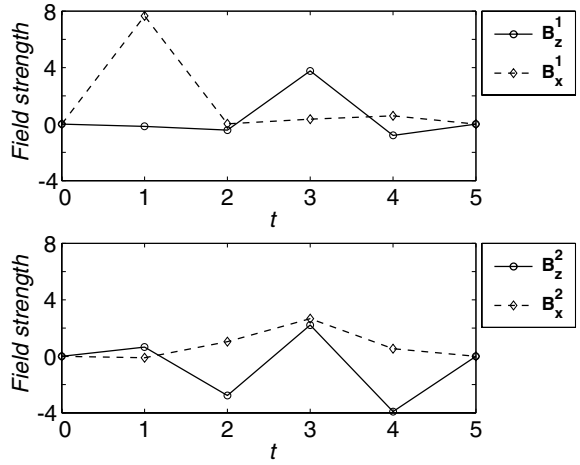

FIG. 4. Control-parameter sequences as functions of time that yield the two-qubit Fourier transform in Eq. (8). The relative error is on the order of 10^{-11} and 100 discretization points per edge were used.

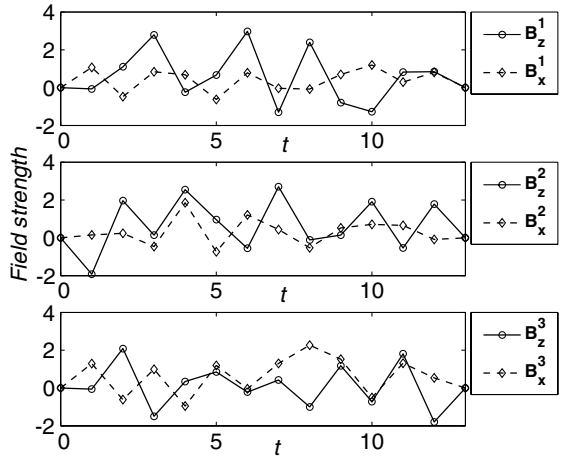

FIG. 5. Control-parameter sequences as functions of time that yield the three-qubit quantum Fourier transform (modulo a global phase). The relative error is on the order of 10^{-5} and 100 discretization points were used.

see Fig. 1. Since these gates would have to be performed sequentially, we would need five polygon edges per two-qubit operation. This results in 20 edges for the whole operation. Using elementary gates would require far more edges. Our optimized three-qubit Fourier transform, though, only requires 13 edges. Since each edge contributes the same amount to the operation time, we conclude that our implementation is improved. What is more, not all multiqubit gates can be decomposed as conveniently as the Fourier transform. For them the gain is higher. Thus, increasing the amount of classical computing resources should yield even better results.

In conclusion, we have described how to efficiently construct two- and three-qubit quantum gates for the Josephson charge qubit using numerical optimization. An immediate strength of the present scenario is that one avoids unnecessary idle time during the logical quantum operations. Since the loops are traversed at a piecewise constant speed, and no fields are instantaneously switched, this method of constructing quantum gates should be viable from the experimental point of view as well. The effect of finite fall and rise times of pulses on the quality of quantum gates has been studied recently [19]. Since we do not use pulses but instead interpolate along linear paths in the parameter space, such errors can be avoided. It seems reasonable to construct large-scale quantum algorithms in multiqubit blocks. This can be accomplished by optimizing the gate realization with the help of classical computers.

The authors thank M. Nakahara for useful discussions and CSC (Finland) for computing resources. This work is supported by the Helsinki University of Technology and Academy of Finland.

Note added.—After submitting our manuscript, work on a parallel switching method was kindly brought to our attention by Burkard *et al.* [20].

*Currently at VTT Information Technology, Microsensing, POB 1207, 02044 VTT, Finland. Electronic address: antti.niskanen@vtt.fi
†Electronic address: juhav@focus.hut.fi

[1] A. Barenco, C. H. Bennett, R. Cleve, D. P. DiVincenzo, N. Margolus, P. Shor, T. Sleator, J. Smolin, and H. Weinfurter, Phys. Rev. A **52**, 3457 (1995).
[2] J. Gruska, *Quantum Computing* (McGraw-Hill, New York, 1999); M. A. Nielsen and I. L. Chuang, *Quantum Computation and Quantum Information* (Cambridge University Press, Cambridge, 2000); A. Galindo and M. A. Martin-Delgado, Rev. Mod. Phys. **74**, 347 (2002).
[3] A. Shnirman, G. Schön, and Z. Hermon, Phys. Rev. Lett. **79**, 2371 (1997); D.V. Averin, Solid State Commun. **105**, 659 (1998).
[4] Yu. Makhlin, G. Schön, and A. Shnirman, Rev. Mod. Phys. **73**, 357 (2001).
[5] J. Q. You, J. S. Tsai, and F. Nori, Phys. Rev. Lett. **89**, 197902 (2002).
[6] W. H. Zurek, Rev. Mod. Phys. (to be published).
[7] Y. Nakamura, Yu. A. Pashkin, and J. S. Tsai, Nature (London) **398**, 786 (1999); Phys. Rev. Lett. **87**, 246601 (2001).
[8] T. P. Orlando, J. E. Mooij, L. Tian, C. H. van der Wal, L. Levitov, S. Lloyd, and J. J. Mazo, Phys. Rev. B **60**, 15 398 (1999).
[9] J. M. Martinis, S. Nam, J. Aumentado, and C. Urbina, Phys. Rev. Lett. **89**, 117901 (2002); Y. Yu, S. Han, X. Chu, S. Chu, and Z. Wang, Science **296**, 889 (2002).
[10] D. Vion, A. Aassime, A. Cottet, P. Joyez, H. Pothier, C. Urbina, D. Esteve, and M. H. Devoret, Science **296**, 886 (2002).
[11] A. O. Niskanen, M. Nakahara, and M. M. Salomaa, Quantum Information and Computation **2**, 560 (2002); Phys. Rev. A **67**, 012319 (2003).
[12] P. Zanardi and M. Rasetti, Phys. Lett. A **264**, 94 (1999).
[13] J. Siewert and R. Fazio, Phys. Rev. Lett. **87**, 257905 (2001).
[14] J. P. Palao and R. Kosloff, Phys. Rev. Lett. **89**, 188301 (2002).
[15] X. Wang, A. Sørensen, and K. Mølmer, Phys. Rev. Lett. **86**, 3907 (2001).
[16] J. C. Lagarias, J. A. Reeds, M. H. Wright, and P. E. Wright, SIAM J. Optim. **9**, 112 (1998).
[17] We have carried out sensitivity analyses on the CNOT and two-qubit QFT gate realizations; the error was found to scale linearly with the rms of the Gaussian noise added at each vertex: error $\approx 6 \times \langle \text{noise} \rangle_{\text{rms}}$.
[18] We assume that one-qubit operations are embedded into two-qubit gates.
[19] S. Oh, Phys. Rev. B **65**, 144526 (2002).
[20] G. Burkard, D. Loss, D. P. DiVincenzo, and J. A. Smolin, Phys. Rev. B **60**, 11 404 (1999).

Reprinted with permission from the publisher.
In: International Journal of Quantum Information
2004. Vol. 2, No. 1, pp. 1–10.

ACCELERATION OF QUANTUM ALGORITHMS USING THREE-QUBIT GATES

JUHA J. VARTIAINEN*

Materials Physics Laboratory, Helsinki University of Technology
POB 2200 (Technical Physics), FIN-02015 HUT, Finland
juhav@focus.hut.fi

ANTTI O. NISKANEN

VTT Information Technology, Microsensing, POB 1207, 02044 VTT, Finland

MIKIO NAKAHARA

Department of Physics, Kinki University, Higashi-Osaka 577-8502, Japan

MARTTI M. SALOMAA

Materials Physics Laboratory, Helsinki University of Technology
POB 2200 (Technical Physics), FIN-02015 HUT, Finland

Received 27 October 2003
Revised 6 January 2004

Quantum-circuit optimization is essential for any practical realization of quantum computation, in order to beat decoherence. We present a scheme for implementing the final stage in the compilation of quantum circuits, i.e. for finding the actual physical realizations of the individual modules in the quantum-gate library. We find that numerical optimization can be efficiently utilized in order to generate the appropriate control-parameter sequences which produce the desired three-qubit modules within the Josephson charge-qubit model. Our work suggests ways in which one can in fact considerably reduce the number of gates required to implement a given quantum circuit, hence diminishing idle time and significantly accelerating the execution of quantum algorithms.

Keywords: decoherence; Josephson charge qubit; multiqubit quantum gates; numerical optimization.

1. Introduction

The most celebrated and potentially useful quantum algorithms, which include Shor's factorization algorithm[1] and Grover's search,[2] manifest the potential of a quantum computer compared to its classical counterparts.

Widely different physical systems have been proposed to be utilized as a quantum computer.[3,4] The main drawback shared by most of the physical realizations is

*Corresponding author.

the short decoherence time. Decoherence[5] destroys the pure quantum state which is needed for the computation and, therefore, strongly limits the available execution time for quantum algorithms. This, combined with the current restricted technical possibilities to construct and control nanoscale structures, delays the utilization of quantum computation for reasonably extensive[6] algorithms.

The execution time of a quantum algorithm can be reduced by optimization. The methods similar to those common in classical computation[7] can be utilized in quantum compiling, constructing a quantum circuit[8] for the algorithm. Moreover, the physical implementation of each gate can and must be optimized in order to achieve gate sequences long enough, for example, to implement Shor's algorithm within typical decoherence times.[9]

Any quantum gate can be implemented by finding an elementary gate sequence[10,11] which, in principle, exactly mimics the gate operation. In the most general case on the order of 4^n elementary gates are needed to implement an arbitrary n-qubit.[12] Fortunately, remarkably shorter polynomial gate sequences are known to implement many commonly used gates, such as the n-qubit quantum Fourier transform (QFT). In addition to the exact methods, quantum gates can be implemented using techniques which are approximative by nature.[9,13–15]

In this paper we consider the physical implementation of nontrivial three-gate operations. As an example of the power of the technique, we show how to find realizations for the Fredkin, Toffoli, and QFT gates through numerical optimization. These gates have been suggested to be utilized as basic building blocks for quantum circuits and would thus act as basic extensions of the standard universal set of elementary gates. However, the method presented can be employed to find the realization of any three-qubit gate. Having more computer resources available would allow one to construct gates acting on more than three qubits.

The numerical method allows us a straightforward and efficient way for finding the physical implementation of any quantum gate. Thus, the method may prove to be practical or even necessary for an efficient experimental realization of a quantum computer.

We concentrate on a hypothetical Josephson charge qubit register,[16] since the experimental investigations of superconducting qubits is active; see, for instance, Refs. 17–19. The scheme utilizes the number degree of freedom of the Cooper pairs in a superconducting Josephson-junction circuit. It is potentially scalable and it offers, in principle, full control over the quantum register. Moreover, the method employed here is easily extended to any physical realization providing time-dependent control over the physical parameters.

2. Physical Model

The physical implementation of a practical quantum algorithm requires that it is decomposed into modules whose physical realizations are explicitly known. In the quantum computer, the gate operations are realized through unitary operations

U that result from the temporal evolution of the physical state of the quantum register. The unitary evolution is governed by the Hamiltonian matrix $H(\gamma)$, which describes the energy of the system for a given setting of physical parameters γ. In general, the parameters are time-dependent, $\gamma = \gamma(t)$. The induced unitary operator is obtained from the formal solution of the Schrödinger equation

$$U = \mathcal{T} \exp\left(-i \int_{\gamma(t)} H(\gamma(t))dt\right), \tag{1}$$

where $\mathcal{T}$ stands for the time-ordering operator and we have chosen $\hbar = 1$.

We consider the Josephson charge qubit register as a realization of a quantum computer, see Fig. 1. The register is a homogenous array of mesoscopic superconducting islands and the states of the qubit correspond to either zero or one extra Cooper pair residing on the island. Each of the islands is capacitively coupled to an adjustable gate voltage, $V_{\rm g}^i(t)$. In addition, they are coupled to a superconducting lead through mesoscopic SQUIDs. We consider an ideal situation, where each Josephson junction in the SQUID devices has the same Josephson energy $E_{\rm J}$ and capacitance $C_{\rm J}$. The magnetic flux $\Phi_i(t)$ through the ith SQUID loop is a control parameter which may be produced by adjustable current I_i. The qubit array is coupled in parallel with an inductor, L, which allows the interaction between the qubits.

In this scheme the Hamiltonian for the qubit register is[9,16]

$$H = \sum_i^n \left\{ -\frac{1}{2} B_z^i \sigma_z^i - \frac{1}{2} B_x^i \sigma_x^i \right\} - \sum_{i \neq j}^{n,n} C B_x^i B_x^j \sigma_y^i \otimes \sigma_y^j, \tag{2}$$

where the standard notation for Pauli matrices has been utilized and σ_x^i stands for $I \otimes \cdots \otimes \sigma_x \otimes I \cdots \otimes I$. Above, B_x^i can be controlled with the help of a flux $\Phi_i(t)$ through the ith SQUID, B_z^i is a tunable parameter which depends on the gate voltage $V_{\rm g}(t)$ and C is a constant parameter describing the strength of the coupling. We set C equal to unity by rescaling the Hamiltonian and time. The approach taken is to deal with the parameters B_z^i and B_x^i as dimensionless control parameters.

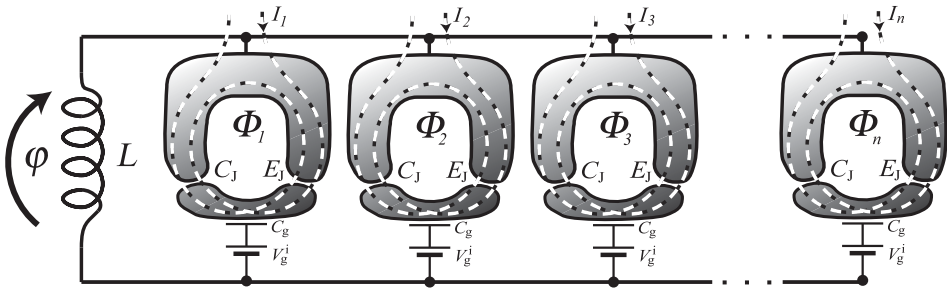

Fig. 1. Schematic of an array of Josephson charge qubits coupled in parallel with an inductor.

In the above Hamiltonian, each control parameter can be set to zero, to the degeneracy point, thereby eliminating all temporal evolution. The implementation of one-qubit operations is straightforward through the Baker–Campbell–Hausdorff formula, since the turning on of the parameters B_z^i and B_x^i one by one does not interfere with the states of the other qubits. Implementation of two-qubit operations is more complex since simultaneous application of nonzero parameter values for many qubits causes undesired interqubit couplings. However, by properly tuning the parameters it is possible to compensate the interference and to perform any temporal evolution in this model setup. This is partly why numerical methods are necessary for finding the required control-parameter sequences.

Finally, we point out that using the above Hamiltonian we are able to perform gates $U \in SU(2^k)$ since the Hamiltonian is traceless. However, for every gate $U \in U(2^k)$ we can find a matrix $U' = e^{i\phi}U$ which has a unit determinant. The global phase factor $e^{i\phi}$ corresponds to redefining the zero level of energy.

3. Numerical Methods

We want to determine the physical realization for the quantum gates. Our aim is to numerically solve the inverse problem of finding the parameter sequences $\gamma(t)$ which would yield the desired gate operation when substituted into Eq. (1). The numerical optimization provides us with the realizations for not only any one- and two-qubit, but also for any three-qubit gates. Using the three-qubit implementation we circumvent the idle time in qubit control which provides us faster execution times, see Fig. 2.

In the Josephson charge qubit model the Hamiltonian for the n-qubit register, Eq. (2), depends on the external parameters

$$\gamma(t) = [B_z^1(t) \cdots B_z^n(t);\ B_x^1 z(t) \cdots B_x^n(t)].$$

To discretize the integration path $\gamma(t)$ for numerical optimization we consider a parametrization in which the values of the control-parameter fields, $\{B_z^i(t)\}$ and $\{B_z^i(t)\}$, are piecewise linear functions of time. Consequently, the path $\gamma(t)$ can be fully described by a set of parameter values at ν control points, where the slopes of the fields changes. We denote the set of these values collectively as X_γ. To obtain a general k-qubit gate $U_k \in SU(2^k)$ one needs to have enough control parameters to parameterize the unitary group $SU(2^k)$, which has a total of $2^{2k} - 1$ generators. Since there are $2k$ free parameters for each control point in γ we must have

$$2k\nu \geq 2^{2k} - 1. \tag{3}$$

We use $\nu = 12$ for the three-qubit gates and $\nu = 4$ for the two-qubit gates. We force the parameter path to be a loop, which starts from and ends at the degeneracy point, where all parameter values vanish. Then we can assemble the modules in arbitrary order without introducing mismatch in the control parameters. We further set the time spent in traversing each interval of the control points to equal unity. Eventually,

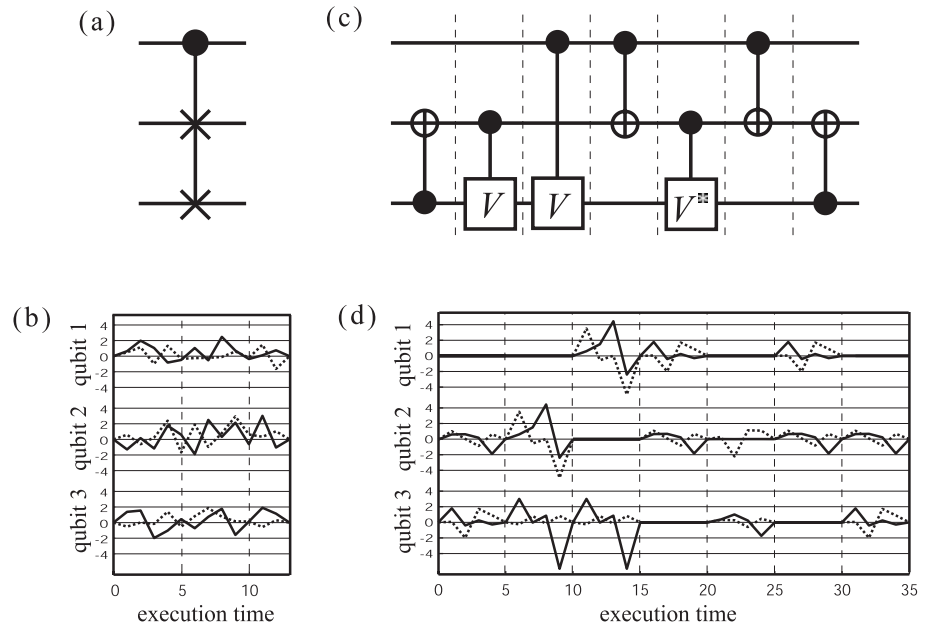

Fig. 2. Implementation of the Fredkin gate on the Josephson charge qubit model. (a) The quantum circuit symbol of the Fredkin gate, and (b) its physical implementation by controlling all three qubits simultaneously. (c) The two-qubit gate decomposition of the Fredkin gate. Here $V = \sqrt{\sigma_x}$ and V^* stands for its Hermitian conjugate. (d) The physical implementation of the gate sequence; note that during each gate operation, one of the qubits is in the idle state. The vertical axis in figures (b) and (d) stands for the control parameter field amplitudes; the solid line describes the parameter B_z^i and the dotted line the parameter B_x^i, see text.

the execution time of U_k is proportional to $\nu + 1$, which gives us a measure to compare different implementations. Figure 2 illustrates our approach and shows the benefits of the three-qubit implementation of the Fredkin gate compared to corresponding implementation through two-qubit gate decomposition. Note that the two-qubit gate implementation could be further optimized.[20]

We evaluate the unitary operator in Eq. (1) in a numerically robust manner by dividing the loop $\gamma(t)$ into tiny intervals that take time Δt to traverse. If γ_i denotes all the values of the parameters in the midpoint of the ith interval, and m is the number of such intervals, we then find to a good approximation

$$U_{X_\gamma} \approx \exp(-iH(\gamma_m)\Delta t) \cdots \exp(-iH(\gamma_1)\Delta t). \tag{4}$$

The evaluation of the U_{X_γ} consists of independent matrix multiplications which can be evaluated simultaneously. This allows straightforward parallelization of the computation. To calculate the matrix exponentials efficiently we use the truncated Taylor-series expansion

$$e^A \approx \sum_{k=0}^{m} \frac{A^k}{k!}, \tag{5}$$

where m is an integer in the range 3–6. Since the eigenvalues of the anti-Hermitian matrix $A = -iH\delta t$ are significantly less than unity, the expansion converges rapidly. The applicability of the approximation can be confirmed by comparing the results with the exact results obtained using spectral decomposition.

Using the above numerical methods we transform the inverse problem of finding the desired unitary operator into an optimization task. Namely, any $\hat{U}$ can be found as the solution of the problem of minimizing the error function

$$f(X_\gamma) = \|\hat{U} - U_{X_\gamma}\|_F \tag{6}$$

over all possible values of X_γ. Here $\|\cdot\|_F$ is the Frobenius trace norm defined as $\|A\|_F = \sqrt{\mathrm{Tr}(A^\dagger A)}$. The minimization landscape is rough, see Fig. 3. Thus we apply the robust polytope search algorithm[21] for the minimization. We have assumed that a suitable limit of sufficient accuracy for the gate operations is given by the requirement of the applicability[6] of quantum error correction

$$\|U_{X_\gamma} - \hat{U}\| < 10^{-4}, \tag{7}$$

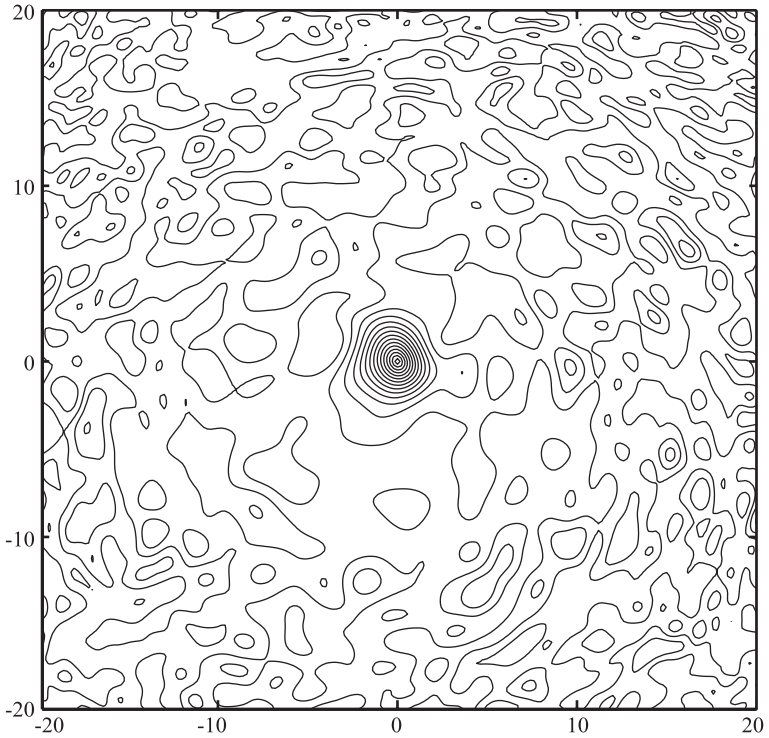

Fig. 3. Typical planar cut of the error function space. The plane through the minimum point $X_{\min}$ has been chosen arbitrarily in the parameter space. The irregular shape of the landscape easily reveals the complexity of finding the global minimum and the reason why the gradient-based methods fail.

where $\hat{U}$ and U_{X_γ} are the target and the numerically optimized gate operations, respectively.

4. Quantum Gate Optimization Results

We have applied the minimization procedure to various three-qubit gates and found that the error functional of Eq. (6) can be minimized to values below 10^{-4} by running the polytope search repetitively. Table 1 represents the optimized control parameters which serve to yield the Fredkin gate when applied to the Josephson charge qubit Hamiltonian. Numerical results for the Toffoli and three-qubit QFT gates are represented in Tables 2 and 3, respectively. Finding the control parameter using the polytope search requires an order of 10^6 error-function evaluations, which

Table 1. Field amplitudes at the control points for the Fredkin gate.

Time	B_z^1	B_z^2	B_z^3	B_x^1	B_x^2	B_x^3
1	0.00000	0.00000	0.00000	0.00000	0.00000	0.00000
2	0.71637	−1.44846	1.54511	0.55428	0.67228	−0.58105
3	2.23337	0.18377	1.73522	1.29275	−0.69463	0.01513
4	1.17895	−1.31725	−2.22145	−1.11461	0.27210	−0.18665
5	−0.92555	1.97326	−1.15875	1.49438	2.69507	1.57872
6	−0.54804	0.66834	0.48872	−0.38981	−1.88659	−0.60226
7	1.18034	−2.13101	−0.81205	−0.27817	2.13894	0.92208
8	−0.59994	2.80989	0.82839	−0.24260	−1.09419	2.09561
9	2.78429	0.35914	1.98896	−0.11839	0.90439	0.83671
10	0.79364	2.40575	−1.78131	0.67600	3.31481	0.17828
11	−0.41098	−0.69585	0.15594	−0.21996	0.70917	0.15377
12	0.12630	3.39809	2.14043	1.65229	0.37794	−0.64223
13	0.84941	−1.17701	1.28801	−1.84075	1.16739	0.33965
14	0.00000	0.00000	0.00000	0.00000	0.00000	0.00000

Table 2. Field amplitudes at the control points for the Toffoli gate.

Time	B_z^1	B_z^2	B_z^3	B_x^1	B_x^2	B_x^3
1	0.00000	0.00000	0.00000	0.00000	0.00000	0.00000
2	0.00286	−0.06484	0.96050	0.72386	0.33310	−0.22026
3	2.85647	−0.08874	2.94358	1.60795	−0.18192	0.03931
4	0.67879	−1.70364	−2.54280	−1.65771	−0.04722	−0.25411
5	−0.17379	0.87916	0.19581	1.55484	2.98447	1.22991
6	0.01847	2.68973	−0.18098	0.02898	−0.54301	−0.15977
7	0.21569	−3.27483	−0.33407	−0.31173	2.26503	0.32031
8	−0.57439	4.25644	1.25986	0.12262	0.06238	1.87619
9	3.40836	−0.48759	0.44296	−0.20867	0.04664	1.00381
10	−0.60520	1.59369	0.87620	0.95412	2.75968	0.37209
11	−0.10762	0.16258	−0.24672	−0.11839	1.38245	0.01990
12	0.20275	1.97553	1.12769	1.07003	0.46081	−0.35437
13	0.99088	−0.23145	0.68050	−2.12999	0.74237	0.01537
14	0.00000	0.00000	0.00000	0.00000	0.00000	0.00000

Table 3. Field amplitudes for the three-qubit QFT gate.

Time	B_z^1	B_z^2	B_z^3	B_x^1	B_x^2	B_x^3
1	0.00000	0.00000	0.00000	0.00000	0.00000	0.00000
2	0.49824	0.41039	1.75837	0.42339	0.67345	1.83257
3	−0.18007	0.55372	−1.79297	0.64987	0.53048	−0.39300
4	0.73625	0.60488	−0.94171	0.61458	0.09641	−0.39863
5	2.21744	1.28419	2.82723	0.47046	1.04206	1.59345
6	0.47037	−0.48092	−0.53215	0.04297	0.21802	1.24063
7	0.69085	0.72558	1.00427	0.22332	1.25082	−0.25144
8	2.61154	0.87134	0.74335	0.31834	−0.00374	1.64643
9	0.24827	0.82952	1.04102	2.31043	1.00804	0.98377
10	−0.90785	−1.32491	1.10923	0.69935	−0.15359	−0.34420
11	0.59315	1.36082	−0.19764	1.83023	0.58541	0.85453
12	0.76819	0.31529	0.24531	−0.40221	1.13052	0.68184
13	−0.85651	0.02093	0.85491	1.33447	0.56580	0.06332
14	0.00000	0.00000	0.00000	0.00000	0.00000	0.00000

Table 4. Comparison of the execution times for various quantum gates.

Gate	Fredkin	Toffoli	QFT	$U \in SU(2^3)$ Decomposed	$U \in SU(2^3)$ 3-qubit Gates
Number of two-qubit gates	5	3	3	206	—
Execution time	25	15	15	1030	13

takes tens of hours of CPU time, but can be done in a reasonable time by using parallel computing.

We found that the error functional grows linearly in the vicinity of the minimum point X_γ, which implies that the parameter sequence found may be robust. The robustness was further analyzed by adding Gaussian noise to the control parameters of the path $\gamma(t)$. Such a sensitivity analysis confirmed that the error scales linearly with the root-mean-square amplitude of the surplus Gaussian noise.

In our scheme, any three-qubit gate requires an integration path $\gamma(t)$ with 12 control points, which takes 13 units of time to execute. Similarly, a two-qubit gate takes 5 units of time to execute. Table 4 summarizes our results by comparing the number of steps that are required to carry out a single three-qubit gate or using a sequence of two-qubit gates. The results are calculated for the Fredkin and Toffoli gates following the decomposition given in Refs. 20 and 10. For a QFT gate the quantum circuit is explicitly shown, for example, in Ref. 22. Any three-qubit gate can be realized by using 68 controlled^2 U and controlled^2 NOT gates. This number can be reduced to 50 using palindromic optimization.[23] The decomposition of the controlled^2 U gate is discussed in Ref. 10. Note that the results in Table 4 are calculated assuming that the physical realization for any two qubit modules is available through some scheme similar to the one which is employed in this paper and one-qubit gates are merged into two-qubit modules. The implementation of

a general three-qubit module using a limited set of gates, for example, one-qubit rotations R_y and R_z and the CNOT gate has recently been discussed in Ref. 12.

5. Discussion

We have shown how to obtain approximative control-parameter sequences for a Josephson charge-qubit register with the help of a numerical optimization scheme. The scheme utilizes well known theoretical methods and the results are obtained through heavy computation. Our method can prove useful for experimental realization of working quantum computers. The possibility to implement nontrivial multiqubit gates in an efficient way may well turn out to be a crucial improvement in making quantum computing realizable. For example, Josephson-junction qubits suffer from a short decoherence time, in spite of their potential scalability, and therefore the runtime of the algorithm must be minimized using all the possible ingenuity imaginable.

Here we have utilized piecewise linear parameter paths. This makes the scheme experimentally more viable than the pulse-gate solutions, since the parameters are adjusted such that no fields are switched instantaneously. However, the numerical method proposed for solving the time evolution operator is not unique. Some implicit methods for the integration in time may turn out to yield the results more accurately in the same computational time. Furthermore, for practical applications it may turn out to be useful to try and describe the parameter paths using a collection of smooth functions and to find whether they would produce the required gates.

To summarize the results of our numerical optimization, we emphasize that more efficient implementations for quantum algorithms can be found using numerically optimized three-qubit gates. In the construction of large-scale quantum algorithms even larger multiqubit modules may prove powerful. The general idea is to use classical computation to minimize quantum computation time, aiming below the decoherence limit.

Acknowledgements

JJV thanks the Foundation of Technology (TES, Finland) for a scholarship and the Emil Aaltonen Foundation for a travel grant to attend EQIS'03 in Japan; MN is grateful for partial support of a Grant-in-Aid from the Ministry of Education, Culture, Sports, Science, and Technology, Japan (Project Nos. 14540346 and 13135215). This research has been supported in the Materials Physics Laboratory at HUT by the Academy of Finland through the Research Grants in Theoretical Materials Physics (No. 201710) and in Quantum Computation (No. 206457). We also want to thank CSC — Scientific Computing Ltd. (Finland) for parallel computing resources.

References

1. P. W. Shor, *Algorithms for quantum computation: Discrete logarithms and factoring* in *Proc. 35nd Annual Symposium on Foundations of Computer Science*, ed. S. Goldwasser (IEEE Computer Society Press, 1994), p. 124.

2. L. K. Grover, *Phys. Rev. Lett.* **79**, 325 (1997).
3. R. Clark (ed.), *Experimental Implementation of Quantum Computation (IQC '01)* (Rinton Press Inc., New Jersey, 2001).
4. F. De Martini (ed.), *Experimental Quantum Computation and Information* (International School of Physics "Enrico Fermi", Vol. **148**) (IOS Press, Amsterdam, 2002).
5. W. H. Zurek, *Rev. Mod. Phys.* **75**, 715 (2003).
6. D. P. DiVincenzo, *Fortschr. Phys.* **48**, 771 (2000).
7. A. V. Aho, R. Sethi and J. D. Ullman, *Compilers: Principles, Techniques and Tools* (Addison-Wesley, Reading, Massachusetts, 1986).
8. D. Deutsch, *Proc. Roy. Soc. London* **A425**, 73 (1989).
9. A. O. Niskanen, J. J. Vartiainen and M. M. Salomaa, *Phys. Rev. Lett.* **90**, 197901 (2003); J. J. Vartiainen, A. O. Niskanen, M. Nakahara and M. M. Salomaa, Implementing Shor's algorithm on Josephson charge qubits, quant-ph/0308171.
10. A. Barenco, C. H. Bennett, R. Cleve, D. P. DiVincenzo, N. Margolus, P. Shor, T. Sleator, J. Smolin and H. Weinfurter, *Phys. Rev.* **A52**, 3457 (1995).
11. J. Zhang, J. Vala, S. Sastry and B. Whaley, *Phys. Rev. Lett.* **91**, 027903 (2003).
12. V. V. Shende, I. L. Markov and S. S. Bullock, On universal gate libraries and generic minimal two-qubit quantum circuits, quant-ph/0308033.
13. A. W. Harrow, B. Recht and I. L. Chuang, *J. Math. Phys.* **43**, 4445 (2002).
14. E. Knill, Approximation by quantum circuits, quant-ph/9508006.
15. G. Burkard, D. Loss, D. P. DiVincenzo and J. A. Smolin, *Phys. Rev.* **B60**, 11404 (1999).
16. Y. Makhlin, G. Schön and A. Shnirman, *Rev. Mod. Phys.* **73**, 357 (2001).
17. Y. A. Pashkin, T. Yamamoto, O. Astafiev, Y. Nakamura, D. V. Averin and J. S. Tsai, *Nature* **421**, 823 (2003).
18. T. Yamamoto, Y. A. Pashkin, O. Astafiev, Y. Nakamura, D. V. Averin and J. S. Tsai, *Nature* **425**, 944 (2003).
19. J. M. Martinis, S. Nam, J. Aumentado and C. Urbina, *Phys. Rev. Lett.* **89**, 117901 (2002).
20. J. A. Smolin and D. P. DiVincenzo, *Phys. Rev.* **A53**, 2855 (1996).
21. J. C. Lagarias, J. A. Reeds, M. H. Wright and P. E. Wright, *SIAM J. Optim.* **9**, 112 (1998).
22. J. Gruska, *Quantum Computing* (McGraw-Hill, New York, NY, 1999), p. 118.
23. A. V. Aho and K. M. Svore, Compiling quantum circuits using the Palindrome transform, quant-ph/0311008.

Reprinted with permission from the publisher.
In: Physical Review 2004. Vol. A 70, pp. 012319-1–11.

Implementing Shor's algorithm on Josephson charge qubits

Juha J. Vartiainen,[1,*] Antti O. Niskanen,[2] Mikio Nakahara,[1,3] and Martti M. Salomaa[1]
[1]*Materials Physics Laboratory, POB 2200 (Technical Physics), Helsinki University of Technology, FIN-02015 HUT, Finland*
[2]*VTT Information Technology, Microsensing, POB 1207, 02044 VTT, Finland*
[3]*Department of Physics, Kinki University, Higashi-Osaka 577-8502, Japan*
(Received 6 October 2003; revised manuscript received 27 February 2004; published 30 July 2004)

We investigate the physical implementation of Shor's factorization algorithm on a Josephson charge qubit register. While we pursue a universal method to factor a composite integer of any size, the scheme is demonstrated for the number 21. We consider both the physical and algorithmic requirements for an optimal implementation when only a small number of qubits are available. These aspects of quantum computation are usually the topics of separate research communities; we present a unifying discussion of both of these fundamental features bridging Shor's algorithm to its physical realization using Josephson junction qubits. In order to meet the stringent requirements set by a short decoherence time, we accelerate the algorithm by decomposing the quantum circuit into tailored two- and three-qubit gates and we find their physical realizations through numerical optimization.

DOI: 10.1103/PhysRevA.70.012319 PACS number(s): 03.67.Lx, 03.75.Lm

I. INTRODUCTION

Quantum computers have potentially superior computing power over their classical counterparts [1,2]. The novel computing principles which are based on the quantum-mechanical superposition of states and their entanglement manifest themselves, for example, in Shor's integer-factorization algorithm [3] and in Grover's database search [4]. In this paper we focus on Shor's algorithm which is important owing to its potential applications in (de)cryptography. Many widely applied methods of public-key cryptography are currently based on the RSA algorithm [5] which relies on the computational difficulty of factoring large integers.

Recently, remarkable progress toward the experimental realization of a quantum computer has been accomplished, for instance, using nuclear spins [6,7], trapped ions [8,9], cavity quantum electrodynamics [10], electrons in quantum dots [11], and superconducting circuits [12–17]. However, the construction of a large multiqubit register remains extremely challenging. The very many degrees of freedom of the environment tend to become entangled with those of the qubit register which results in undesirable decoherence [18]. This imposes a limit on the coherent execution time available for the quantum computation. The shortness of the decoherence time may present fundamental difficulties in scaling the quantum register up to large sizes, which is the basic requirement for the realization of nontrivial quantum algorithms [19].

In this paper, we consider an inductively coupled charge-qubit model [20]. Josephson-junction circuits provide two-state pseudospin systems whose different spin components correspond to distinct macroscopic variables: either the charges on the superconducting islands or the phase differences over the Josephson junctions. Thus, depending on the parameter values for the setup, one has flux [12,13], or charge qubits [14–17,21]. Thus far the largest quantum register, comprising seven qubits, has been demonstrated for nuclear magnetic resonance (NMR) in a liquid solution [7]. However, the NMR technique is not believed to be scalable to much larger registers. In contrast, superconducting Josephson-junction circuits are supposed to provide scalable registers and hence to be better applicable for large quantum algorithms [22]. Furthermore, they allow integration of the control and measurement electronics. On the other hand, the coupling to the environment, e.g., through the electrical leads, [23] causes short decoherence times.

In addition to the quantum register, one needs a quantum gate "library," i.e., a collection of control parameter sequences which implements the gate operations on the quantum register. The quantum gate library must consist of at least a set of universal elementary gates [24], which are typically chosen to be the one-qubit unitary rotations and the CNOT gate. Some complicated gates may also be included in the library.

The quantum circuit made of these gates resembles the operational principle of a conventional digital computer. To minimize the number of gates, the structure of the quantum circuit can be optimized using methods similar to those in digital computing [25]. Minimizing the number of gates is important not only for fighting decoherence but also for decreasing accumulative errors of classical origin. If some tailored two-, three- or arbitrary k-qubit gates are included in the gate library, the quantum circuits may be made much more compact. The implementation of gates acting on more than two qubits calls for numerical optimization [26]. For further discussion on the implementation of non-standard gates as the building blocks for quantum circuits, see Refs. [27–30].

We propose an implementation of Shor's algorithm for factoring moderately large integers—we deal with both algorithmic and hardware issues in this paper. These are two key aspects of quantum computation which, however, have traditionally been topics of disjoint research communities. Hence

*Electronic address: juhav@focus.hut.fi

we aim to provide a unifying discussion where an expert on quantum algorithms can gain insight into the realizations using Josephson junctions and experimentalists working with Josephson devices can choose to read about the quantum algorithmic aspects. The background material on the construction of a quantum circuit needed for the evaluation of the modular exponential function [31,32] is presented in Appendix A and a derivation of the effective Hamiltonian for a collection of inductively coupled Josephson qubits is given in Appendix B.

This paper is organized as follows: The construction of a quantum gate array for Shor's algorithm is discussed in Sec. II. In Sec. III, we consider the Josephson charge-qubit register. Section IV presents the numerical methods we have employed to find the physical implementations of the gates. Section V discusses in detail how one would realize Shor's algorithm using Josephson charge qubits to factor the number 21. Section VI is devoted to discussion.

II. SHOR'S FACTORIZATION ALGORITHM

With the help of a quantum computer, one could factor large composite numbers in polynomial time using Shor's algorithm [3,33–35]. In contrast, no classical polynomial time factorization algorithm is known to date, although the potential existence of such an algorithm has not been ruled out, either.

A. Quantum circuit

The strategy for the factoring of a number $N=pq$, both p and q being primes, using a quantum computer relies on finding the period r of the modular exponential function $f(x)=a^x \pmod N$, where $0<a<N$ is a random number coprime to N. For an even r and if $a^{r/2}\neq -1 \pmod N$ at least one prime factor of N is given by $\gcd(a^{r/2}\pm 1, N)$. It can be shown [3] that this happens with a probability higher than one half. Otherwise, a quantum algorithm must be executed for different values for a until a proper r is found.

The evaluation of $f(x)$ can be implemented using several different techniques. To obtain the implementation which involves the minimal number of qubits, one assumes that the numbers a and N are hardwired in the quantum circuit. However, if a large number of qubits is available, the design can be easily modified to take as an input the numerical values of the numbers a and N residing in separate quantum registers. The hardwired approach combined with as much classical computing as possible is considerably more efficient from the experimental point of view.

Figure 1 represents the quantum circuit[1] needed for finding the period r. Shor's algorithm has five stages: (1) Initialization of the quantum registers. The number N takes $n=\lceil \log_2(N+1)\rceil$ bits to store into memory, where $\lceil v\rceil$ stands for the nearest integer equal to or greater than the real number v. To extract the period of $f(x)$, we need at least two registers: $2n$ qubits for the register $|x\rangle_{2n}$ to store numbers x and n qubits for the register $|y\rangle_n$ to store the values of $f(x)$. The register $|x\rangle_{2n}$ is initialized as $|0\rangle_{2n}$, whereas $|y\rangle_n=|1\rangle_n$. (2) The elegance of a quantum computer arises from the possibility to utilize arbitrary superpositions. The superposition state of all integers $0\leqslant x\leqslant 2^{2n}-1$ in the register $|x\rangle_{2n}$ is generated by applying the Hadamard gate H on each qubit separately. (3) The execution of the algorithm, the unitary operator U_f, entangles each input value x with the corresponding value of $f(x)$:

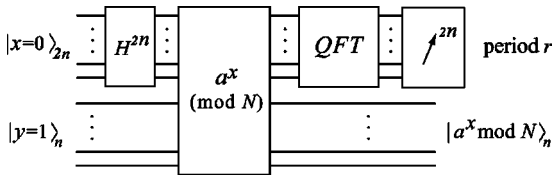

FIG. 1. Quantum circuit for Shor's algorithm.

$$U_f \sum_x |x\rangle|1\rangle = \sum_x |x\rangle|a^x \pmod N\rangle. \tag{1}$$

(4) The quantum Fourier transformation (QFT) is applied to the register $|x\rangle_{2n}$, which squeezes the probability amplitudes into peaks due to the periodicity $f(x)=f(x+r)$. (5) A measurement of the register $|x\rangle_{2n}$ finally yields an indication of the period r. A repetitive execution of the algorithm reveals the probability distribution which is peaked at the value $2^{2n}/r$ and its integer multiples of output values in the register $|x\rangle_{2n}$.

Besides the quantum algorithm which is used to find r, a considerable amount of classical precomputing and postprocessing is required as well. However, all this computing can be performed in polynomial time.

B. Implementing the modular exponential function

We are looking for a general scalable algorithm to implement the required modular exponential function. The implementation of this part of the algorithm sets limits for the spatial and temporal requirements of computational resources, hence it requires a detailed analysis. The remarkable experimental results [7] to factor the number 15 involve an elegant quantum circuit of seven qubits and only a few simple quantum gates. The implementation definitely exploits the special properties of the number 15, and the fact that the outcome of the function $a^x \pmod N$ can be calculated classically in advance for all input values x when N is small. For arbitrary N, reversible arithmetic algorithms must be employed [36,37]. The classical arithmetic algorithms [38], can be implemented reversibly by replacing the irreversible logic gates by their reversible counterparts. The longhand multiplication algorithm, which we use below, should be optimal up to very large numbers, see Sec. VI, requiring only $O(n)$ qubits and $O(n^3)$ steps.

The implementation of the modular exponential function using a longhand multiplication algorithm and a QFT-based adder [31] requires only a small scratch space, for a total of $4n+2$ qubits. The details of the implementation are given in Appendix A. The conventional approach to longhand multi-

[1]In the quantum circuit diagrams, we have indicated the size of a register $|x\rangle_m$ with the subscript m.

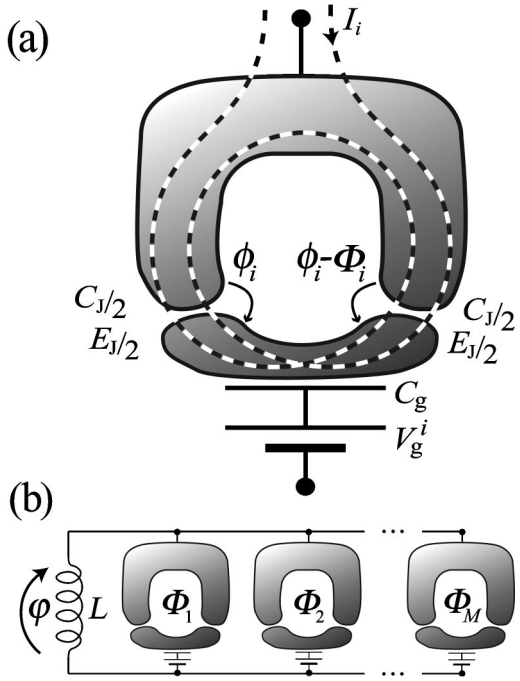

FIG. 2. (a) Schematic of a Josephson charge qubit with the relevant parameters. (b) An array of Josephson charge qubits coupled in parallel with an inductor.

plication without a QFT-based adder would require on the order of $5n$ qubits. The price of the reduced space is the increase in the execution time, which now is $O(n^4)$, but which can be reduced down to $O(n^3 \log_2(n/\epsilon))$, allowing for a certain error level ϵ. According to Ref. [31] one would achieve an algorithm requiring only $2n+3$ qubits with intermediate measurements. However, we do not utilize this implementation since the measurements are likely to introduce decoherence.

III. JOSEPHSON CHARGE-QUBIT REGISTER

The physical model studied in this paper is the so-called inductively coupled Cooper pair box array. This model, as well as other related realizations of quantum computing, has been analyzed in Ref. [20]. The derivation of the Hamiltonian is outlined in Appendix B for completeness. Our approach to quantum gate construction is slightly different from those found in the literature and it is therefore worthwhile to consider the physical model in some detail.

A schematic picture of a homogeneous array of qubits is shown in Fig. 2. Each qubit i comprises a superconducting island coupled capacitively to a gate voltage and a superconducting quantum interference device (SQUID) loop through which Cooper pairs may tunnel. The gate voltage may be used to tune the effective gate charge n_g^i of the island whereas the external magnetic flux through the SQUID can be used to control the effective Josephson energy. Each qubit is characterized by a charging energy E_C and a tunable Josephson energy $E_J(\Phi_i)$, where Φ_i is the flux threading the SQUID. The Hamiltonian for the ith qubit can be written as

$$\mathcal{H}^i_{\text{single}} = -\tfrac{1}{2}B^i_z\sigma^i_z - \tfrac{1}{2}B^i_x\sigma^i_x \tag{2}$$

and the coupling between the ith and jth qubits as

$$\mathcal{H}^{i,j}_{\text{coupling}} = -CB^i_xB^j_x\sigma^i_y \otimes \sigma^j_y. \tag{3}$$

The qubit state $|0\rangle$ ("spin up") corresponds to zero extra Cooper pairs residing on the island and the state $|1\rangle$ ("spin down") corresponds to one extra pair on the island. Above $B^i_x = E_J(\Phi_i)$, $B^i_z = E_C(1-2n^i_g)$, and $C = \pi^2 L/\Phi_0^2(C_{qb}/C_J^2)$ denotes the strength of the coupling between the qubits, whereas C_{qb} is the total capacitance of a qubit in the circuit, C_J is the capacitance of the SQUID, L is the inductance which may in practice be caused by a large Josephson junction operating in the linear regime and finally $\Phi_0 = h/2e$ is the flux quantum. The approach taken is to deal with the parameters B^i_z and B^i_x as dimensionless control parameters. We assume that they can be set equal to zero which is in principle possible if the SQUID junctions are identical. We set $C=1$ and choose natural units such that $\hbar = 1$.

The Hamiltonian in Eqs. (2) and (3) is a convenient model for studying the construction of quantum algorithms for a number of reasons. First of all, the total Hamiltonian can be set to zero thereby eliminating all temporal evolution. Second, setting the effective Josephson coupling to zero eliminates the coupling between any two qubits. This is achieved by applying half a flux quantum through the SQUID loops. If the Josephson energy of any two qubits is nonzero, there will automatically emerge a coupling between them. This is partly why numerical methods are necessary for finding the control-parameter sequences. By properly tuning the gate voltages and fluxes it is possible to compensate undesired couplings and to perform any temporal evolution in this model setup.

We note that the generators $i\sigma_x$ and $i\sigma_z$ are sufficient to construct all the SU(2) matrices through the Baker-Campbell-Hausdorff formula and thus single-qubit gates need not be constructed numerically. It is even possible to do this in a piecewise linear manner avoiding abrupt switching since the only relevant parameter is the time integral of either B^i_z or B^i_x if only one of them is nonzero at a time. That is, any $U \in \mathrm{SU}(2)$ acting on the ith qubit can be written as

$$U = \exp\left(i\sigma^i_z\int_{t_2}^{t_3} B^i_z(t)dt/2\right)\exp\left(i\sigma^i_x\int_{t_1}^{t_2} B^i_x(t)dt/2\right) \times \exp\left(i\sigma^i_z\int_{t_0}^{t_1} B^i_z(t)dt/2\right), \tag{4}$$

where we assume that from t_0 to t_1 only B^i_z is nonzero, from t_1 to t_2 only B^i_x is nonzero and from t_2 to t_3 only B^i_z is again nonzero. For instance, the gate $iH \in \mathrm{SU}(2)$, equivalent to the Hadamard gate $H \in \mathrm{U}(2)$ up to a global phase, can be realized as in Fig. 3 by properly choosing the time-integrals in Eq. (4). We cannot achieve $\mathrm{U}(2^n)$ for n qubits since the Hamiltonian for the entire quantum register turns out to be traceless, thus producing only $\mathrm{SU}(2^n)$ matrices. However, the global phase factor is not physical.

The above Hamiltonian is an idealization and does not take any decoherence mechanisms into account. To justify

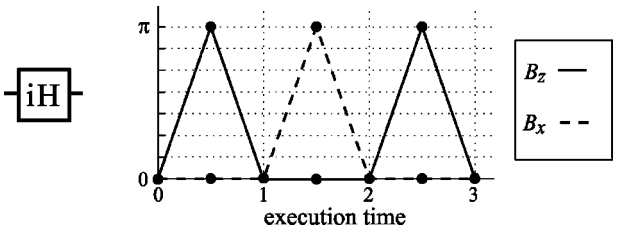

FIG. 3. Pulse sequence implementing an equivalent of the Hadamard gate. Solid line indicates B_x^i while the dashed line shows B_z^i.

this omission, we have to ensure that a charge-qubit register is decoherence-free for time scales long enough to execute a practical quantum algorithm. In addition, we have neglected the inhomogenity of the SQUIDs. It may be extremely challenging to fabricate sufficiently uniform junctions. A three-junction design might alleviate this problem. Whereas for the control of M two-junction SQUIDs one needs at least M independent sources of flux, the three-junction design would call for $2M$ independent sources. The extra sources may be used to compensate the structural nonuniformities. The noise in the control parameters has also been neglected but it will turn out that the error will grow linearly with the rms displacement of uncorrelated Gaussian noise. Correlated noise may only be tolerated if it is very weak. We have also neglected the issue of quantum measurement altogether in the above.

A crucial assumption is that $k_B T \ln N_{qp} \ll E_J \ll E_C \ll \Delta_{BCS}$, where N_{qp} is the number of quasiparticle modes. Typical operation frequencies would be in the GHz range and the operation temperature could be tens of mK. For our two-state Hamiltonian to apply, we should actually insist that, instead of $E_J \ll E_C$, the requirement $E_J(\Phi_i) \ll E_C$ holds. It may appear at first that B_x^i cannot take on values exceeding B_z^i. However, this does not hold since the gate charge also plays a role; values of B_z^i can be very small if n_g^i is tuned close to one half. Since we employ natural units we may freely rescale the Hamiltonian while rescaling time. This justifies our choice $C=1$ above. Furthermore, it is always possible to confine the parameter values within an experimentally accessible range. For more discussion, see Ref. [20].

IV. IMPLEMENTING A QUANTUM-GATE LIBRARY

The evaluation of the time-development operator U is straightforward once the externally controlled physical parameters for the quantum register are given. Here we use numerical optimization to solve the inverse problem; namely, we find the proper sequence for the control variables which produce the given quantum gate.

A. Unitary time evolution

The temporal evolution of the Josephson charge-qubit register is described by a unitary operator

$$U_{\gamma(t)} = \mathcal{T} \exp\left(-i \int_{\gamma(t)} \mathcal{H}(\gamma(t)) dt \right), \tag{5}$$

where $\mathcal{T}$ stands for the time-ordering operator and $\mathcal{H}(\gamma(t))$ is the Hamiltonian for the qubit register. The integration is performed along the path $\gamma(t)$ which describes the time evolution of the control parameters in the space spanned by $\{B_x^j(t)\}$ and $\{B_z^j(t)\}$.

Instead of considering paths $\gamma(t)$ with infinitely many degrees of freedom, we focus on paths parametrized by a finite set of parameters X_γ. This is accomplished by restricting the path $\gamma(t)$ to polygons in the parameter space. Since the pulse sequence starts and ends at the origin, it becomes possible to consistently arrange gates as a sequence. For an n-qubit register, the control-parameter path $\gamma(t)$ is of the vector form

$$\gamma(t) = [B_z^1(t), \ldots, B_z^n(t); B_x^1(t), \ldots, B_x^n(t)]^T, \tag{6}$$

where $B_z^i(t)$ and $B_z^i(t)$ are piecewise linear functions of time for the chosen parametrization. Hence, in order to evaluate Eq. (5), one only needs to specify the $2n$ coordinates for the ν vertices of the polygon, which we denote collectively as X_γ. We let the parameter loop start at the origin, i.e., at the degeneracy point where no time development takes place. We further set the time spent in traversing each edge of the polygon to be unity.

In our scheme, the execution time for each quantum gate depends linearly on the number ν of the vertices in the parameter path. This yields a nontrivial relation between the execution time of the algorithm and the size of the gates. First note that each k-qubit gate represents a matrix in $SU(2^k)$. To implement the gate, one needs to have enough vertices to parametrize the unitary group $SU(2^k)$, which has $2^{2k}-1$ generators. In our model, we have $2k$ parameters for each vertex, which implies $2k\nu \geqslant 2^{2k}-1$. We have used $\nu = 4$ for the two-, and $\nu = 11$ for the three-qubit gates.

To evaluate the unitary operator $U_{\gamma(t)}$ we must find a numerical method which is efficient, yet numerically stable. We divide the path $\gamma(t)$ into tiny intervals that take a time Δt to traverse. If γ_i collectively denotes the values of all the parameters in the midpoint of the ith interval, and m is the number of such intervals, we then find to a good approximation

$$U_{X_\gamma} \approx \exp[-i\mathcal{H}(\gamma_m)\Delta t] \ldots \exp[-i\mathcal{H}(\gamma_1)\Delta t]. \tag{7}$$

We employ the truncated Taylor series expansion

$$e^{-i\mathcal{H}\Delta t} \approx \sum_{k=0}^{l} \frac{(-i\mathcal{H}\Delta t)^k}{k!} \tag{8}$$

to evaluate each factor in Eq. (7). We could have used the Cayley form

$$e^{-i\mathcal{H}\Delta t} \approx (1 - i\mathcal{H}\Delta t/2)(1 + i\mathcal{H}\Delta t/2)^{-1}, \tag{9}$$

or an adaptive Runge-Kutta method to integrate the Schrödinger equation as well. It turns out that the Taylor expansion with $l=3$ is fast and yields enough precision for our purposes. The precision of the approximation is verified by comparing the results with those obtained with an exact spectral decomposition of $\mathcal{H}$.

B. Minimization of the error function

Given an arbitrary unitary matrix $\hat{U}$, our aim is to find a parameter sequence X_γ for the Josephson charge-qubit regis-

ter that yields a unitary matrix $U_{X_\gamma} = \hat{U}$. We convert the inverse problem into an optimization task; namely, that of finding the zeroes of the error function

$$p(X_\gamma) = \|\hat{U} - U_{X_\gamma}\|_{\mathrm{F}}. \tag{10}$$

Minimizing $p(X_\gamma)$ over all the possible values of X_γ will produce an approximation U_{X_γ} for the desired gate $\hat{U}$. Above $\|\cdot_{\mathrm{F}}\|$ denotes the Frobenius trace norm, defined as $\|A\|_{\mathrm{F}} = \sqrt{\mathrm{Tr}(A^\dagger A)}$, which is numerically efficient to compute. Since all the matrix norms are mathematically equivalent, a small value of $\|A\|_{\mathrm{F}}$ implies a small value in all other norms as well, see, e.g., Ref. [39].

For this minimization problem, the error-function landscape is rough consisting of many local minima. Consequently, any gradient-based minimization algorithm will encounter serious problems. Thus, we have found the minimum point $X_{\min}$ for all the gates presented in Sec. V using repeated application of a robust polytope algorithm [30,40,41]. In the first search, the initial condition was chosen randomly. At the next stage, the outcome of the previous search was utilized. In order to accelerate the evaluation of $U_{\gamma(t)}$ we varied the time steps Δt; at an early stage of the optimization a coarse step was employed while the final results were produced using very fine steps. Typical convergence of the search algorithm is illustrated in Fig. 4.

The required accuracy for the gate operations is in the range 10^{-4}–10^{-5} for $p(X_\gamma)$ for two reasons: (i) in quantum circuits with a small number of gates, the total error remains small, and (ii) for large circuits, quantum-error correction can in principle be utilized to reduce the accumulated errors [19]. Our minimization routine takes on the order of 10^6 function evaluations to reach the required accuracy.

V. EXAMPLE

To demonstrate the level of complexity for the quantum circuit and the demands on the execution time, we explicitly present the quantum circuit and some physical implementation for the gates needed for Shor's algorithm to factor the number $N=21$. We choose $a=11$ and hardwire this into the quantum circuit.

A. Quantum circuit

Figure 5 illustrates the structure of the quantum part of the factorization algorithm for the number 21. Since it takes 5 bits to store the number 21, a 5-qubit register $|y\rangle_5$ and a 10-qubit register $|x\rangle_{10}$ are required.

For scratch space we need a six-qubit register $|z\rangle_6$ and one ancilla qubit $|a\rangle$. Each thirteen-qubit controlled-MMUL (modular multiplier) gate in the algorithm can be further decomposed as indicated in Fig. 5. The controlled-MADD (modular adder) gates can also be decomposed. The ten-qubit QFT breaks down to 42 two-qubit gates and one three-qubit QFT. Similarly, the six-qubit QFT can be equivalently implemented as a sequence of 18 two-qubit gates and one three-qubit QFT. In this manner we can implement the entire algorithm using only one-, two- and three-qubit gates. The control parameter sequence realizing each of them can then be found using the scheme outlined in Sec. IV. Two examples of the pulse sequences are also shown in Fig. 5 (bottom insets).

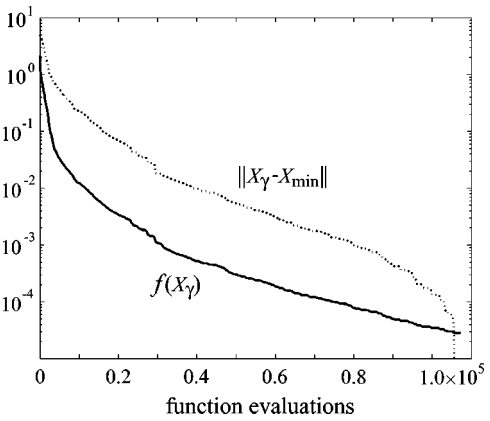

FIG. 4. Convergence of the algorithm for the Fredkin gate. The error function values are indicated by the solid line and the distance of the parameter sequence from the numerical optimum $X_{\min}$ by the dotted line.

B. Physical implementation

The experimental feasibility of the algorithm depends on how complicated it is compared to the present state of technology. Following the above construction of the quantum circuit, the full Shor algorithm to factor 21 requires about 2300 three-qubit gates and some 5900 two-qubit gates, in total. Also a few one-qubit gates are needed but alternatively they can all be merged into the multi-qubit gates. If only two-qubit gates are available, about 16 400 of them are required. If only a minimal set of elementary gates, say the CNOT gate and one-qubit rotations are available, the total number of gates is remarkably higher. In our scheme the execution time of the algorithm is proportional to the total length of the piecewise linear parameter path which governs the physical implementation of the gate operations. Each of the three-qubit gates requires at least a 12-edged polygonal path $\gamma(t)$ whereas two-qubit gates can be implemented with 5 edges. Consequently, on the order of 57100 edges are required for the whole algorithm if arbitrary three-qubit gates are available, whereas $\sim$82 000 edges would be required for an implementation with only two-qubit gates.

The ability to find the physical implementation of the gate library for Shor's algorithm is demonstrated with some further examples. Figure 6 shows how to physically implement the controlled swap gate. We have taken advantage of tailored three-qubit implementations: a one-qubit phase-shift gate and a three-qubit controlled^2 phase-shift gate are merged into one three-qubit gate, see Fig. 7.

The control parameter sequences presented will yield unitary operations which approximate the desired gate operations with an accuracy better than 10^{-4} in the error-function values for the three-qubit gates. For two-qubit gates the error is negligible. Since the whole factorization circuit consists of some 10^3 three-qubit gates, we obtain a total error of $\sim 10^{-1}$.

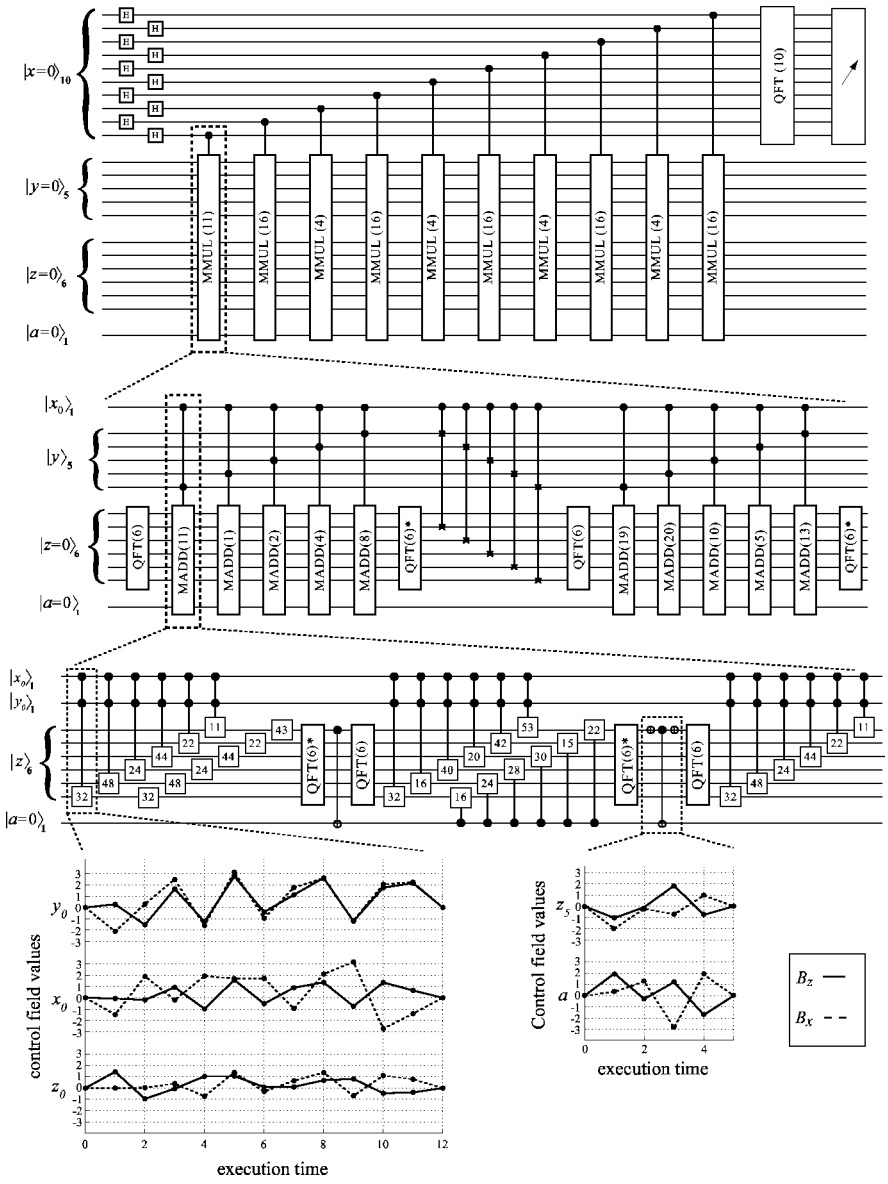

FIG. 5. Quantum circuit for Shor's algorithm factoring the number 21 with the parameter value $a=11$. The full circuit is shown topmost and the decompositions of the modular multiplier and adder blocks are indicated with dashed lines. The gates in the circuit have their conventional meanings, except that we denote a phase-shift gate by a box with a single number ϕ in it meaning that the phase of the state $|1\rangle$ is shifted by $e^{2\pi i\phi/2^n}$ with respect to the state $|0\rangle$. Two examples of numerically optimized parameter sequences are also shown.

This is sufficient for the deduction of the essential information from the output. The robustness of the gates obtained was studied numerically by adding Gaussian noise to the vertices of the path. The error function was found to scale linearly with the rms of the variance of the Gaussian noise: error $\approx 6\times\langle\text{noise}\rangle_{\text{rms}}$, which is probably acceptable.

VI. DISCUSSION

In this paper we have discussed the implementation of Shor's factorization algorithm using a Josephson charge-qubit register. This method is suitable for the first experimental demonstration of factoring a medium-scale integer 2^4-2^{20}. As an example of this method we have studied the algorithm for factoring 21. The only integer smaller than 21 for which Shor's algorithm is applicable is 15, but this is a special case having only the periods 2 and 4. For the experimental factoring of 15 one should consider more direct methods [7] to implement the modular exponential function. For a

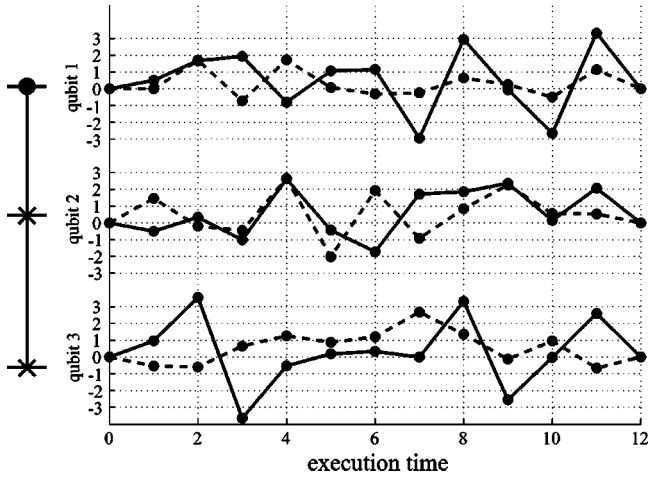

FIG. 6. Control parameters for the Fredkin gate. Solid line indicates B_z^i while the dashed line shows B_x^i.

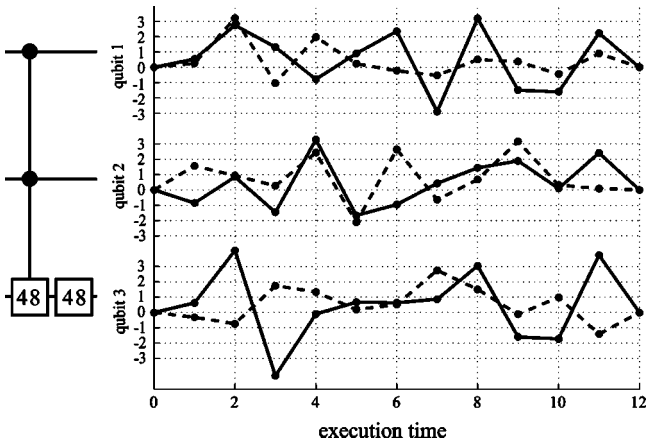

FIG. 7. Control parameters for a composite gate consisting of a twice controlled phase shift and a one-qubit rotation, see the text. Solid line indicates B_z^i while the dashed line shows B_x^i.

larger integer N other approaches, e.g., the Schönhage-Strassen [38] multiplication algorithm, will provide a more efficient quantum circuit. Our approach of numerically determining the optimized gates can be generalized to other physical realizations with tunable couplings as well. The only requirement is that the system allows total control over the control parameters.

We have found that the number of qubits and quantum gates that are involved in carrying out the algorithm is rather large from the point of view of current technology. Thus the realization of a general factorization algorithm for a large integer N will be challenging. Consequently, the scaling of the chosen algorithm, both in time and space, will be of prime importance.

The method we propose utilizes three-qubit gates, which compress the required quantum-gate array, resulting in a shorter execution time and smaller errors. One should also consider other implementations of the quantum algorithms that employ gates acting on a larger number of qubits to further decrease the number of gates and execution time. For example, four-qubit gates may be achievable, but this involves harder numerical optimization.

Finally, let us consider the experimental feasibility of our scheme. To factor the number 21, we need on the order of

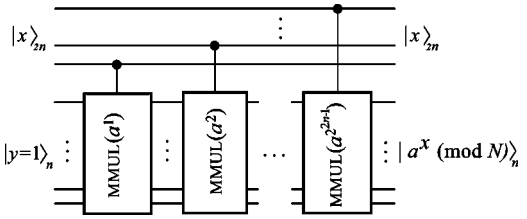

FIG. 8. Quantum circuit required for performing the evaluation of the modular exponential function utilizing the CMMUL(b) gates.

10^4 edges along the control-parameter path. Assuming that the coherence time is on the order of 10^{-6} s implies that the upper limit for the duration of each edge is 10^{-10} s. Since our dimensionless control parameters in the examples are on the order of unity, the energy scale in angular frequencies must be at least on the order of 10^{10} s^{-1}. Typical charging energies for, say, thin-film aluminum structures may be on the order of 10^{-23} J which corresponds to 10^{11} s^{-1}. The ultimate limiting energy scale is the BCS gap, which for thin-film aluminum corresponds to an angular frequency of about 3×10^{11} s^{-1}. Based on these rough estimates, we argue that factoring the number 21 on Josephson charge qubits is, in principle, experimentally accessible.

Constructing a quantum algorithm to decrypt RSA-155 coding which involves a 512-bit integer N with the scheme that we have presented would require on the order of 2000 qubits. Since the execution time scales as $n^3 \log n$ tens of seconds of decoherence time is needed. This agrees with the estimates in Ref. [42] and poses a huge experimental challenge. This can be compared to the 8000 MIPS (million instructions per second) years of classical computing power which is needed to decrypt the code using the general numeric field sieve technique [1]. Thus Shor's algorithm does appear impractical for decrypting RSA-155. However, it provides the only known potentially feasible method to factor numbers having 1024 or more bits.

We conclude that it is possible to demonstrate the implementation of Shor's algorithm on a Josephson charge-qubit register. Nevertheless, for successful experimental implementation of large-scale algorithms significant improvements in coherence times, fabrication, and ultrafast control of qubits is mandatory.

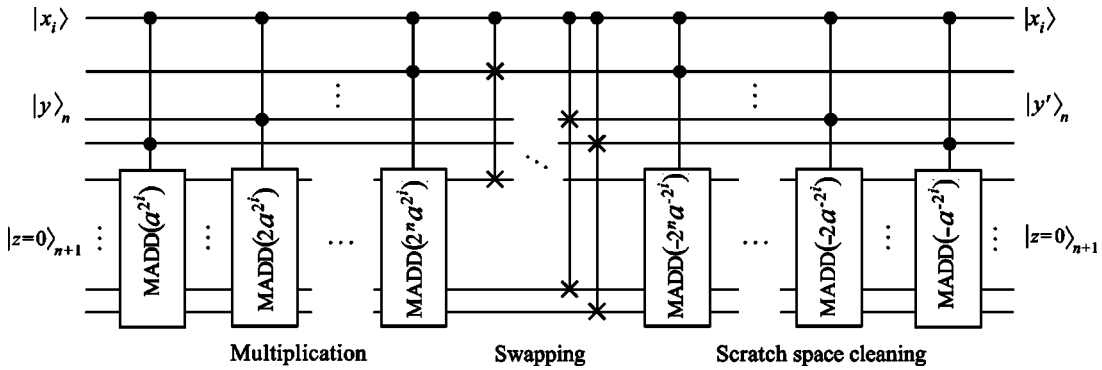

FIG. 9. Decomposition of the CMMUL(a^{2^i}) gate using C^{2}MADD(b) and controlled swap gates. If the controlling qubit $|x_i\rangle$ is active the resulting state is $y' \equiv y + a^{2^i} \pmod N$, otherwise $y' = y$. Note that the gate utilizes an additional ancilla register $|z\rangle_{n+1}$ to perform the calculation.

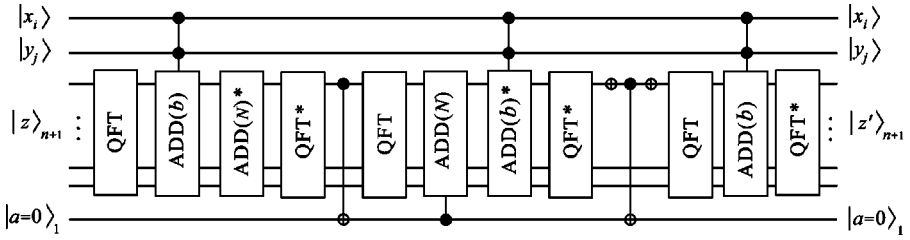

FIG. 10. Decomposition of the C²MADD(b) gate into elementary gates, QFT gates, and additions in the Fourier basis (C²ADD). The asterisk stands for a Hermitian conjugate; it corresponds to a gate for subtraction. The gate takes an input value $z<N\leq 2^n$ and yields $|z'\rangle_{n+1}=|z+b(\mathrm{mod}\ N)\rangle_{n+1}$ if the control qubits $x_i=1$ and $y_j=1$. Otherwise $|z'\rangle_{n+1}=|z\rangle_{n+1}$. The ancilla qubit $|a\rangle$ is one if $z+b>N$ and zero otherwise.

Note added. Recently, it was brought to our attention that a similar circuit implementing Shor's algorithm has been constructed for a linear nearest-neighbor (LNN) qubit array [43] independent of any specific physical realization.

ACKNOWLEDGMENTS

J.J.V. thanks the Foundation of Technology (TES, Finland) and the Emil Aaltonen Foundation for financial support. M.N. thanks the Helsinki University of Technology for financial support; he is grateful for partial support of a Grant-in-Aid from the MEXT and JSPS, Japan (Project Nos. 14540346 and 13135215). The research has been supported in the Materials Physics Laboratory at HUT by Academy of Finland through Research Grants in Theoretical Materials Physics (No. 201710) and in Quantum Computation (No. 206457). We also thank Robert Joynt, Jani Kivioja, Mikko Möttönen, Jukka Pekola, Ville Bergholm, and Olli-Matti Penttinen for enlightening discussions. We are grateful to CSC—Scientific Computing Ltd., Finland for parallel computing resources.

APPENDIX A: CONSTRUCTION OF A QUANTUM CIRCUIT

Here we represent the construction of a quantum circuit needed for an evaluation of the modular exponential function $a^x(\mathrm{mod}\ N)$. We assume the values of a and N to be constant integers coprime to each other. This approach takes advantage of the fast powers trick, see Eq. (A1) below, as well as the construction of a multiplier suggested by Beauregard [31], which in part employs the adder of Draper [32].

The modular exponential function can be expressed in terms of modular products:

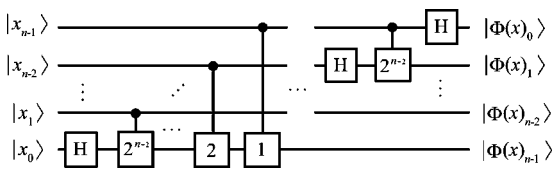

FIG. 11. Quantum circuit for an n-qubit Fourier transformation. Here H stands for the Hadamard gate. The controlled phase-shift gates are labeled with the numbers k which correspond to the phase shifts $e^{i2\pi k/2^n}$. Note the reversed order of the qubits on the right-hand side.

$$a^x \equiv \prod_{i=0}^{2n-1} (a^{2^i x_i}(\mathrm{mod}\ N))(\mathrm{mod}\ N), \tag{A1}$$

where we have used the binary expansion $x=2^0x_0+2^1x_1+2^{n-1}x_{n-1}$, $x_i\in\{0,1\}$. Note that the number of factors in Eq. (A1) grows only linearly for increasing n. The longhand multiplication is based on the relation

$$a^{2^i}x \equiv \sum_{k=0}^{2n-1} (a^{2^i 2^k x_k}(\mathrm{mod}\ N))(\mathrm{mod}\ N), \tag{A2}$$

which again involves only a linear number of terms.

Equation (A1) yields a decomposition of the modular exponential function into controlled modular multiplication gates [CMMUL(a^{2^i})], see Fig. 8. According to Eq. (A2), each of the MMUL(a^{2^i}) gates can be implemented with the sequence of the modular adders, see Fig. 9. Since this decomposition of CMMUL(a^{2^i}) requires extra space for the intermediate results, we are forced to introduce a scratch space $|z\rangle_{n+1}$ into the setup. Initially, we set $|z\rangle_{n+1}=|0\rangle_{n+1}$. Moreover, we must reset the extra scratch space after each multiplication. This is accomplished by multiplication with the inverse element b^{-1} where $b=a^{2^i}$. Let us consider how the gate CMMUL(b) works:

$$\begin{aligned}
|x\rangle|0\rangle &\rightarrow |x\rangle|0+bx(\mathrm{mod}\ N)\rangle \quad \text{(product)}\\
&\rightarrow bx(\mathrm{mod}\ N)|x\rangle \quad \text{(swap)}\\
&\rightarrow |bx(\mathrm{mod}\ N)\rangle|x+(-b^{-1})(bx(\mathrm{mod}\ N))\rangle\\
&= bx(\mathrm{mod}\ N)|0\rangle \quad \text{(result)}.
\end{aligned}$$

Euler's totient theorem guarantees that for every b which is coprime to N, a modular inverse $b^{-1}\in\mathbb{N}$ exists. Furthermore, the extended Euclidean algorithm provides an efficient way to find the numerical value for b^{-1}.

Figure 10 presents the decomposition of the C²MADD(b) gate ($b\in\mathbb{N}$) using adders in the Fourier space. The idea is first to calculate $z'=z+b-N$. If $z'<0$ the ancilla a, which is initially zero, is flipped and N is added to z' yielding $z'=z+b$. The rest of the circuit is needed to reset a to zero.

The circuit simplifies when multiple C^2MADD(b) gates are applied since the final QFT* will cancel against the initial QFT of two consecutive gates. This is taken into account in counting the total number of gates and in Fig. 5. An obvious

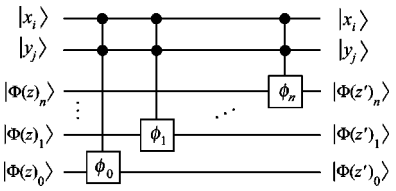

FIG. 12. Quantum circuit for the twice controlled addition of a classical number b into the quantum register $|z\rangle_{n+1}$ in the Fourier basis. The twice controlled phase-shift gates serve to yield the phase shift $e^{2\pi i\phi_k/2^n}$ provided that the control qubits $|x_i\rangle$ and $|y_j\rangle$ are active.

drawback of this implementation is the need for a number of QFT gates. However, we need to introduce only one ancilla qubit $|a\rangle$.

The decomposition of the gate C²MADD(b) consists of twice controlled adders, $(n+1)$-qubit QFTs, one-qubit NOTS, and CNOTS. The decomposition of a QFT-gate into one- and two-qubit gates [2] is represented in Fig. 11. Since Fourier space is utilized, the C²ADD(b) gates can be implemented [32] using controlled^2 phase shifts. The quantum gate sequence for an adder working in the Fourier space is depicted in Fig. 12. The values of the phase shifts for the gate C²ADD(b) are given by $e^{2\pi i\phi_j/2^n}$, where $\phi_j=2^j b$.

Finally, we are in the position to perform the unitary transformation which implements the modular exponential function using only one-, two- and three-qubit gates. If the three-qubit gates are not available, further decomposition into one- and two-qubit gates is needed, see Ref. [24]. For instance, each three-qubit twice controlled U gate decomposes into five two-qubit gates and each Fredkin gate takes seven two-qubit gates to implement.

APPENDIX B: DERIVATION OF THE HAMILTONIAN

1. The Lagrangian

Consider a homogenous array of mesoscopic superconducting islands as an idealized model of a quantum register, see Fig. 2. The basis states of the qubit correspond to either zero or one extra Cooper pair residing on the superconducting island, denoted by $|0\rangle$ and $|1\rangle$, respectively. Each of the islands, or Cooper-pair boxes, is capacitively coupled to a gate voltage, $V_{\rm g}^i$. In addition, they are coupled to a superconducting lead through a mesoscopic SQUID with identical junctions, each having the same Josephson energy $E_{\rm J}/2$ and capacitance $C_{\rm J}/2$. All these qubits are then coupled in parallel with an inductor, L. The lowest relevant energy scale is set by the thermal energy $k_{\rm B}T$ and the highest scale by the BCS gap $\Delta_{\rm BCS}$.

We assume that the gate voltage $V_{\rm g}^i$ and the time-dependent flux Φ_i through each SQUID can be controlled externally. The flux Φ_i may be controlled with an adjustable current I_i through an external coil, see the dotted line in Fig. 2(a). In this setup, the Cooper pairs can tunnel coherently to a superconducting electrode. We denote the time-integral of voltage, or difference in flux units, over the left junction of the ith SQUID by ϕ_i and the flux through the inductor by φ. The phase difference in flux units over the rightmost junction is $\phi_i-\Phi_i$. We take the positive direction for flux to be directed outward normal to the page.

We adopt ϕ_i and φ as the dynamical variables, whereas Φ_i and $V_{\rm g}^i$ are external adjustable parameters. With the help of elementary circuit analysis [44], we obtain the Lagrangian for the qubit register

$$\mathcal{L}=\frac{1}{2}\sum_{i=1}^{M}\left[\frac{C_{\rm J}}{2}\dot{\phi}_i^2+\frac{C_{\rm J}}{2}(\dot{\phi}_i-\dot{\Phi}_i)^2+C_{\rm g}(\dot{\phi}_i+\dot{\varphi}-V_{\rm g}^i)^2-\right]\frac{\varphi^2}{2L}$$
$$+\frac{1}{2}\sum_{i=1}^{M}\left[E_{\rm J}\cos\left(\frac{2e}{\hbar}\phi_i\right)+E_{\rm J}\cos\left(\frac{2e}{\hbar}(\phi_i-\Phi_i)\right)\right]. \quad \text{(B1)}$$

We now perform the following changes of variables

$$\phi_i\rightarrow\phi_i+\frac{\Phi_i}{2}-\frac{C_{\rm g}}{C_{\rm J}+C_{\rm g}}\varphi, \quad \text{(B2)}$$

which yields

$$\mathcal{L}=\frac{1}{2}\sum_{i=1}^{M}\left[(C_{\rm J}+C_{\rm g})\dot{\phi}_i^2-2C_{\rm g}\left(V_{\rm g}^i-\frac{\dot{\Phi}_i}{2}\right)\dot{\phi}_i\right.$$
$$\left.+E_{\rm J}\cos\left(\pi\frac{\Phi_i}{\Phi_0}\right)\cos\left(\frac{2e}{\hbar}\phi_i-\frac{2\pi C_{\rm qb}}{\Phi_0 C_{\rm J}}\varphi\right)\right]+\frac{1}{2}MC_{\rm qb}\dot{\varphi}^2$$
$$-\sum_{i=1}^{M}C_{\rm qb}\left(V_{\rm g}^i-\frac{\dot{\Phi}_i}{2}\right)\dot{\varphi}-\frac{\varphi^2}{2L}+\text{const.} \quad \text{(B3)}$$

Above, $\Phi_0=h/2e$ is the flux quantum and $C_{\rm qb}=C_{\rm J}C_{\rm g}/(C_{\rm J}+C_{\rm g})$ is the qubit capacitance in the LC circuit. Note that the effective Josephson energy of each SQUID can now be tuned. We denote this tunable energy parameter in Eq. (B3) as

$$E_{\rm J}(\Phi_i)=E_{\rm J}\cos\left(\pi\frac{\Phi_i}{\Phi_0}\right). \quad \text{(B4)}$$

The canonical momenta are given by $Q=\partial\mathcal{L}/\partial\dot{\varphi}$ and $q_i=\partial\mathcal{L}/\partial\dot{\phi}_i$. We interpret Q as the charge on the collective capacitor formed by the whole qubit register, whereas q_i is the charge on the ith island. Note that the charge q_i is related to the number n_i of Cooper pairs on the island through $q_i=-2en_i$.

2. The Hamiltonian

We are now in the position to write down the Hamiltonian for the quantum register. We will also immediately replace the canonical variables by operators in order to quantize the register. Moreover, we will employ the number of excess Cooper pairs n_i on the island and the superconducting phase difference instead of the usual quantum-mechanical conjugates. We will also change to the more common phase difference θ_i related to ϕ_i through $\theta_i=(2e/\hbar)\phi_i$. Hence the relevant commutation relations are $[\theta_i,n_i]=-i$ and $[\varphi,Q]=i\hbar$. All the other commutators vanish. Using the Legendre transformation

$$\mathcal{H} = Q\dot{\varphi} + \sum_{i=1}^{M} q_i \dot{\phi}_i - \mathcal{L} \tag{B5}$$

we obtain

$$\mathcal{H} = \sum_{i=1}^{M} \left[\frac{2e^2(n_i - n_g^i)^2}{C_J + C_g} - E_J(\Phi_i)\cos\left(\theta_i - \frac{2\pi C_{qb}}{\Phi_0 C_J}\varphi\right)\right] + \frac{(Q+Q_g)^2}{2MC_{qb}} + \frac{\varphi^2}{2L}. \tag{B6}$$

We have denoted the effective gate charge by

$$n_g^i = \frac{C_g}{2e}\left(V_g^i - \frac{\dot{\Phi}_i}{2}\right) \tag{B7}$$

and

$$Q_g = \sum_{i=1}^{M} C_{qp}\left(V_g^i - \frac{\dot{\Phi}_i}{2}\right). \tag{B8}$$

In addition to the usual voltage contribution, the time dependence of the flux also plays a role. In practice, the rates of change of the flux are negligible in comparison to the voltages and this term may safely be dropped.

The Hamiltonian in Eq. (B6) describes the register of qubits (n_i, ϕ_i) coupled to a quantum-mechanical *LC* resonator, i.e., a harmonic oscillator (Q, φ). We will now assume that the rms fluctuations of φ are small compared to the flux quantum Φ_0 and also that the harmonic oscillator has a sufficiently high frequency, such that it stays in the ground state. The first assumption implies that

$$\cos\left(\theta_i - \frac{2\pi C_{qb}}{\Phi_0 C_J}\varphi\right) \approx \cos\,\theta_i + \frac{2\pi C_{qb}}{\Phi_0 C_J}\varphi\,\sin\,\theta_i. \tag{B9}$$

The second assumption will cause an effective coupling between the qubits. Namely, the Hamiltonian may now be rewritten in the more suggestive form

$$\mathcal{H} \approx \sum_{i=1}^{M}\left[\frac{2e^2(n_i - n_g^i)^2}{C_J + C_g} - E_J(\Phi_i)\cos\,\theta_i\right] + \frac{(Q+Q_g)^2}{2MC_{qb}} + \frac{(\varphi - \hat{\varphi}^2)}{2L} - \frac{\hat{\varphi}^2}{2L}, \tag{B10}$$

where the operator $\hat{\varphi}$ is given by

$$\hat{\varphi} = \frac{2\pi L C_{qb}}{\Phi_0 C_J}\sum_{i=1}^{M} E_J(\Phi_i)\sin\,\theta_i. \tag{B11}$$

We now see from Eq. (B10) that in the high-frequency limit the harmonic oscillator is effectively decoupled from the qubit register. The effect of the qubit register is thus to redefine the minimum of the potential energy for the oscillator. This does not affect the spectrum of the oscillator, since it will adiabatically follow its ground state in the low-temperature limit. We may therefore trace over the degrees of freedom of the harmonic oscillator and the harmonic-oscillator energy will merely yield a zero-point energy contribution, $\hbar\omega_{LC}/2$. The effective Hamiltonian describing the dynamics of the coupled qubit register alone is thus

$$\mathcal{H} \approx \sum_{i=1}^{M}\left[\frac{2e^2(n_i - n_g^i)^2}{C_J + C_g} - E_J(\Phi_i)\cos\,\theta_i\right] - \frac{2\pi^2 L C_{qb}^2}{\Phi_0^2 C_J^2}\left(\sum_{i=1}^{M} E_J(\Phi_i)\sin\,\theta_i\right)^2. \tag{B12}$$

This result is in agreement with the one presented in Ref. [20]. We conclude that the *LC*-oscillator has created a virtual coupling between the qubits.

For the purposes of quantum computing, it is convenient to truncate the Hilbert space such that each Cooper-pair box will have only two basis states. In the limit of a high charging energy $E_C = 2e^2/(C_g + C_J)$ relative to the Josephson energy E_J, we may argue that in the region $0 \leqslant n_g^i \leqslant 1$ only the states with $n_i = 0,1$ can be occupied. We use the vector representation for these states, in which $|0\rangle_i = (1\ 0)_i^T$ and $|1\rangle_i = (0\ 1)_i^T$.

The basis states of the Hilbert space are orthogonal $\langle k|e^{\pm i\theta}|l\rangle = \delta_{k,l\mp 1}$. Hence, in this two-state approximation, $\cos\,\theta_i = \frac{1}{2}\sigma_x^i$ and $\sin\,\theta_i = \frac{1}{2}\sigma_y^i$, where, e.g.,

$$\alpha_x^i = \underbrace{I \otimes \ldots \otimes I}_{i-1 \text{ times}} \otimes \alpha_x \otimes \underbrace{I \otimes I \ldots \otimes I}_{M-i \text{ times}}.$$

Finally, omitting the constant terms, we obtain the Hamiltonian in the Pauli-matrix representation

$$\mathcal{H}_{qb} = \sum_{i=1}^{M}\left[-\frac{E_C}{2}(1 - 2n_g^i)\sigma_z^i - \frac{E_J(\Phi_i)}{2}\sigma_x^i\right] - \frac{\pi^2 L}{\Phi_0^2}\left(\frac{C_{qb}}{C_J}\right)^2 \sum_{i=1}^{M}\sum_{j=i+1}^{M} E_J(\Phi_i)E_J(\Phi_j)\sigma_y^i \otimes \sigma_y^j, \tag{B13}$$

which results in Eqs. (2) and (3) of the main text.

[1] A. Galindo and M. A. Martín-Delgado, Rev. Mod. Phys. **74**, 347 (2002).

[2] M. A. Nielsen and I. L. Chuang, *Quantum Computation and Quantum Information* (Cambridge University Press, Cambridge, 2000).

[3] P. W. Shor, in *Proceedings of the 35th Annual Symposium on Foundations of Computer Science*, edited by S. Goldwasser (IEEE Computer Society Press, Los Alamitos, CA, 1994), Vol. 124.

[4] L. K. Grover, Phys. Rev. Lett. **79**, 325 (1997).

[5] D. R. Stinson, *Cryptography: Theory and Practice* (CRC Press, Boca Raton, FL, 1995).
[6] M. Steffen, W. van Dam, T. Hogg, G. Breyta, and I. Chuang, Phys. Rev. Lett. **90**, 067903 (2003).
[7] L. M. K. Vandersypen, M. Steffen, G. Breyta, C. S. Yannoni, M. H. Sherwood, and I. L. Chuang, Nature (London) **414**, 883 (2001).
[8] D. Leibfried, B. DeMarco, V. Meyer, D. Lucas, M. Barrett, J. Britton, W. M. Itano, B. Jelenkovi, C. Langer, T. Rosenband, and D. J. Wineland, Nature (London) **422**, 412 (2003).
[9] F. Schmidt-Kaler, H. Häffner, M. Riebe, S. Gulde, G. P. T. Lancaster, T. Deuschle, C. Becher, C. F. Roos, J. Eschner, and R. Blatt, Nature (London) **422**, 408 (2003).
[10] C.-P. Yang, Shih.-I. Chu, and S. Han, Phys. Rev. A **67**, 042311 (2003).
[11] W. G. van der Wiel, S. De Franceschi, J. M. Elzerman, T. Fujisawa, S. Tarucha, and L. P. Kouwenhoven, Rev. Mod. Phys. **75**, 1 (2003).
[12] T. P. Orlando, J. E. Mooij, L. Tian, C. H. van der Wal, L. Levitov, S. Lloyd, and J. J. Mazo, Phys. Rev. B **60**, 15398 (1999).
[13] Y. Yu, S. Han, X. Chu, S. Chu, and Z. Wang, Science **296**, 889 (2002).
[14] Y. A. Pashkin, T. Yamamoto, O. Astafiev, Y. Nakamura, D. V. Averin, and J. S. Tsai, Nature (London) **421**, 823 (2003); T. Yamamoto, Y. A. Pashkin, O. Astafiev, Y. Nakamura, D. V. Averin, and J. S. Tsai, *ibid.* **425**, 944 (2003).
[15] Y. Nakamura, Yu. A. Pashkin, and J. S. Tsai, Nature (London) **398**, 786 (1999); Phys. Rev. Lett. **87**, 246601 (2002); Y. Nakamura, Yu. A. Pashkin, T. Yamamoto, and J. S. Tsai, *ibid.* **88**, 047901 (2002).
[16] J. M. Martinis, S. Nam, J. Aumentado, and C. Urbina, Phys. Rev. Lett. **89**, 117901 (2002).
[17] D. Vion, A. Aassime, A. Cottet, P. Joyez, H. Pothier, C. Urbina, D. Esteve, and M. H. Devoret, Science **296**, 886 (2002).
[18] W. H. Zurek, Rev. Mod. Phys. **75**, 715 (2003).
[19] D. P. DiVincenzo, Fortschr. Phys. **48**, 771 (2000).
[20] Yu. Makhlin, G. Schön, and A. Shnirman, Rev. Mod. Phys. **73**, 357 (2001).
[21] D. V. Averin and C. Bruder, Phys. Rev. Lett. **91**, 057003 (2003).
[22] J. Q. You, J. S. Tsai, and F. Nori, Phys. Rev. Lett. **89**, 197902 (2002).
[23] M. J. Storcz and F. K. Wilhelm, Phys. Rev. A **67**, 042319 (2003).
[24] A. Barenco, C. H. Bennett, R. Cleve, D. P. DiVincenzo, N. Margolus, P. Shor, T. Sleator, J. A. Smolin, and H. Weinfurter, Phys. Rev. A **52**, 3457 (1995).
[25] A. V. Aho, R. Sethi, and J. D. Ullman, *Compilers: Principles, Techniques and Tools* (Addison-Wesley, Reading, MA, 1986).
[26] A. O. Niskanen, J. J. Vartiainen, and M. M. Salomaa, Phys. Rev. Lett. **90**, 197901 (2003).
[27] G. Burkard, D. Loss, D. P. DiVincenzo, and J. A. Smolin, Phys. Rev. B **60**, 11404 (1999).
[28] N. Schuch and J. Siewert, Phys. Rev. Lett. **91**, 027902 (2003).
[29] J. Zhang, J. Vala, S. Sastry, and K. B. Whaley, Phys. Rev. Lett. **91**, 027903 (2003).
[30] J. J. Vartiainen, A. O. Niskanen, M. Nakahara, and M. M. Salomaa, Int. J. Quantum Inf. **2**, 1 (2004).
[31] S. Beauregard, Quantum Inf. Comput. **3**, 175 (2003).
[32] T. Draper, e-print quant-ph/0008033.
[33] J. Gruska, *Quantum Computing* (McGraw-Hill, New York, 1999).
[34] A. Ekert and R. Jozsa, Rev. Mod. Phys. **68**, 733 (1996).
[35] M. Hirvensalo, *Quantum Computing* (Springer, Berlin, 2001).
[36] V. Vedral, A. Barenco, and A. Ekert, Phys. Rev. A **54**, 147 (1996).
[37] D. Beckman, A. N. Chari, S. Devabhaktuni, and J. Preskill, Phys. Rev. A **54**, 1034 (1996).
[38] D. E. Knuth, *The Art of Computer Programming, Vol. 2: Seminumerical Algorithms*, 3rd ed. (Addison-Wesley, Reading, MA, 1998).
[39] G. H. Golub and C. F. Van Loan, *Matrix Computations*, 3rd ed. (The Johns Hopkins University Press, Baltimore, MD, 1996).
[40] A. O. Niskanen, M. Nakahara, and M. M. Salomaa, Phys. Rev. A **67**, 012319 (2003).
[41] J. C. Lagarias, J. A. Reeds, M. H. Wright, and P. E. Wright, SIAM J. Optim. **9**, 112 (1998).
[42] R. J. Hughes, Philos. Trans. R. Soc. London, Ser. A **356**, 1853 (1998).
[43] A. G. Fowler, S. J. Devitt, and L. C. L. Hollenberg, e-print quant-ph/0402196.
[44] M. H. Devoret, *Quantum Fluctuations in Electrical Circuits, Quantum Fluctuations*, edited by S. Reymaud, E. Giacobino, and J. Zinn-Justin (Elsevier Science, Amsterdam, 1997).

Reprinted with permission from the publisher.
In: Physical Review Letters 2003. Vol. 91,
No. 17, pp. 177003-1–4.

Fast and Accurate Single-Island Charge Pump: Implementation of a Cooper Pair Pump

Antti O. Niskanen,[1,2,*] Jukka P. Pekola,[2] and Heikki Seppä[1]
[1]*VTT Information Technology, Microsensing, POB 1207, 02044 VTT, Finland*
[2]*Low Temperature Laboratory, Helsinki University of Technology, POB 2200, FIN-02015 HUT, Finland*
(Received 1 April 2003; published 24 October 2003)

We introduce a Cooper pair "sluice" for the implementation of a frequency-locked current source. The device consists of two mesoscopic SQUIDs and of a single superconducting island with a gate. We demonstrate theoretically that it is possible to obtain a current as high as 0.1 nA at better than ppm accuracy via periodically modulating both the gate charge and the effective Josephson coupling. We find that the device is tolerant against background charge noise and operates well even in a dissipative environment. The effect of the imperfect suppression of the Josephson coupling and the finite operating frequency are also investigated.

DOI: 10.1103/PhysRevLett.91.177003 PACS numbers: 74.50.+r, 03.65.Vf, 73.23.–b, 74.78.Na

Single-electron and Cooper pair devices have attracted considerable attention recently. Applications such as the single-electron pump [1] and the Cooper pair box for quantum computing [2] have demonstrated that at sufficiently low temperatures and high charging energies the quantization of charge leads to some very interesting effects. Especially, it has been shown that single electrons can be pumped extremely accurately at frequencies f of a few MHz with a relative uncertainty of 10^{-8} in normal metal devices according to the relation $I = ef$ [3]. This has resulted in a standard of capacitance. However, the pump frequencies, and thus current levels, have been too low for the realization of a practical accurate current source for nanoelectronic applications or for realizing the quantum measurement triangle [4]. The attempts to generalize the single-electron pump to a superconducting Cooper pair pump [5,6] that, in theory, would allow for higher-frequency pumping have been unsuccessful so far due to a variety of reasons. In particular, Landau-Zener tunneling between energy levels induces pumping errors. In addition, there is always a considerable amount of supercurrent leaking through the pump. Also, the interplay of the two conjugate variables, the phase and the number of Cooper pairs, results in a coherent correction such that the current is no longer given by the relation $I = 2ef$ [7]. Further, the coherent correction is proportional to $\cos\varphi$, where φ is the phase difference over the whole pump, whereas the supercurrent is proportional to $\sin\varphi$ rendering it impossible to choose φ to eliminate both of these simultaneously. The effect of nonidealities can be reduced by adding more junctions, but this will complicate the practical implementation due to the increasing number of control parameters and cross capacitances. Furthermore, one has to take into account the effect of the fluctuating background charges responsible for the $1/f$ noise and the phase fluctuations caused by the electromagnetic environment. The latter, however, may help in achieving $\langle\cos\varphi\rangle = \langle\sin\varphi\rangle = 0$ if desired.

In this Letter we propose and critically analyze a simplified scenario for implementing a Cooper pair sluice that ideally has no dynamical supercurrent leaking through the junctions and is governed by the relation $I = 2ef$ or more generally $I = 2nef$, where n is the number of pairs carried per cycle. First, we present the general idea of the device. We also study the viability of implementing the device by considering different sources of error and show that the sluice is tolerant against several kinds of nonidealities. We demonstrate that it is possible to construct a frequency-locked current source that has, with realistic assumptions, a yield of 0.1–0.2 nA with better than 1 ppm error.

The device consists of just one superconducting island that works as the sluice chamber and of two mesoscopic SQUIDs; see Fig. 1. The role of the SQUID loops is to serve as the sluice doors for the flow of Cooper pairs. The control parameters which are varied periodically and adiabatically include the gate voltage V_g and the magnetic fluxes Φ_a (a = l, r) through the SQUID loops. The idea of controlling the effective Josephson coupling is used throughout in the Josephson qubit literature; see, e.g., Ref. [2]. Utilizing flux pulses in Cooper pair shuttles [8] has also been suggested in Ref. [9] but in a nonadiabatic context. Here we work in the adiabatic limit. Note that the device is particularly simple; there is only one voltage

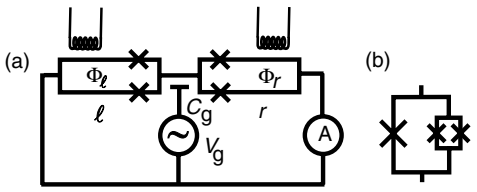

FIG. 1. (a) Schematic illustration of the device, the "sluice." The role of the coils is to apply controlled flux pulses through the SQUID loops, and they are synchronized with the periodic gate voltage. (b) An improved three-junction SQUID.

gate to adjust. The current through the sluice is given by the time integral of the expectation value of the current operator of either of the two SQUIDs. The dynamics is governed by the Schrödinger equation and the Hamiltonian of the device is (in the case of identical junctions)

$$\hat{H} = \frac{2e^2}{2C_\mathrm{J} + C_\mathrm{g}}(\hat{n} - n_\mathrm{g})^2 - E_\mathrm{J}^\mathrm{r}\left(\pi\frac{\Phi_\mathrm{r}}{\Phi_0}\right)\cos(\phi + \varphi/2) - E_\mathrm{J}^\mathrm{l}\left(\pi\frac{\Phi_\mathrm{l}}{\Phi_0}\right)\cos(\varphi/2 - \phi). \quad (1)$$

Here $C_\mathrm{J}/2$ is the capacitance of a single junction, C_g is the capacitance of the gate, $n_\mathrm{g} = C_\mathrm{g}V_\mathrm{g}/2e$ is the gate charge in $2e$ units, $\Phi_0 = h/2e$, and φ is the phase difference over the sluice. Furthermore, $E_\mathrm{J}^\mathrm{a}(\pi\frac{\Phi_\mathrm{a}}{\Phi_0}) = E_\mathrm{J}^\mathrm{max}\cos(\pi\frac{\Phi_\mathrm{a}}{\Phi_0})$ (a = l, r) denotes the effective flux-dependent signed Josephson energy of the left and the right SQUID, respectively. The Josephson energy of a single junction is thus $E_\mathrm{J}^\mathrm{max}/2$. The factor $E_\mathrm{C} \equiv (2e^2)/(2C_\mathrm{J} + C_\mathrm{g})$ is the charging energy. The quantum mechanical conjugate variables are the number of Cooper pairs on the island $\hat{n}$ and the superconducting phase ϕ. They obey the canonical commutation relation $[\hat{n}, \phi] = i$. The case of nonidentical junctions is modeled below by not allowing the Josephson energy to vanish during the cycle. We note that it is possible to use more complicated SQUIDs [see Fig. 1(b)] for which one of the junctions is replaced by a SQUID biased with a static field to match the E_J of the other half when $\Phi_0/2$ threads the primary loop. Self-inductance may be ignored for two junctions (other sources of error dominate) but for the three-junction design the self-inductance sets a limit for suppression at $\pi LI_\mathrm{C}/\Phi_0$ where $I_\mathrm{C} = 2\pi E_\mathrm{J}/\Phi_0$. An achievable value for this could be 10^{-3}. The current operator of the, say, right SQUID is

$$I^\mathrm{r} = \frac{2e}{\hbar}E_\mathrm{J}^\mathrm{r}\left(\pi\frac{\Phi_\mathrm{r}}{\Phi_0}\right)\sin(\phi + \varphi/2). \quad (2)$$

The total charge flowing through the system over one cycle has two components in the adiabatic limit [7], namely, the contribution from the dynamical supercurrent

$$Q_\mathrm{s} = \int_0^{t_\mathrm{cycle}}\langle 0; \mathbf{q}(t)|I^\mathrm{r}|0; \mathbf{q}(t)\rangle dt, \quad (3)$$

and the pumped charge (γ is the loop in parameter space)

$$Q_\mathrm{p} = 2\hbar\,\mathrm{Im}\left[\sum_{n\neq 0}\oint_\gamma \frac{\langle 0; \mathbf{q}|I^\mathrm{r}|n; \mathbf{q}\rangle}{E_0(\mathbf{q}) - E_n(\mathbf{q})}\langle n; \mathbf{q}|\nabla_\mathbf{q}|0; \mathbf{q}\rangle \cdot d\mathbf{q}\right]. \quad (4)$$

We have denoted above the control parameters collectively by the vector $\mathbf{q}$ which is varied in time. In the present context $\mathbf{q} = (n_\mathrm{g}, E_\mathrm{J}^\mathrm{r}, E_\mathrm{J}^\mathrm{l})^T$. Because of the adiabaticity criterion, the sluice stays at all times in the ground state with negligible Zener tunneling. The nth eigenstate at the point $\mathbf{q}$ is denoted by $|n; \mathbf{q}\rangle$ and the energy eigenvalue by $E_n(\mathbf{q})$.

Figure 2 illustrates a model control-parameter sequence. Note that the SQUIDs are biased in such a manner that one door is always closed, such that the dynamical contribution of Eq. (3) vanishes. Moreover, the signal is designed such that the system Hamiltonian (1) is always nondegenerate. This validates the use of Eq. (4). Varying just the gate voltage would lead to a degeneracy at $n_g = 0.5$, but because just one of the doors is open at this point, the problem is resolved. The sluice is ideally a switchable Cooper pair box. During the first half of the sequence one of the SQUIDs works as a Josephson junction while the other is effectively a capacitor. Then the roles are exchanged. It is easy to see that this sequence leads to the transport of exactly one Cooper pair through the sluice per cycle. In the beginning of the sequence the system is in the eigenstate of charge (zero pairs) due to the fact that the effective Josephson couplings are set to zero. In the middle of the sequence when both doors are again closed, the island is in the eigenstate of charge but now with one extra Cooper pair. The Cooper pair has tunneled through the right SQUID since the left one was closed. Finally, in the end of pulse the system is again at the eigenstate of charge with zero Cooper pairs and the charge must have gone through the left SQUID. Repeating this sequence results in $I = 2ef$, where $f = 1/t_\mathrm{cycle}$. The form of the pulse may also be generalized for the purpose of allowing n Cooper pairs to flow through the sluice over t_cycle, thus increasing the current to $I = 2nef$, simply by operating between $n_g = 0$ and $n_g = n$.

Assuming that the SQUIDs can be closed to a high degree renders the system almost entirely insensitive to the actual operating point of voltage. Instead of operating

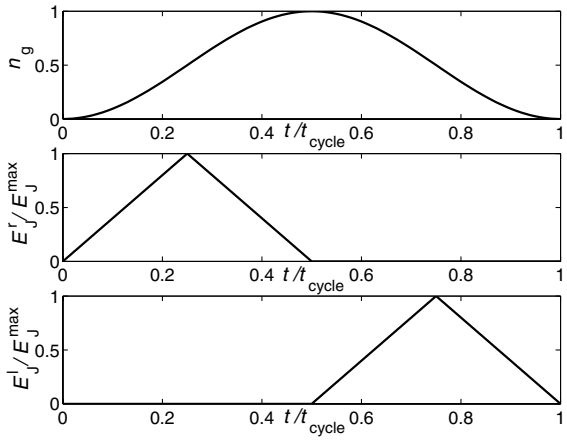

FIG. 2. Pulse sequence for pumping a single Cooper pair through the sluice. The exact form of the pulses is not crucial as long as the synchronization is maintained. The gate charge (or voltage) pulse, which is a shifted harmonic one here, may be generalized to have a larger amplitude and thus a larger number of pairs could be pumped.

between $n_g = 0$ and $n_g = 1$ (or $n_g = 0$ and $n_g = n$) we may just as well operate between $n_g = \delta$ and $n_g = \delta + 1$ (or $n_g = \delta$ and $n_g = n + \delta$) as long as $\delta \neq \frac{1}{2}$. However, the adiabaticity criterion becomes harder to fulfill if we start close to the degeneracy point. Considering that a typical measured power spectrum of the background $1/f$ charge noise is $S(f) = 10^{-8}e^2/f$ [2,10], there will be a need to reconfigure the sluice only after time scales of hours. This is a definite strength of the present approach and it is attributable to the use of the controllable SQUIDs. It should be emphasized that the exact shape of the pulses is not crucially important as long as the maxima and minima are synchronized as in Fig. 2. Even though we consider imperfections in suppressing E_J below, the effect of flux noise still needs to be studied in an experiment.

Let us comment on the maximum operating frequency of the device. Because of imperfections in the flux control and nonidentical Josephson junctions, there is always some residual E_J^{res}. This implies that one should have $E_J^{max} < E_C$ to avoid excess leakage and to make the sluice insensitive to background charge fluctuations. Furthermore, since the minimum gap in the energy spectrum of the sluice is roughly E_J^{max} whenever $E_J^{max} \leq E_C$ holds, one should have $hf \ll E_J^{max}$. It is often asserted that one should also have $E_C \ll \Delta_{BCS}$ in order to avoid quasiparticle effects. It follows that there would be an inequality chain $hf \ll E_J^{max} < E_C \ll \Delta_{BCS}$ which seriously limits the operation frequency of the device. However, it suffices to have

$$hf \ll E_J^{max} \approx E_C \lesssim \Delta_{BCS} \tag{5}$$

in the present context. Namely, the criterion $E_C \ll \Delta_{BCS}$ is now superfluous because, assuming adiabaticity, the sluice is never in its excited state. That is, it is sufficient to have Δ_{BCS} such that the second band [11] is just slightly below the lowest quasiparticle state which cannot be excited due to adiabaticity. In the case of nonadiabatic evolution $E_C \ll \Delta_{BCS}$ is, of course, necessary whenever we consider exciting the system, as in the case of the Josephson charge qubit [2]. We can also set $E_J^{max} \approx E_C$ in Eq. (5) and still get satisfactory performance as we show below.

We proceed to present numerical results obtained by integrating the Schrödinger equation corresponding to the Hamiltonian Eq. (1) over discrete time steps. The pumped charge was then obtained by numerically integrating the time-dependent expectation value of the current operator in Eq. (2). This nonadiabatic method reveals the effect of the finite operating frequency. We also estimate the effect of several kinds of nonidealities. We choose for the rest of the paper the typical parameters $C_J = C$, $C_g = 0.1C$, and $E_J^{max} = e^2/C$ such that $E_J^{max} \approx E_C$. Integrating the system at varying frequencies results in the pumped charge illustrated in Fig. 3. The path of

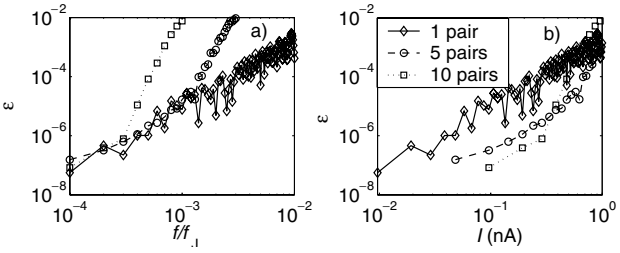

FIG. 3. Error (a) in the pumped charge over a single period and (b) in the current as a function of (a) frequency and (b) current. Here $C_J = C$, $C_g = 0.1C$, $E_J^{max} = e^2/C$, and $f_J = E_J^{max}/\hbar$. The error is $\varepsilon \equiv 1 - Q_P/2ne \equiv \Delta I/I$. The line marked by diamonds represents pumping a single Cooper pair, the line marked by circles represents pumping five Cooper pairs, whereas the squared line represents pumping ten Cooper pairs per cycle. In (b) we assume $f_J = 300 \times 10^9\ \mathrm{s}^{-1}$.

integration is the ideal sequence of Fig. 2. In light of Fig. 3, it seems that we could quite safely pump single Cooper pairs at the frequency $f = E_J^{max}/\hbar \times 10^{-3}$ and still have an accuracy of 7 ppm. Fabricating the island and the leads out of aluminum is the most viable option for the present, and by standard lithography one obtains $C < 10^{-15}$ fF. The well known BCS gap would be roughly $\Delta_{BCS}/h \approx 50$ GHz. Choosing the charging energy optimally, that is, $E_C \lesssim \Delta_{BCS}$, results in an operating frequency of some 300 MHz and a current of about 0.1 nA. However, Fig. 3 also illustrates the adiabaticity error for pumping five Cooper pairs; that is, the gate charge pulse has an amplitude of $C_g \Delta V_g/2e = 5$. When this is converted to current, we conclude that it may be possible to pump 0.2 nA with better than 1 ppm error. The result of pumping altogether ten Cooper pairs per cycle is also shown, and it turns out that a current of about 0.1 nA at 0.1 ppm error is possible. Ramps of the Josephson energy cause adiabaticity errors and, in comparison, varying the gate voltage does not contribute as much at least when pumping only a few Cooper pairs. The optimum number of pairs per cycle is yet an open question which we have not solved due to numerical difficulties.

The quantitative effect of background charge and the residual value of E_J, E_J^{res}, is illustrated in Fig. 4. We calculated the actual pumped charge, in the case of a single attempted Cooper pair in Fig. 4(a), over one cycle as a function of the gate charge deviation δ and E_J^{res}. The result has been averaged over different evenly spaced phase bias values, namely, $\varphi = \pi/2$, π, $3\pi/2$, and 2π (for justification see below). The frequency was $f = E_J^{max}/\hbar \times 10^{-4}$ which corresponds roughly to 0.1 nA. The performance of the sluice degrades rapidly with increasing E_J^{res} at fixed phase bias values. However, a physical sample would always be subject to some phase fluctuations. Keeping the phase constant over one cycle, as done above, is a realistic assumption if the dephasing time is long compared to t_{cycle}. We see that the error

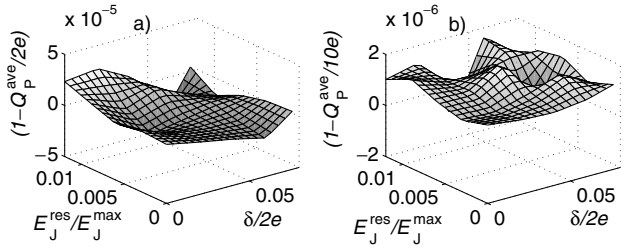

FIG. 4. (a) Averaged pumping error over the phase bias values $\varphi = \pi/2$, π, $3\pi/2$, and 2π as a function of δ and $E_{\rm J}^{\rm res}$ at $f = E_{\rm J}^{\rm max}/\hbar \times 10^{-3} (\approx 300$ MHz). (b) The same as (a) but for pumping five Cooper pairs at $f = 4E_{\rm J}^{\rm max}/\hbar \times 10^{-4} \approx 120$ MHz which corresponds to $I \approx 0.2$ nA.

averages out to a great accuracy even though the deviation from the ideal point (i.e., $E_{\rm J}^{\rm res}/E_{\rm J}^{\rm max} = 0$ and $\delta = 0$) is quite large. Note that the span of gate charge is some 10% and the span of the residual $E_{\rm J}^{\rm res}$ some 1%. Achieving even $E_{\rm J}^{\rm res}/E_{\rm J}^{\rm max} = 10^{-3}$ should be possible with the design of Fig. 1(b). A similar calculation for pumping five Cooper pairs was also performed at a frequency corresponding to $I \approx 0.2$ nA, and the averaged result is shown in Fig. 4(b). A yield of at least 0.2 nA is possible even in the presence of nonidealities with a relative error of some 10^{-6}.

It is easy to see why phase averaging suppresses the errors when $E_{\rm J}^{\rm res} \neq 0$ as suggested by Fig. 4. Namely, the supercurrent is proportional to $E_{\rm J}^{\rm r} E_{\rm J}^{\rm l} \sin\varphi$ [12] and the average of this is clearly zero. It is identically zero whenever one of the sluice doors is closed. We obtain in a two-state adiabatic approximation a perturbative formula in $E_{\rm J}^{\rm res}$ (for pumping a single Cooper pair)

$$\frac{Q_{\rm P}}{2e} \approx 1 - \frac{2\sqrt{(E_{\rm J}^{\rm max})^2 + E_{\rm C}^2}}{E_{\rm J}^{\rm max} E_{\rm C}} E_{\rm J}^{\rm res} \cos\varphi \qquad (6)$$

such that we may confirm that the error is proportional to $\cos\varphi$ as in the conventional pump [7]. We have utilized the fact that $Q_{\rm P} = -2e\frac{d}{d\varphi}\gamma$, where γ is the Berry phase associated with the adiabatic loop [13]. The effect of δ on the performance of the sluice is negligible compared to the effect of nonzero $E_{\rm J}^{\rm res}$ with fixed φ. Phase averaging, i.e., placing the sluice in a dissipative environment, may be used to cancel the effect of small nonidealities. Figure 4 clearly indicates that the sluice is quite insensitive to background charge fluctuations.

We assumed that choosing the phases evenly is a representative sample of the whole. Over time scales of seconds one may consider the phase to be evenly distributed between 0 and 2π due to dissipation. The even distribution is asymptotically identical to a wide Gaussian distribution on the whole real axis. The Gaussian nature can be justified by assuming a thermal bath of harmonic oscillators coupled to the phase with a sufficiently high effective impedance. The variance of the phase increases with the real part of the impedance seen by the device due to the fluctuation-dissipation theorem. Thus $\langle \exp(\pm i\varphi) \rangle = \exp(\pm i\langle\varphi\rangle - \langle\Delta\varphi^2\rangle/2)$ decays exponentially as do the pumping errors. Phase averaging has been used in the R-pump scenarios [6] by inserting large series resistors. At high currents this leads inevitably to overheating. In the present context the phase averaging is needed only as a second order mechanism since most of the errors are suppressed by the controlled modulation of the Josephson coupling. Finally, we comment on the effect of the ammeter. An ammeter with high R can cause a significant voltage over the sluice. A good choice would be a cryogenic current comparator modeled by L and C in parallel. With, e.g., $L = 10$ H, $C = 1$ nF, and $E_{\rm J}^{\rm max} \approx E_{\rm C}$ we would get $V(t) \approx V_0 \sin(2\pi f t)$ with $V_0 \approx e/C\pi \approx 50$ pV which is negligible.

To conclude, we have introduced and analyzed an idea of a Cooper pair sluice with just three control parameters. Compared to other Cooper pair pumping scenarios, we have suppressed undesired cotunneling, supercurrent leakage, and, most importantly, the need to have a long error-prone array of junctions with numerous gates. The idea for the control of the sluice is similar to the control of Josephson junction qubits. The sluice is much simpler, though, since superpositions and entanglement are not pursued and relatively slow pulses are sufficient.

We thank F. Hekking and O. Buisson for useful discussions and the Academy of Finland for financial support.

*Electronic address: antti.niskanen@vtt.fi

[1] See, e.g., articles in H. Grabert and M. H. Devoret, *Single Charge Tunneling* (Plenum Press, New York, 1992).
[2] Yu. Makhlin, G. Schön, and A. Shnirman, Rev. Mod. Phys. **73**, 357 (2001).
[3] M.W. Keller, J. M. Martinis, N. M. Zimmerman, and A. H. Steinbach, Appl. Phys. Lett. **69**, 1804 (1996).
[4] K. K. Likharev and A. B. Zorin, J. Low Temp. Phys. **59**, 347 (1985).
[5] L. J. Geerligs, S. M. Verbrugh, P. Hadley, J. E. Mooij, H. Pothier, P. Lafarge, C. Urbina, D. Esteve, and M. H. Devoret, Z. Phys. B **85**, 349 (1991).
[6] A. B. Zorin, S.V. Lotkhov, S. A. Bogoslovsky, and J. Niemeyer, cond-mat/0105211.
[7] J. P. Pekola, J. J. Toppari, M. Aunola, M. T. Savolainen, and D.V. Averin, Phys. Rev. B **60**, R9931 (1999).
[8] L. Y. Gorelik, A. Isacsson, Y. M. Galperin, R. I. Shekhter, and M. Jonson, Nature (London) **411**, 454 (2001).
[9] A. Romito, F. Plastina, and R. Fazio, cond-mat/0212414.
[10] A. B. Zorin, F.-J. Ahlers, J. Niemeyer, T. Weimann, H. Wolf, V. A. Krupenin, and S.V. Lotkhov, Phys. Rev. B **53**, 13682 (1996).
[11] A. Widom, G. Megaloudis, T. D. Clark, J. E. Mutton, R. J. Prance, and H. Prance, J. Low Temp. Phys. **57**, 651 (1984).
[12] M. Tinkham, *Introduction to Superconductivity* (McGraw-Hill, New York, 1996), 2nd ed., pp. 274–278.
[13] M. Aunola and J. J. Toppari, cond-mat/0303176.

Submitted for publication 2004. 4 p.
cond-mat/0410758

Evidence of Cooper pair pumping with combined flux and voltage control

Antti O. Niskanen,[1,2,*] Jani M. Kivioja,[2] Heikki Seppä,[1] and Jukka P. Pekola[2]

[1] *VTT Information Technology, Microsensing, POB 1207, FIN-02044 VTT, Finland*
[2] *Low Temperature Laboratory, Helsinki University of Technology, POB 2200, FIN-02015 HUT, Finland*

We have experimentally demonstrated pumping of Cooper pairs in a single-island mesoscopic structure. The island was connected to leads through SQUID (Superconducting Quantum Interference Device) loops. Synchronized flux and voltage signals were applied whereby the Josephson energies of the SQUIDs and the gate charge were tuned adiabatically. From the current-voltage characteristics one can see that the pumped current increases in $1e$ steps which is due to quasiparticle poisoning on the measurement time scale, but we argue that the transport of charge is due to Cooper pairs.

PACS numbers: 74.50.+r, 74.78.Na, 73.23.-b
Keywords: Josephson effect, charge pumping

A device that yields a DC current in response to an AC signal at frequency f according to the relation $I = Qf$ is called a charge pump. In the case of electron pumps $Q = me$ while for Cooper pair pumps $Q = 2me$, where m is an integer denoting the number of charges being pumped per cycle. Typically pumping electrons in mesoscopic structures requires an array of at least three tunnel junctions with voltage gates coupled to the islands in between the junctions. A Cooper pair pump is obtained when the tunnel junctions are replaced by Josephson junctions. These devices appear at first sight to be very similar and actually the very same samples may serve as both Cooper pair and electron pumps depending on whether the device is in the superconducting state or not. However, major differences exist. Besides the doubled charge in the superconducting state, the nature of the tunneling processes is very different, too. Electrons can tunnel downhill in energy due to the inherent dissipation mechanisms in normal metals with the relevant time scale given by the RC time constant, where R is the tunnel resistance and C the tunnel capacitance. Cooper pairs, on the other hand, try to conserve their energy, and in the absence of an electromagnetic environment, (i.e. zero impedance) only elastic processes are possible. Their maximum pumping frequency is proportional to $E_{\rm J}^2/(E_{\rm C}\hbar)$, where $E_{\rm J}$ and $E_{\rm C}$ are the Josephson and charging energies, respectively. What is more, superconducting circuits may behave coherently in the quantum-mechanical sense. The first attempt to pump Cooper pairs dates back to over a decade ago[1]. However, Cooper pair pumps have not been even nearly as accurate as single-electron pumps. The best example of the latter ones is the NIST seven-junction pump[2]. The motivation behind pumping Cooper pairs is two-fold. First of all, Cooper pair pumps are hoped to be able to pump larger currents than their normal state counterparts while still being accurate. This is roughly because increasing $E_{\rm J}^2/(E_{\rm C}\hbar)$ is easier than increasing $1/(RC)$. Secondly, the operation of Cooper pair pumps is interesting from the point of view of secondary "macroscopic" quantum phenomena and the structures are quite similar to the superconducting qubits (see, e.g., Refs. 3,4). Pumping of electrons using surface acoustic waves is another active field of study, see, e.g., Ref. 5.

In this work we report on the experimental demonstration of pumping Cooper pairs in a structure nicknamed the Cooper pair "sluice" introduced and theoretically analyzed recently by us, see Ref. 6. The device is particularly simple; it has just one superconducting island, like the single Cooper pair transistor, but the bare Josephson junctions are replaced by SQUID loops. The device may be alternatively viewed as a tunable Cooper pair box, a Josephson charge qubit[7]. Here the control is achieved via adiabatically manipulating both the fluxes through the two loops and the gate voltage. Ideally the SQUIDs act as tunable Josephson junctions whose coupling energy can be varied between a value close to zero and the sum of the couplings of the individual junctions. First we describe the experimental setup and discuss the theoretical idea briefly. Then we present measured data of the pumping experiment. We demonstrate that the pumped current obeys nicely the theoretical predictions. We also comment on possible ways of improving the results should the device be used in applications and discuss the significance of the results.

Figure 1 shows an SEM image of the sample used in the experiments along with a schematic of the measurement setup in Fig 1(c). The device was fabricated out of aluminum using standard e-beam lithography and two-angle shadow evaporation. It consists of a superconducting island that connects to the leads via SQUID loops. These are relatively large (10 μm by 100 μm) in order to have good inductive coupling but the island and the junctions are still small such that the charging energy is large enough ($\approx$1 K) to suppress thermal effects. The sample was attached to a dilution cryostat with a base temperature of 20 mK with the RF-lines connected.

Ideally, the pumping of m Cooper pairs is achieved by applying the three pulses in Fig 2(b) through the attenuated RF-lines. The upmost signal is applied to the gate while the two lower ones represent the currents flowing in the input coils. Two different versions of the gate pulse are shown, one for pumping "forward" and one for pumping "backward". To understand how the device works,

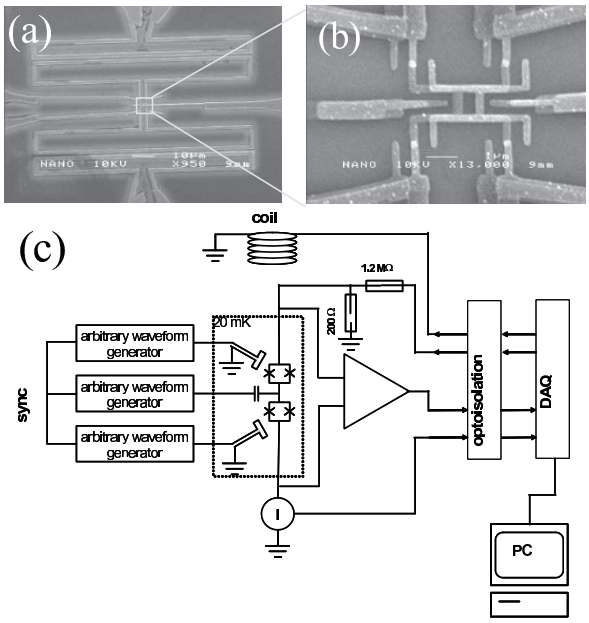

FIG. 1: (a) Scanning electron micrograph of the sample. The two input coils can be seen on top and bottom, respectively. The gate extends to the far right and the gate capacitance is $C_{\rm g} = 0.24$ fF based on DC measurements. The current flows between the two leads on the left side. (b) Closeup of the island. The measured total capacitance of the island is 3.7 fF which corresponds to a charging energy of about 1 K for Cooper pairs. The maximum $E_{\rm J}$ per SQUID is estimated to be around 0.5 K based on the normal state resistance. (c) Schematic illustration of the measurement setup. We used commercial room temperature electronics for the current measurement and three synchronized arbitrary waveform generators for the control pulse. The external coil for tuning the background of the SQUIDs is at 20 mK. The voltage biasing happens via voltage division through resistive lines. A surface mount capacitor of 680 pF and an on-chip capacitor on the order of 10 pF were also used.

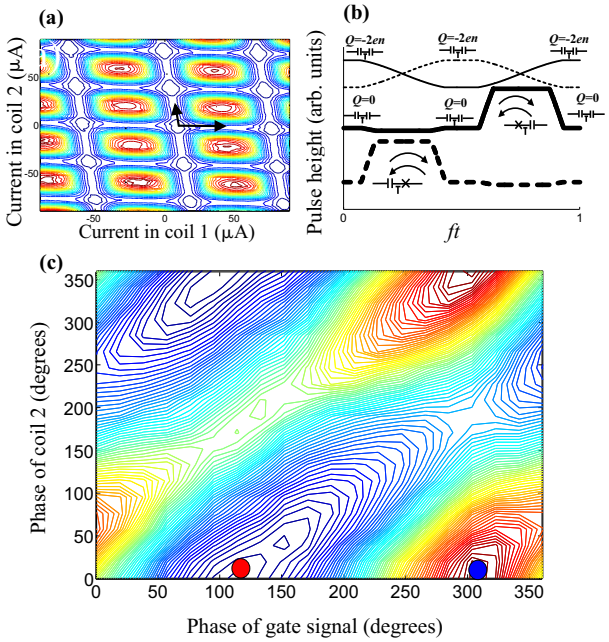

FIG. 2: (a) Contour plot of the measured DC current at constant voltage against DC currents in the two input coils. The total variation in the current is around 40 pA at this bias point (150 μV). The arrow line indicates the path along which the flux pulsing is performed in the pumping experiment. The lines of minimum current along which the arrows are aligned are the lines along which half a flux quantum threads one of the two SQUIDs. The slight tilting of the lines is a signature of the inductive cross-coupling. Arranging the pulsing as shown compensates for the cross coupling. (b) Waveforms that were used in the experiment. The thin almost sinusoidal pulse is the gate signal for pumping in, say, "forward" direction, and the dashed π-shifted signal is for pumping in the "backward" direction. The low level of the gate pulse is zero. The thick lines are the current signals corresponding to the arrowed path in the previous contour plot. (c) Contour plot of the measured current at a constant voltage of 250 μV against the relative phase differences between the signals with the pumping signal being applied at 2 MHz. The blue circle is the optimal choice for pumping "forward" while the red circle is the optimal point for pumping "backward". The amplitude was set large (over $400e$) and the variation in current was 150 pA. This operation point is far from optimal, but we still obtain a clear modulation for calibration purposes.

it is instructive to look at the Hamiltonian of the device, which reads

$$\begin{aligned}\hat{H} =& E_{\rm C}(\hat{n} - n_{\rm g})^2 - E_{\rm J}^1(\Phi_1)\cos(\phi + \varphi/2) \\ & - E_{\rm J}^2(\Phi_2)\cos(\varphi/2 - \phi). \end{aligned} \quad (1)$$

Here $E_{\rm C} = 2e^2/C_\Sigma$ is the charging energy for Cooper pairs where C_Σ is the total capacitance seen from the island. Furthermore, $E_{\rm J}^j$ with $j = 1, 2$ are the (signed) Josephson energies of the two SQUIDs which can be tuned with the external fluxes Φ_j. For identical junctions $E_{\rm J}^j = E_{\rm J}^{\rm max}\cos(\pi\Phi_j/\Phi_0)$, where $\Phi_0 \approx 2\times10^{-15}$ Wb is the flux quantum and $E_{\rm J}^{\rm max}$ is proportional to the critical current $I_{\rm C}$ of the individual junctions via $E_{\rm J}^{\rm max} = (\hbar/e)I_{\rm C}$. Furthermore, $n_{\rm g} = C_{\rm g}V_{\rm g}/2e$ is the gate charge in $2e$ units, $\hat{n}$ is the number operator for Cooper pairs, ϕ is the phase on the island and their commutator is $[\hat{n}, \phi] = i$. The environment couples to the pump through φ which is the phase difference over the pump. If the SQUIDs were to have perfectly identical junctions as well as vanishing self-inductance and if the flux control were perfect then the effective Josephson couplings could be set to zero.

Figure 2(a) shows a contour plot based on the measurement of the current through the device at a constant voltage against the DC currents in the two input coils. Along the lines of minimum current the flux through either of the loops is $(k+1/2)\Phi_0$, where k is an integer. The measurement reveals not only the mutual inductances M_{ij} between coil i and SQUID j, which were $M_{11} = 30$ pH, $M_{12} = 2$ pH, $M_{21} = 3$ pH and $M_{22} = 50$ pH, but also the proper offsets at any given time, i.e. the background

fluxes threading the loops. This measurement does not fully demonstrate to which extent it is possible to suppress the Josephson energy.

In the beginning of an ideal pumping cycle the $E_{\rm J}$'s of both loops are set as close to zero as possible and the position of the gate determines the ground state. We see that initially the ground state of the island is an eigenstate of charge. We then adiabatically "open" one of the SQUIDs, i.e. move to the tip of the, say, horizontal arrow in Fig 2(a) which means that the $E_{\rm J}$ of the SQUID 1 is maximized while for the other it is still zero. We stay at the tip of the arrow for some time and start to either decrease or increase the gate charge $n_{\rm g}$ depending on the direction we have chosen. When the gate reaches its extremum we "close" the SQUID again. Now if everything has been adiabatic the system is still in its ground state. The charge is again a good quantum number at this point but since the position of the gate is different, the number of charges is different too. The only possibility is that the excess charges have tunneled through the SQUID whose $E_{\rm J}$ has been non-vanishing during the cycle. The $E_{\rm J}$ of the second SQUID is then opened and the gate put back to its initial position. Finally the second SQUID is also closed. The number of Cooper pairs pumped is given by the difference between the integers closest to the high and low level of the gate charge. Fixing the low level and sweeping the high level should result in a $2e$-periodic staircase in the pumped current.

The phase of the gate determines naturally the direction, i.e. a 180-degree phase shift reverses the pumped current. Fig 2(c) illustrates the measured behavior of the current when the relative phases between the pulses are varied. The phase of coil 1 is fixed at 180 degrees and the phases of the other two are swept. The two circles shown are the optimal choices for pumping. Note that the extrema of current are indeed 180 degrees apart in the gate as expected and the optimal choices are the ones illustrated in Fig. 2. For practical reasons we were forced to use frequencies in the MHz range, but in the present pumping scheme it is possible to increase the value of current conveniently by increasing the gate amplitude. We tried out different shapes of pulses such as a mere sinusoidal gate signal, but it was found that it is better to keep the gate constant while the $E_{\rm J}$ is not maximized which is in accordance with the adiabaticity requirement. In practice we have arranged for a 15% dead time between the flux pulses although no systematic optimization of the pulses was performed.

Figure 3(a) shows an example of characteristic IV-curves (i.e., current-voltage curves) with the pumping signal being applied at $f = 3$ MHz. The effect of the change of direction is shown. The curves correspond to eight different values of gate amplitude. We see immediately that a leakage current exists on top of the pumped current that is on the same order or less than the pumped current. The IV-curves, however, clearly shift and the curves for pumping in opposite directions are far apart. The total current flowing through the device is a sum

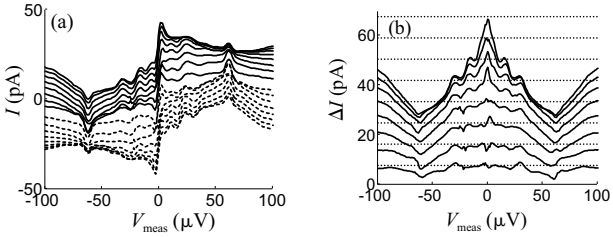

FIG. 3: (a) Examples of measured IV-curves with the pumping signal applied at 3 MHz. The gate charge (in $2e$ units) varies between 4 and 34. The solid curves correspond to pumping forward and the dashed curves correspond to pumping backward. Here $V_{\rm meas}$ is the measured value of voltage over the pump. (b) Difference of current, ΔI, in the IV-curves of (a) for pumping in opposite directions. The dotted lines indicate the expected values.

of two contributions, one being the leakage supercurrent that can be associated with the dynamical phase of the wave function and the other being the less trivial pumping contribution attributable to the geometric phase. If one assumes that the leakage is the same for the pumping in both directions at a definite voltage bias point, then the difference between the IV-curves should be twice the magnitude of current pumped in this case. Fig. 3(b) reveals that at low voltages (tens of μV) and at smaller amplitudes this pumping contribution is indeed close to the expected level shown with dotted lines. The leakage current which is due to the nonideal environment and flux control is undesirable from an application point of view, but the physical phenomenon is clearly visible. The voltage bias is not sufficiently good to eliminate the leakage, i.e. the P(E)-curve[8] for tunneling events is not sufficiently peaked at the origin.

These considerations suggest that it is interesting to study the difference in the currents ΔI with the gate shifted by 180 degrees. Figure 4(a) shows the measured behavior of ΔI at 2.5 MHz versus the high level of gate voltage with the low level set to zero. The current may be seen to increase in clear steps. The expected height of a step is twice the pumped current, i.e. $4ef$ which in this case is some 1.6 pA. Since we sweep the high level of the gate signal and not just the amplitude with constant offset, the steps should occur at $2e$ intervals in the gate charge. However, due to random parity changes (quasiparticle "poisoning") at time scales that are much shorter than our measurement time scale (0.1 s) but longer than the pumping cycle (10^{-6} s) we observe the time average of two $2e$-periodic staircases that are shifted by e in the gate charge. For instance in Ref. 9 the tunneling time for quasiparticles was estimated to be 10 μs in a similar structure while in Ref. 10 it was some 10^{-2} s for a coupled system of two superconducting transistors with one grounded. We were unable to measure the corresponding time in our setup, but based on this supporting evidence we argue that the transport of current is due to Cooper

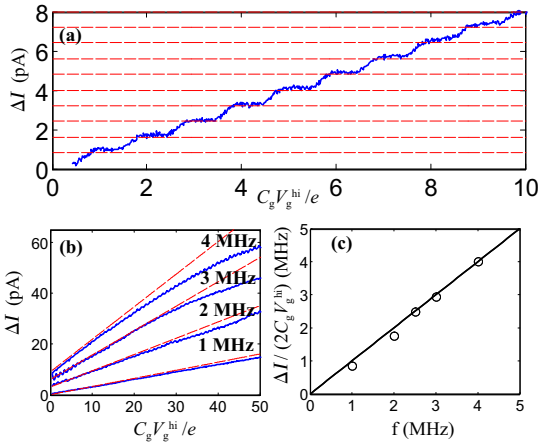

FIG. 4: (a) Difference ΔI in current of forward and backward pumping at 2.5 MHz against the high level of the gate signal V_g^{hi} with the low level at zero. The dashed lines are drawn at $2ef$ intervals. (b) Large gate amplitude behavior of ΔI at a few frequencies. The dashed lines show the expected gate dependece, i.e. their slope is $2ef$. The curves are offset for clarity. (c) Fitted slopes to the data of the previous plots up to $V_g C_g/e = 10$ are shown by circles. The solid line indicates the expected behavior. The voltage bias point was around 10 μV in all the above plots.

pairs since the order in which the E_J's are manipulated changes the direction of current. The quasiparticles effectively shift the gate charge by e but rarely enough such that the pumping is undisturbed on the level of precision of the present measurement. If this interpretation is made then one sees that the obtained results are in very good agreement with theory. Figure 4(b) illustrates the measured large amplitude behavior of the pumped current at frequencies between 1 MHz and 4 MHz. We see that the current lacks behind the prediction with increasing frequency and amplitude. At 1 MHz no clear bending of the curve is seen up to gate amplitude of $40e$, while at 4 MHz the performance starts to degrade after $10e$. One can observe by looking at Fig. 3(b) that the "bending" is more pronounced at larger bias voltage values (voltage is on the order of 10 μV in Fig. 4) while no visible bending happens up to amplitudes of $68e$ when $V \approx 0$. Small amplitude behavior in Fig. 4, however, is linear aside from the steps with a slope of $2ef$. Figure 4(c) shows the slopes obtained from linear fits to the data of Fig. 4(a) and the ten first steps of Fig. 4(b). One sees that the agreement is again good.

The above results prove that the flux and voltage driven pumping of Cooper pairs is experimentally possible in a single-island device. However, in order to serve as a practical device the leakage current needs to be taken care of as well as the quasiparticle poisoning. The quasiparticles may possibly be handled by either quasiparticle "traps" or by BCS gap profile engineering[9]. As to the reduction of the leakage, several options exist. One option is the engineering of the electromagnetic environment such that the voltage biasing is good also at frequencies on the order of the charging energy. This would result in DC IV-characteristics heavily peaked at zero voltage with negligible leakage current. Another way to cut down the leakage is to fabricate a longer chain of junctions. A multiloop SQUID would possibly improve the suppression of E_J without increasing the number of controls. Improved RF-engineering would also be of benefit in arranging the flux pulses. To conclude, the results are encouraging in spite of several nonidealities observed and the pumping of Cooper pairs with flux control looks much more attractive than with a mere multiple gate voltage control.

We thank H. Sipola and S. Franssila for help with the measurement set-up and device fabrication, and A. Anthore, T. Heikkilä, P. Helistö and M. Paalanen for useful discussions. The Academy of Finland and EU IST-FET-SQUBIT2 are acknowledged for financial support.

* Electronic address: antti.niskanen@vtt.fi

[1] L. J. Geerligs, S. M. Verbrugh, P. Hadley, J. E. Mooij, H. Pothier, P. Lafarge, C. Urbina, D. Esteve, and M. H. Devoret, Z. Phys. B: Condens. Matter **85**, 349 (1991).
[2] M. W. Keller, J. M. Martinis, N. M. Zimmerman, and A. H. Steinbach, Appl. Phys. Lett. **69**, 1804 (1996).
[3] D. Vion, A. Aassime, A. Cottet, P. Joyez, H. Pothier, C. Urbina, D. Esteve, and M. H. Devoret, Science **296**, 886 (2002).
[4] Y.A. Pashkin, T. Yamamoto, O. Astafiev, Y. Nakamura, D.V. Averin, and J.S. Tsai, Nature **421**, 823 (2003).
[5] J. M. Shilton, V. I. Talyanskii, M. Pepper, D. A. Ritchie, J. E. F. Frost, C. J. B. Ford, C. G. Smith, and G. A. C. Jones, J. Phys.: Condens. Matter **8**, L531 (1996).
[6] A. O. Niskanen, J. P. Pekola, and H. Seppä, Phys. Rev. Lett. **91**, 177003 (2003).
[7] Yu. Makhlin, G. Schön, and A. Shnirman, Rev. Mod. Phys. **73**, 357 (2001).
[8] G.-L. Ingold and Yu. V. Nazarov, in Single Charge Tunneling, edited by H. Grabert and M.H. Devoret (Plenum Press, New York, 1992), pp. 21–106.
[9] J. Aumentado, M. W. Keller, J. M. Martinis, and M. H. Devoret, Phys. Rev. Lett. **92**, 066802 (2004).
[10] J. Männik and J. E. Lukens, Phys. Rev. Lett. **92**, 057004 (2004).

Published by

Series title, number and report code of publication

VTT Publications 552
VTT–PUBS–552

Author(s)
Niskanen, Antti O.

Title

Control of Quantum Evolution and Josephson Junction Circuits

Abstract

Ever since Peter Shor's ground-breaking discovery in 1994 of an algorithm capable of factoring large integers on a quantum-mechanical computer exponentially faster than using any known classical method, research on quantum computing has boomed. Quantum information – a unique mixture of computer science, physics and mathematics – has developed into a new branch of information theory. On the experimental side, physicists from many different disciplines including atomic, solid-state and low-temperature physics, as well as optics, are striving today towards a practical quantum computer. All the candidate quantum bit (qubit) technologies have one thing in common: They rely on the controlled time-evolution of a closed quantum system, a seemingly paradoxical task.

In this Thesis the temporal control of quantum systems is studied. The topics included can be divided into two according to the type of temporal evolution; geometrical or dynamical. Geometrical realization-independent methods for quantum computing are studied first. Then the study is extended into dynamical quantum computing and the so-called Josephson charge-qubit register is considered as a test bench. Finally, a spin-off application of the geometrical evolution of a Josephson junction system is studied, i.e. Cooper pair pumping. A novel Cooper pair pump, the Cooper pair "sluice", is introduced.

The work on quantum computing reported in this Thesis is theoretical while the Cooper pair "sluice" is studied both theoretically and experimentally. Numerical simulations, both sequential and parallel, are used extensively throughout the Thesis. The experiments were carried out under cryogenic mK conditions and the sample fabrication was done using e-beam nanolithography.

Because the execution time of a quantum algorithm is always limited by the inevitable process of decoherence, it is important to utilize any measure available for accelerating quantum computations. It is found that practical quantum algorithms could greatly benefit from classical computer-aided optimization. Moreover, it is found that even a modest demonstrator of a full quantum algorithm using Josephson charge qubits is just barely realizable within present-day coherence times. However, the experimental part of this Thesis shows clear evidence of the functioning of the "sluice". While the worldwide effort of improving the coherence properties of qubits is underway, the "sluice" could well find practical use, e.g., in metrology in the foreseeable future.

Keywords
quantum systems, quantum mechanics, quantum computing, quantum algorithms, Cooper pair pumping

Activity unit
VTT Information Technology, Tietotie 3, P.O.Box 1207, FIN–02044 VTT, Finland

ISBN			Project number
951–38–6420–0 (soft back ed.) 951–38–6421–9 (URL:http://www.inf.vtt.fi/pdf/)			
Date	Language	Pages	Price
October 2004	English	46 p. + app. 61 p.	C.
Series title and ISSN		Sold by	
VTT Publications 1235–0621 (soft back ed.) 1455–0849 (URL: http://www.vtt.fi/inf/pdf/)		VTT Information Service P.O.Box 2000, FIN–02044 VTT, Finland Phone internat. +358 9 456 4404 Fax +358 9 456 4374	

Ever since Peter Shor's ground-breaking discovery in 1994 of an algorithm capable of factoring large integers on a quantum-mechanical computer exponentially faster than using any known classical method, research on quantum computing has boomed. Quantum information – a unique mixture of computer science, physics and mathematics – has developed into a new branch of information theory. On the experimental side, physicists from many different disciplines including atomic, solid-state and low-temperature physics, as well as optics, are striving today towards a practical quantum computer. All the candidate quantum bit technologies have one thing in common: They rely on the controlled time-evolution of a closed quantum system, a seemingly paradoxical task. This work investigates the temporal control of various quantum systems. While the bulk of the work is theoretical, also experimental results are reported. The topics discussed include both geometrical and dynamical quantum computing as well as adiabatic charge pumping. Particular attention is paid to Josephson junction systems.

Tätä julkaisua myy
VTT TIETOPALVELU
PL 2000
02044 VTT
Puh. (09) 456 4404
Faksi (09) 456 4374

Denna publikation säljs av
VTT INFORMATIONSTJÄNST
PB 2000
02044 VTT
Tel. (09) 456 4404
Fax (09) 456 4374

This publication is available from
VTT INFORMATION SERVICE
P.O.Box 2000
FIN–02044 VTT, Finland
Phone internat. +358 9 456 4404
Fax +358 9 456 4374

ISBN 951–38–6420–0 (soft back ed.)
ISSN 1235–0621 (soft back ed.)

ISBN 951–38–6421–9 (URL: http://www.vtt.fi/inf/pdf/)
ISSN 1455–0849 (URL: http://www.vtt.fi/inf/pdf/)

VTT PUBLICATIONS 552 Control of Quantum Evolution and Josephson Junction Circuits Antti O. Niskanen